Saturation vapor pressures and transition enthalpies of low-volatility organic molecules of atmospheric relevance: from dicarboxylic acids to complex mixtures

Journal:	*Chemical Reviews*
Manuscript ID:	cr-2014-005502.R1
Manuscript Type:	Thematic Review
Date Submitted by the Author:	n/a

Complete List of Authors:	Bilde, Merete; Aarhus University, Chemistry Barsanti, Kelley; Portland State University, Civil & Environmental Engineering Booth, Alastair; University of Manchester, SEAES Cappa, Christopher; University of California - Davis, Civil and Environmental Engineering Donahue, Neil; Carnegie Mellon University, Center for Atmospheric Particle Studies Emanuelsson, Eva; Aarhus University, Department of Chemistry McFiggans, Gordon; University of Manchester, SEAES Krieger, Ulrich; ETH , Institut für Atmosphäre und Klima Marcolli, Claudia; ETH Zurich, Institute for Atmospheric and Climate Science Topping, David; University of Manchester, School of Earth, Atmospheric and Environmental Science; University of Manchester, National Centre for Atmospheric Science (NCAS) Ziemann, Paul; University of Colorado, Department of Chemistry and Biochemistry and Cooperative Institute for Research in Environmental Sciences (CIRES) Barley, Mark; University of Manchester, Centre for Atmospheric Science Clegg, Simon; University of East Anglia, School of Environmental Sciences Dennis-Smither, Benjamin; University of Bristol, School of Chemistry Hallquist, Mattias; Atmospheric Science, Chemistry and Molecular Biology Hallquist, Åsa; IVL Swedish Environmental Research Institute, Khlystov, Andrey; Desert Research Institute, Division of Atmospheric Sciences Kulmala, Markku; University of Helsinki, Dept. of Physical Sciences Mogensen, Ditte; University of Helsinki, Dept. of Physical Sciences Percival, Carl; University of Manchester, SEAES Pope, Francis; University of Cambridge, Department of Chemistry Reid, Jonathan; University of Bristol, School of Chemistry Rosenoern, Thomas; University of Copenhagen, Department of Chemistry Ribeiro da Silva, Manuel; University of Porto, Chemistry Salo, Kent; Chalmers University of Technology, Shipping and Marine Technology Soonsin, Vacharaporn; ETH Zurich, Institute for Atmospheric and Climate Science; Chulalongkorn University, Center of Excellence on Hazardous Substance Management

	Yli-Juuti, Taina; University of Helsinki, Department of Physics; University of Eastern Finland, Department of Applied Physics Prisle, Nønne; University of Helsinki, Pagels, Joakim; Lund University, Division of Aerosol Technology Rarey, Juergen; University of KwaZulu-Natal, School of Chemical Engineering; DDBST GmbH, ; Carl von Ossietzky University , Industrial Chemistry Zardini, Alessandro; Institute for Energy and Transport, European Commission, Joint Research Centre (JRC) Riipinen, Ilona; Stockholm University, Department of Analytical Chemistry and Environmental Science (ACS) and Bolin Centre for Climate research

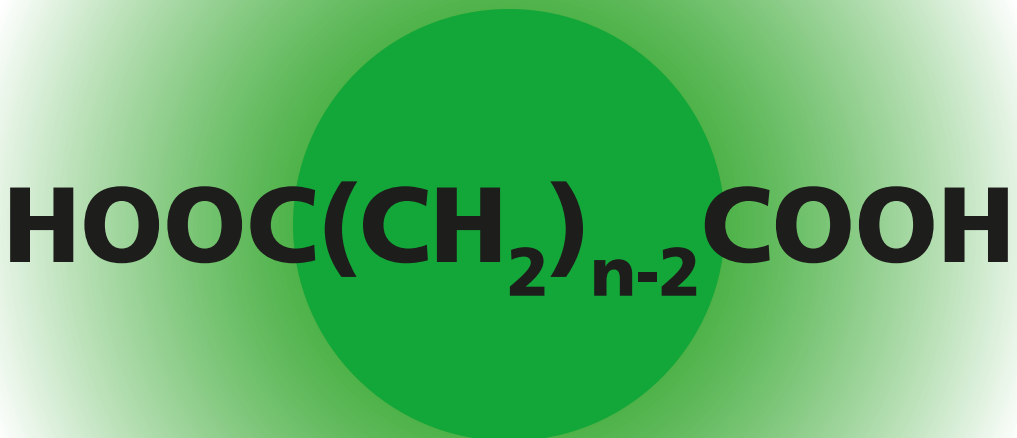
HOOC(CH2)n-2COOH

Saturation vapor pressures and transition enthalpies of low-volatility organic molecules of atmospheric relevance: from dicarboxylic acids to complex mixtures

Merete Bilde,[1*] Kelley Barsanti,[2] Murray Booth,[3] Christopher D. Cappa,[4] Neil M. Donahue,[5] Eva U. Emanuelsson,[1] Gordon McFiggans,[3] Ulrich K. Krieger,[6] Claudia Marcolli,[6,7] David Topping,[3,8] Paul Ziemann,[9] Mark Barley,[3] Simon Clegg,[10,11] Benjamin Dennis-Smither,[12] Mattias Hallquist,[13] Åsa M. Hallquist,[14] Andrey Khlystov,[15] Markku Kulmala,[16] Ditte Mogensen,[16] Carl J. Percival,[3] Francis Pope,[17] Jonathan P. Reid,[12] M. A. V. Ribeiro da Silva,[18] Thomas Rosenoern,[19] Kent Salo,[20] Vacharaporn Pia Soonsin,[6,21] Taina Yli-Juuti,[16,22] Nønne L. Prisle,[16] Joakim Pagels,[23] Juergen Rarey,[24,25,26] Alessandro A. Zardini,[27] Ilona Riipinen[28]

1 Department of Chemistry, Aarhus University, Aarhus, Denmark

2 Department of Civil and Environmental Engineering, Portland State University, Portland OR, USA

3 Centre for Atmospheric Science, School of Earth, Atmospheric and Environmental Sciences, University of Manchester, Manchester United Kingdom

4 Department of Civil and Environmental Engineering, University of California, Davis, USA,

5 Centre for Atmospheric Particle Studies, Carnegie Mellon University, Pittsburgh, USA

6 Institute for Atmospheric and Climate Science, ETH Zurich, Zurich, Switzerland

7 Marcolli Chemistry and Physics Consulting GmbH, Zurich, Switzerland

8 National Centre for Atmospheric Science (NCAS), University of Manchester,

Manchester, United Kingdom

9 Department of Chemistry and Biochemistry and Cooperative Institute for Research in Environmental Sciences (CIRES), University of Colorado, Boulder, USA

10 School of Environmental Sciences, University of East Anglia, Norwich, United Kingdom

11 Air Quality Research Center, University of California, Davis, CA 95616, USA

12 School of Chemistry, University of Bristol, United Kingdom

13 Atmospheric Science, Department of Chemistry and Molecular Biology, University of Gothenburg, Gothenburg, Sweden

14 IVL Swedish Environmental Research Institute, Gothenburg, Sweden

15 Division of Atmospheric Sciences, Desert Research Institute, Reno, USA

16 Department of Physics, University of Helsinki, Helsinki, Finland17 School of Geography, Earth and Environmental Sciences, University of Birmingham, Birmingham, United Kingdom

18 Centro de Investigação em Química, Department of Chemistry and Biochemistry, Faculty of Science, University of Porto, Porto, Portugal

19 Department of Chemistry, University of Copenhagen, Copenhagen, Denmark

20 Maritime Environment, Shipping and Marine Technology, Chalmers University of Technology, Gothenburg, Sweden

21 Center of Excellence on Hazardous Substance Management, Chulalongkorn University, Bangkok, Thailand

22 Department of Applied Physics, University of Eastern Finland, Kuopio, Finland

23 Ergonomics & Aerosol Technology, Lund University, Lund, Sweden

24 School of Chemical Engineering, University of KwaZulu-Natal, South Africa

25 DDBST GmbH, Oldenburg, Germany

26 Industrial Chemistry, Carl von Ossietzky University Oldenburg, Oldenburg, Germany

27 European Commission, Joint Research Centre (JRC), Institute for Energy and Transport, Ispra, Italy

28 Department of Analytical Chemistry and Environmental Science (ACS), and Bolin Centre for Climate research, Stockholm University, Stockholm, Sweden

* Author to whom correspondence should be addressed (bilde@chem.au.dk)

Contents

1. Introduction

Aerosol particles are important constituents of the atmosphere. They impact modern society through their effects on visibility,[1] human health[2] and global climate.[3] Despite this great importance, they continue to represent a challenge to scientists due to their complexity.

Atmospheric aerosols have both natural and anthropogenic sources and consist of both organic and inorganic molecules. Organic compounds constitute 20-90% of the atmospheric aerosol particle mass, depending on location.[4] The term primary aerosol particle is used to describe particles that are emitted directly into the atmosphere as particles. These primary particles are transformed in the atmosphere through the continuous exchange between the gas and particle phases via evaporation and condensation. Additionally, a large fraction of the organic particulate mass results from condensation of vapors that are produced by chemical reactions in the gas phase[4-5] and is termed secondary organic aerosol (SOA). To predict the temporal and spatial distribution of aerosols, particularly SOA, it is necessary to understand the fundamental parameters that govern the distribution of organic compounds between the gas and particle phases. Key thermodynamic properties describing the equilibrium gas-particle partitioning of organic compounds are the saturation vapor pressures[6] and the enthalpies of vaporization and sublimation.

The majority of organic molecules, especially those produced from chemical reactions, that are partitioned to the condensed phase in the atmosphere are characterized as being oxidized and multifunctional,[7] and likely have molecular weights between 150–300 g mol^{-1} and relatively low saturation vapor pressures (< 10^{-2} Pa).[8] Recent laboratory and field observations have brought

attention to a potentially important contributor to SOA and atmospheric new-particle formation, namely organic molecules with extremely low vapor pressures (less than ~10^{-7} Pa).[9]

During the past four decades several experimental techniques have been developed to probe thermodynamic properties of low-volatility organic molecules present in atmospheric aerosols. Measurements of low vapor pressures are challenging due to the low gas-phase concentrations that need to be probed - the lower the vapor pressure the more difficult the measurement. Given that the number of different organic molecules in the atmosphere may be in the range of 10,000 to 100,000,[10] the number of experimentally determined saturation vapor pressures for compounds of atmospheric relevance is distressingly limited. Predictions of gas-particle partitioning thus must rely on estimation methods. Several estimation methods are available for predicting saturation vapor pressure of organic molecules. Yet there is a scarcity of low-volatility benchmark molecules available for testing of such methods due, in large part, to measurement challenges.

One class of low volatility compounds that has received extensive study using a wide variety of experimental techniques are dicarboxylic acids, which are commonly found in atmospheric aerosols[7c] and which are also commercially available. This, in principle, makes them ideal benchmark molecules for testing of estimation methods. However, experimental results repeated for dicarboxylic acid saturation vapor pressures and vaporization enthalpies are in some cases in good agreement, while in other cases (as discussed herein) the reported vapor pressures disagree by several orders of magnitude and the enthalpies by some tens of kJ mol^{-1}. While this provides an excellent base for stimulating scientific discussions, it also presents and obvious problem and limits wider use of the data. This review is motivated by the need for a synthesis of the current

state-of-science on saturation vapor pressure measurement and estimation techniques, a discussion of best practices in applications of gas-particle partitioning in the atmosphere, and recommendations for future measurement and modeling efforts. The basis for this review article was laid at a workshop in Copenhagen in 2010 on the measurement and prediction of saturation vapor pressures and gas to particle partitioning in the atmosphere. Discussions have continued and evolved since. This review is focused around the well-studied dicarboxylic acids, with the ambition of providing a comprehensive review of the existing data on their saturation vapor pressures, along with retrieving new general insights into the advantages and limitations associated with the different measurement and prediction techniques, as well as producing a set of saturation vapor pressures and enthalpies based on combined literature datasets that span the 20th century through today. Furthermore, strategies to help bridge the gap in complexity between single-component saturation vapor pressures, simple mixtures and multi-component atmospheric organic aerosols and provide directions for future research in this field are discussed.

2. Theoretical background and framework for atmospheric aerosols

In this section the theoretical framework for discussing evaporation and condensation, from and to atmospheric aerosol particles is provided. The framework and approaches outlined in this section are used in the interpretation and application of the data presented in the following sections.

2.1 Saturation vapor pressures

We use the IUPAC[11] definition of saturation vapor pressure: "*The pressure exerted by a pure substance (at a given temperature) in a system containing only the vapor and condensed phase (liquid or solid) of the substance"*. The surface of the condensed phase is flat and the vapor and condensed phases are in thermodynamic equilibrium with each other. The saturation vapor pressure of compound *i* is in this work denoted p_i^0 where superscript ^{0} indicates *saturation* vapor pressure. In phase equilibrium, there is no net molecular flux between the vapor and condensed phases (chemical equilibrium condition), no temperature gradients (thermal equilibrium condition) and no net forces (mechanical equilibrium condition) acting on the interface. The saturation vapor pressure p_i^0 depends on the molecular interactions of *i* in the condensed phase, and is a strong function of temperature.[12] The temperature dependence of p_i^0 is given by the Clausius-Clapeyron equation:

$$\frac{dp_i^0}{dT} = \frac{\Delta H_{trs,i}}{T \cdot \Delta v_{m,i}} \quad (1)$$

where T is the temperature, $\Delta H_{trs,i}$ and $\Delta v_{m,i}$ are the changes of molar enthalpy and molar volume upon the phase transition (vaporization or sublimation), respectively.

At temperatures below the critical temperature, the change in molar volume upon transition to gas phase can normally be approximated by the molar volume of the gas. Assuming that the gas phase behaves ideally, Equation 1 can thus be written:

$$\frac{dp_i^0(T)}{dT} = \frac{\Delta H_{trs,i}}{R \cdot T^2} \cdot p_i^0 \qquad (2)$$

where R is the molar gas constant. The Clausius-Clapeyron equation can be integrated, yielding an exponential dependence of p_i^0 on temperature. Assuming that $\Delta H_{trs,i}$ is independent of temperature, the integrated Clausius-Clapeyron equation is

$$p_i^0(T) = p_i^0(T^{ref}) \exp\cdot\left[\frac{\Delta H_{\mathrm{trs},i}}{R} \cdot \left(\frac{1}{T^{ref}} - \frac{1}{T}\right)\right] \qquad (3)$$

where T^{ref} and p_i^0 (T^{ref}) are the temperature and saturation vapor pressure at a reference state *e.g.,* at the boiling point. The temperature-dependence of the saturation vapor pressure can then be expressed as:

$$\ln p_i^0(T) = -\frac{\Delta H_{trs,i}}{R \cdot T} + C \qquad \text{or} \qquad \log_{10} p_i^0(T) = -\frac{\Delta H_{trs,i} \log_{10} e}{R \cdot T} + C' \qquad (4)$$

where C and C' are constants containing information about the reference state (see Equation 3). Similar equations can be derived with more accurate representations of the temperature dependence of $\Delta H_{trs,i}$ resulting in more terms on the right hand side of the equations.

The saturation vapor pressure and transition enthalpy of a pure component *i* can be defined with respect to a liquid phase $p^0_{l,i}$, $\Delta H_{vap,i}$ or a solid phase $p^0_{s,i}$, $\Delta H_{sub,i}$. At a given temperature *T* below the melting point, the saturation vapor pressure over the solid phase is lower than that over the subcooled liquid. The Gibbs free energy difference $\Delta G_{fus,i}$ between two condensed phases, liquid and solid, of the same compound, *i*, is related to the ratio of their saturation vapor pressures by

$$\Delta G_{fus,i} = R \cdot T \cdot \ln\left(\frac{p^0_{l,i}}{p^0_{s,i}}\right) \quad (5)$$

Hence, the saturation vapor pressures over subcooled liquid and solid pure compound *i* can be linked with the formula[12]

$$\ln \frac{p^0_{l,i}}{p^0_{s,i}} = \frac{\Delta H_{fus,i}}{R \cdot T_m} \cdot \left(\frac{T_t}{T} - 1\right) - \frac{\Delta c_{p,sl,i}}{R} \cdot \left(\frac{T_t}{T} - 1\right) + \frac{\Delta c_{p,sl,i}}{R} \cdot \ln \frac{T_t}{T} \quad (6)$$

where ΔH_{fus} is the enthalpy of fusion, T_t is the triple point temperature, and $\Delta c_{p,sl}$ is the change in the molar heat capacity upon the solid-liquid transition at the triple point. In practical applications of Equation 6, the triple point is often approximated with the melting point temperature at atmospheric pressure, and the enthalpy of fusion is also calculated at the melting temperature.[12]

The solid state can be crystalline or amorphous. The amorphous state is here referred to as something that is not crystalline (without long range order). The amorphous state thus includes gels, rubber and glasses. The phase state of the solid (crystalline or amorphous) is important because the saturation vapor pressures over the two different solid phases are different. The saturation vapor pressure of an amorphous solid is very close to the one of the subcooled liquid at a given temperature and they are treated herein to be the same. The formula linking the two vapor

pressures derived from Equation 5 is similar to Equation 6, but does not contain the first term, since there is no equivalent to the enthalpy of fusion in the liquid to amorphous solid transition. The change in in the molar heat capacity $\Delta c_{p,l\rightarrow amorphous}$ may be approximated upon the liquid to amorphous transition to be constant and equal to the heat capacity change at the so-called glass transition. This approximation will yield an upper limit of the expected effect, since $\Delta c_{p,l\rightarrow amorphous}$ will converge to zero at the triple point. Few data are available on the $\Delta c_{p,l\rightarrow amorphous}$ and the glass transition temperature for atmospherically relevant organic molecules. To illustrate the magnitude of the expected ratio in saturation vapor pressures, examples for two molecules[13] for which data are available are provided: citric acid with the glass transition temperature, T_g = 282 K close to room temperature and $\Delta c_{p,l\rightarrow amorphous}$ = 184 J mol^{-1} K^{-1}, and glycerol with T_g = 192 K and $\Delta c_{p,l\rightarrow amorphous}$ = 88 J mol^{-1} K^{-1}. Here the subscript g refers to glass. For an upper limit of the ratio of amorphous solid to subcooled vapor pressure at 298 K values of 0.97, 0.40, and 0.36 are obtained for citric acid, glycerol and water, respectively. The ratio in vapor pressure between amorphous solid and liquid state is most significant for compounds of low molecular weight with low glass transition temperatures but stays above 0.36 at 298 K even for those. For most compounds under consideration here the difference in saturation vapor pressure is estimated to be below 20% and will be ignored in our analysis. Hence, in the following, p_s^0 refers to the crystalline solid and p_l^0 to the vapor pressure of the subcooled liquid and the amorphous solid. If the crystalline solid can exist in different polymorphic forms, transitions between those have to be accounted for in Equation 6, as well.

2.2 Vapor-liquid or vapor-solid equilibria over mixed solutions

In a multi-component system, the thermodynamic phase equilibria are altered as compared with the single-component pure liquid or solid state. The equilibrium vapor pressure, p_i^{eq}, of an organic compound *i* over a flat surface of a mixture, depends strongly on the pure-component saturation vapor pressure p_i^0, but is also linked to the chemical composition of the mixture through the modified Raoult's law equation[12]

$$p_i^{eq} = \gamma_{x,i} \cdot x_i \cdot p_i^0 \quad (7)$$

where $\gamma_{x,i}$ is the (mole fraction based) activity coefficient and x_i is the mole fraction of *i* in the mixture. The activity coefficient reflects the molecular interactions in the condensed phase, and depends on the composition of the mixture and temperature. If the interactions of molecules *i* with the other molecules in the mixture are equal to the interactions of *i* with itself, the mixture is said to be ideal with respect to *i*, and $\gamma_{x,i} = 1$. The saturation vapor pressure p_i^0 is thus a special case of the equilibrium vapor pressure p_i^{eq} referring to the case of a gas over a single-component, condensed-phase surface ($x_i = 1$, $\gamma_{x,i} = 1$).

Equilibrium thermodynamics require the equilibrium vapor pressure, $p_{ss,i}^{eq}$, over a saturated solution, *ss*, to be the same as over the corresponding thermodynamically stable solid (crystalline) phase *s* at the same temperature. This is in turn relatable to the liquid-phase vapor pressure because the three phases must be in equilibrium, and there is only a single gas phase:

$$p_{ss,i}^{eq} = p_{s,i}^0 = \gamma_{x,ss,i} \cdot x_{ss,i} \cdot p_{l,i}^0 \quad (8)$$

This equation allows for assessment of consistency between different measurement data obtained from samples in different physical states. For example the equilibrium vapor pressure of *i* measured over a saturated solution $p_{ss,i}^{eq}$ should be the same as that measured over the crystalline solid $p_{s,i}^{0}$.

2.3 Equilibria over curved surfaces

The above formulations (Equations 7-8) for the equilibrium vapor pressures of *i* were defined over a flat surface. If the surface is curved, however, the mechanical equilibrium condition is altered due to the surface tension (surface free energy) at the vapor-liquid (vapor-solid) interface. This results in an increase in the equilibrium vapor pressure as compared with the flat surface case, formulated through the Kelvin equation

$$p_i(D_p) = p_i^0 \cdot \exp\left(\frac{4 \cdot \sigma \cdot \nu_{m,i}}{R \cdot T \cdot D_p}\right) \quad (9)$$

where σ is the surface tension (surface free energy) of the condensed-phase surface, $v_{m,i}$ the molar volume of *i* in the mixture, and D_p the diameter of curvature.[14] The equilibrium vapor pressure of i over a multicomponent particle is thus given as:

$$p_i^{eq}(D_p) = \gamma_{x,i} \cdot x_i \cdot p_i^0 \cdot \exp\left(\frac{4 \cdot \sigma \cdot \nu_{m,i}}{R \cdot T \cdot D_p}\right) \quad (10)$$

Curvature effects increase as diameter decreases and, for typical σ values, become important for diameters smaller than about 100 nm. The term $\frac{4 \cdot \sigma \cdot \nu_{m,i}}{R \cdot T}$ in Equation 9 has units of length and scales with the particle diameter, and can thus be called the *Kelvin diameter*. For many organic compounds of atmospheric relevance it is of order 7-15 nm.[15] While this is important to account

for in deriving single component saturation vapor pressures from measurements of nano-particle evaporation (Section 3), for partitioning calculations involving complex mixed aerosols, the Kelvin term is very significant only for the smallest particles with $D_p \lesssim 20$ nm (it rapidly diminishes above that value being 15-30% for 50 nm particles and 7-16% for 100 nm particles), especially compared with the many orders of magnitude variation in equilibrium vapor pressure for constituents in a typical ambient mixture.

2.4 Dynamic evaporation and condensation from and to an aerosol particle

Since direct observations of the saturation gas-phase concentrations of low-volatility compounds are challenging, saturation vapor pressure values are often inferred from measurements of dynamic evaporation, or condensational growth of small condensed-phase samples such as aerosol particles. In practice, this is done by monitoring changes in the size of the sample or the gas phase concentrations as a function of time. To determine values of saturation vapor pressures from such measurements, the data need to be interpreted using a dynamic model of the mass transport between the gas and condensed phase.

In general, the mass transport of compound *i* to or from a condensed phase sample (such as an aerosol particle), is driven by a difference between the ambient partial vapor pressure of *i* far from the sample surface $p_{\infty,i}$ and the partial pressure at the sample surface $p_{a,i}$. It is usually assumed that the surface composition and properties resemble that of the bulk phase, and that the particle surface is in thermodynamic equilibrium with the vapor immediately adjacent to the surface, *i.e.* $p_{a,i} = p_i^{eq}$.

In the case of aerosol particles, the appropriate theory for describing the mass transport of substance i to and from the particles depends on particle diameter D_p relative to the mean free path λ_i of i in the gas mixture described by the Knudsen number Kn_i.

$$Kn_i = \frac{2 \cdot \lambda_i}{D_p} \tag{11}$$

The mean free path in air is 66 nm at standard conditions[16] and does not change much over ambient temperatures. Thus the Knudsen number is ~1 for a particle of diameter of ~132 nm. If the mean free path is much smaller than the particle diameter ($Kn_i << 1$), the mass transport is limited by gas phase diffusion and can be derived from diffusional mass transport equations.[14] This is called the continuum regime. A key parameter is the gas phase diffusivity $D_{i,gas}$. In the case where the mean free path is much larger than the particle ($Kn_i >> 1$), the mass transport can be derived using kinetic gas theory, and the transport is limited by the mass accommodation. This is called kinetic regime, where a key parameter is the mass accommodation coefficient α_m, which is the fraction of the molecules impinging on the surface that stick and absorb to the bulk of the particle. If the mean free path is similar to the particle size ($Kn_i \approx 1$), both gas phase diffusion and mass accommodation are important for mass transport. This is called the transition regime. To describe evaporation or condensation in this regime, it is necessary to match the equations governing the diffusional transport with those describing kinetic transport. The flux matching results in a formula for the mass flux I to and from a spherical particle due to condensation and evaporation that is applicable throughout the Kn_i regimes.[17]

$$I_i = \frac{2 \cdot \pi \cdot D_p \cdot D_{i,gas} \cdot M_i \cdot \beta_{i,m}}{R \cdot T} \cdot \left(p_{i,\infty} - p_{i,a} \right) \quad (12)$$

where $D_{i,gas}$ is the diffusion coefficient of i in the gas mixture, M_i the molar mass of i and

$$\beta_i = \frac{1 + \mathrm{Kn}_i}{1 + \left(\frac{4}{3 \cdot \alpha_{mi}} + 0.377 \right) \cdot \mathrm{Kn}_i + \frac{4}{3 \cdot \alpha_{mi}} \cdot \mathrm{Kn}_i^{\,2}} \quad (13)$$

is the transition regime correction factor resulting from the flux-matching procedure.

In this version of β, λ is given as $\lambda = \frac{3 \cdot D_{i,gas}}{\bar{c}}$ where $\bar{c}$ is the mean speed of the molecules, $\bar{c} = \left(\frac{8 \cdot k \cdot T}{\pi \cdot M_i} \right)^{1/2}$. It should be noted that this definition of λ is specific to this formulation of β.

Equation 12 is a special case of the mass transport to and from a spherical particle, and several assumptions have been made in its derivation. Most importantly: 1) the gas-phase compounds behave as ideal gases; 2) the system is homogeneous and under no external forces; 3) pressure and temperature are constant throughout the system; 4) ordinary diffusion is the main form of mass transport (*i.e.* that there is, for instance, no significant convection or temperature gradient present); 5) the mass fluxes of the condensing/evaporating compounds i are not influencing each other; 6) the system is in quasi-stationary state *i.e.* the timescale of condensation is long enough for the position of the surface to be well defined; and 7) the concentration of the condensing vapor is low as compared with the inert gas concentration, and the Stefan flow (the flow of inert gas to maintain the constant pressure) can be neglected. If evaporation or condensation rates are

large as compared with the heat conduction by the gas-phase molecules, the latent heat release or absorption will influence mass transfer and needs to be accounted for.

A detailed discussion on mass and heat transfer is beyond the scope of this review. For a broad overview the reader is referred to *e.g.* Seinfeld & Pandis,[14] Pruppacher & Klett[18] and for a more thorough discussion of the approximations typically used in aerosol science, the reader is referred to the specialized literature.[19]

The mass accommodation coefficient of organic compounds of atmospheric relevance is still uncertain within an order of magnitude,[20] while the diffusivity can be estimated with better accuracy. Consequently, the mass accommodation coefficient is among the most important sources of uncertainty in the evaporation and condensation rate calculations for atmospheric low-volatility vapors, and for deriving saturation vapor pressures from measurements of evaporation rates.[21] Well-defined laboratory data on the mass accommodation coefficients of organic molecules is still scarce, largely due to similar difficulties as encountered in determining the saturation vapor pressures.[22] Saleh et al.[23] reported α_m values of 0.07, 0.08, and 0.24 for succinic-, adipic-, and pimelic acids, respectively, based on experiments using the Integrated Volume Methods described in Section 3.3.3. Recently, Julin et al.[20] studied the pure-component mass accommodation of a selection of organic molecules (succinic acid, adipic acid, naphtalene and nonane) by molecular simulations complemented with expansion chamber measurements for nonane only, and found no clear evidence for α_m values below unity for any of the molecules, but constrained the coefficients to be between about 0.1-1 for all the studied molecules. For subcooled liquids there is no evidence for the accommodation coefficient to be substantially lower than 1.[20]

2.5 Ambient partitioning

Atmospheric aerosols are almost always incompletely described; they consist of a complex mixture of possibly hundreds of thousands of different organic compounds,[10,24] as well as inorganic material, including elemental carbon, crustal minerals, and metals. In almost all cases only a fraction of the mass concentration of total suspended particulate matter, *TSP*, constitutes one or more organic rich phases important for organic partitioning. This complexity poses challenges for thermodynamic descriptions of atmospheric aerosols. The partitioning of a given molecule *i* is often described by the parameter f_i^{cond}, which is the fraction of molecule *i* residing in the condensed phase. The partitioning can thus be expressed as:

$$f_i^{cond} = \frac{C_i^{cond}}{C_i^{cond} + C_i^{vap}} = \frac{1}{1 + C_i^{vap} / C_i^{cond}} \quad (14)$$

where C_i^{cond} and C_i^{vap} are the mass concentrations of *i* in the condensed phase and the vapor phase, respectively in units of mass per volume of air (typically μg m^{-3}).

In the context of atmospheric studies, organic molecules are often classified according to their distribution between the vapor and condensed phases under ambient conditions. Accordingly, the following terms have recently been introduced, defined based on saturation mass concentrations: volatile organic compounds (VOCs), intermediate volatility organic compounds (IVOCs), semi-volatile organic compounds (SVOCs), low volatility organic compounds (LVOCs), and extremely low volatility organic compounds (ELVOCs).[25] IVOCs generally are vapors but may be in the condensed phase in extremely concentrated smoke and exhaust plumes, SVOCs have substantial fractions in both the gas and condensed phases, LVOCs are principally in the

condensed phase but still subject to curvature effects, while ELVOCs have negligible equilibrium gas-phase fractions and condense more or less irreversibly to the condensed phase if they are formed in the gas phase.[25-26] While potentially useful, these terms and definitions are not yet universally adopted.

Partitioning of organic molecules from the gas to the condensed phase can take place in two ways: adsorption on a surface and absorption into the bulk. The latter process, absorption, describes the partitioning of organic molecules into an organic matrix, and plays a dominant role in the formation of ambient SOA.[6] Absorptive gas to particle partitioning theory[6,27] is therefore used in most atmospheric models to represent SOA formation. Applying the modified Raoult's law, Equation 7, and the ideal gas law, a gas-particle partitioning coefficient (K_p) has been defined:[6]

$$K_{p,i} = \frac{R \cdot T \cdot f_{OM}}{M_{OM} \cdot \gamma_{x,i} \cdot p^0_{l,i}} = \frac{C_i^{cond} / TSP}{C_i^{vap}} \quad (15)$$

Partitioning of a given compound *i* between the vapor C_i^{vap} and condensed C_i^{cond} phases is largely driven by its equilibrium vapor pressure and its activity coefficient in the absorbing phase. The quantity f_{OM} describes the fraction of *TSP* that serves as the absorbing bulk organic phase, which typically is assigned a mean molecular weight M_{OM}.

In many atmospherically relevant cases the appropriate equilibrium vapor pressure is the sub-cooled liquid-phase vapor pressure. It is *not* necessary that the condensed phase actually be a liquid, but it is conventionally assumed (and supported by several studies)[28] that the thermodynamically stable complex condensed phase is amorphous; it may be a liquid, a glass, or

an amorphous solid (see Section 2.1). As the difference between a liquid and a crystalline phase is the regular arrangement of molecules in a crystalline lattice, it is thus generally assumed that the sub-cooled liquid vapor pressure is reasonable for partitioning calculations,[6] especially as most atmospheric particles contain some water.

The interpretation of field observations is challenging using the above framework because neither the mole fraction nor the average molar weight of the absorbing bulk organic phase is known, and both vary in time and space. However, the mass concentration of compound *i* in the absorbing organic phase can be readily obtained using gravimetric and mass-spectrometer measurements from the mass fraction φ_i of compound *i* in that phase:

$$C_i^{cond} = x_i \cdot \left(\frac{M_i}{M_{OM}} \right) \cdot C_{OA} = \varphi_i \cdot C_{OA} \quad (16)$$

where C_{OA} is the total mass concentration of the absorbing bulk organic phase. Analogous to Equation 7, the equilibrium mass concentration of *i* in the vapor phase C_i^{eq} can be expressed as:

$$C_i^{eq} = \frac{M_i}{R \cdot T} \cdot \gamma_{x,i} \cdot x_i \cdot p_{l,i}^0 = \gamma_{x,i} \cdot x_i \cdot C_{l,i}^0 \quad (17)$$

where, $C_{l,i}^0$ is the saturation mass concentration of *i* over the condensed phase. To account for curvature effects, a Kelvin term can be added (see Equation 9).

Equation 17 can then be re-written in terms of the mass fraction and a mass-based activity coefficient $\gamma_{m,i}$

$$C_i^{eq} = \varphi_i \cdot \gamma_{m,i} \cdot C_{l,i}^0 = \varphi_i \cdot C_i^* \quad (18)$$

The product $\gamma_{m,i} \cdot C_{l,i}^0$ is called the effective saturation concentration of *i* and abbreviated C_i^*. At equilibrium, with $C_i^{vap} = C_i^{eq}$, Equation 14 can be re-written.[29]

$$f_i^{cond} = \frac{1}{1 + C_i^* / C_{OA}} \quad (19)$$

In the case where $f_{OM} = 1$, the effective saturation concentration of *i*, C_i^* is the inverse of the partitioning coefficient $K_{p,i}$, *i.e.* $C_i^* = 1/K_{p,i}$.

Activity coefficients are calculated on the mole fraction or molality scale. A number of models [7a,30] all use the molar-based partitioning approach in a manner consistent with equations 15 through 19. To account for non-ideality in the mass-based partitioning as formulated in equations 16, 17 and 18, it would be necessary to develop a mass-fraction based activity coefficient model covering all the functional groups encountered in the atmosphere. No such approach exists or is envisaged.

3. Experimental methods

Ideally, the equilibrium, and thus saturation vapor pressure of a specific compound is measured directly by monitoring the gas phase concentration of the compound in thermodynamic phase equilibrium over the condensed (liquid or solid, pure or mixture) phase. Unfortunately the gas phase concentrations corresponding to the saturation vapor pressures of the least volatile atmospheric molecules are often unreachable with the currently available instrumentation – particularly at ambient conditions where air molecules are present in orders of magnitude higher numbers than the investigated compounds. To reduce the lower limit of equilibrium vapor pressure measurements and quantify the saturation vapor pressures of the least volatile atmospheric organic compounds, several methods have been used. Some methods have also

probed the equilibrium vapor pressure of organic compounds over simple mixtures with water and common atmospheric inorganic salts.

In many studies size or mass changes due to evaporation or condensation of small condensed phase samples, often in form of airborne or trapped particles, have been monitored *in lieu* of direct observation of the gas phase in equilibrium. Other studies apply mass spectrometric analysis of the gas phase, but typically at total pressures well below the atmospheric. Working at elevated temperatures,[31] compared to atmospheric conditions, is an additional means to overcome some of the problems that the very small equilibrium concentrations pose to measurement techniques since the saturation vapor pressures are a strong increasing function of temperature (Equation 1). Some studies operate as close to equilibrium conditions as possible,[31e,32] while others infer the equilibrium and saturation vapor pressures from observations of dynamic evaporation or condensation.[31d,33] In the dynamic case, calculations on the dynamic mass transport are needed to interpret the experimental observations of evaporation or condensation rates (see Section 2.4).

In this section, an overview of a selection of the methods that have been applied to study the thermodynamic properties of pure C_2-C_{12} dicarboxylic acids, and their simple mixtures with water and common atmospheric inorganic constituents is presented. The methods differ from each other in terms of the sample generation method, size, phase (liquid or solid) as well as the time scales, relative humidity, temperature and vapor pressure ranges that can be probed. Additionally, the primary observable tracked in the experiments and used for determining the saturation vapor pressure varies between methods. Consequently, the different methods represent

a range of sensitivities to the p^o and p^{eq} as well as $\Delta H_{(vap\ or\ sub)}$ values, and thus different confidence intervals for these quantities. For an experimentally based determination of ΔH, the temperature-dependence of p^o needs to be obtained from the measurements. Table 1 and Figure 1A-D summarize some of the main features of the experimental methods outlined in this paper.

3.1 Knudsen cell based methods

Knudsen cells are temperature controlled cylindrical cells connected to vacuum chambers with spherical orifices. Knudsen cells are utilized for measurements of equilibrium vapor pressures of solid state compounds of atmospheric relevance by placing a macroscopic sample inside the cell, letting the sample equilibrate with the gas phase, and measuring either the changes in the sample mass over time[31a,31g,34] or the effusion rate of gas phase molecules from the cell.[35] It can be shown that if the Knudsen number *Kn* of the orifice, defined as the ratio of the mean free path λ of the effusing vapor molecules to the radius of the effusion orifice r_0, is high enough, loss of the effusing gas molecules does not significantly disturb the equilibrium in the cell[36] and the steady state pressure in the Knudsen cell can be approximated with the equilibrium vapor pressure of the effusing compound. The basic principles of the Knudsen cell based methods are outlined in Figure 1A and described in more detail below (see also Table 1).

3.1.1 Knudsen mass loss methods

In the Knudsen mass loss methods applied by Ribeiro da Silva and co-workers,[31a,31g,34] the pure macroscopic crystalline sample is placed at the base of the Knudsen cell. Through an orifice located coaxially at the top of the cell, the vapor effuses into the vacuum (pressure of the order of

10^{-2} Pa) outside the cell. The change in mass of the sample (Δm) during time t is recorded with an accuracy of ±0.1 mg by weighing before and after an effusing time period, while the system temperature (within ±0.01 to 0.001 K) and experiment time are set such that sufficient sample has been lost to be measured with a balance. The mass loss rate is proportional to the difference between the vapor pressure in the cell (assuming the sample surface is in equilibrium with the gas phase) and the vacuum chamber (where the gas phase concentration of the effusing vapor is assumed to be zero). The equilibrium vapor pressure p_i^0 of the effusing compound i can therefore be formulated using the kinetic theory of gases as

$$p_i^0 = \left(\frac{\Delta m_i}{A_0 \cdot \omega_0 \cdot t} \right) \cdot \sqrt{\frac{2 \cdot \pi \cdot R \cdot T}{M_i}} \qquad (20)$$

where A_0 is the area of the orifice (given by $\pi \cdot r_0^2$, where r_0 is the radius of the orifice, with typical orifice areas of the order of 10^{-6} m^2), and ω_0 is the Clausing probability factor[31a] which accounts for the geometry of the system, and can be calculated using the expression

$$\omega_0 = \left[1 + \frac{3 \cdot l_0}{8 \cdot r_0} \right]^{-1} \qquad (21)$$

where l_0 is the length of the orifice, *i.e.* thickness of the plate, typically of the order of 0.05 mm. The detection limit of Knudsen mass loss is limited by having to effuse enough material to be measured using a balance. Typical problems with the technique are the need to extrapolate from higher temperatures to obtain values for 298 K with most low volatility compounds, and sample contamination by components with a higher volatility.

3.1.2 Knudsen Effusion Mass Spectrometry (KEMS)

In Knudsen Effusion Mass Spectrometry (KEMS) the change in concentration of the gas phase as the vapor from a macroscopic crystalline sample effuses from a Knudsen cell is measured using mass spectrometry. The KEMS system built and applied at University of Manchester[35] consists of two separately pumped vacuum chambers connected via a gate valve, and operating at total gas phase pressures within the cell of approximately 10^{-4}–10^{-6} Pa. The lower chamber contains a coaxially heated Knudsen cell with a chamfered effusion orifice. The upper chamber is connected to a Balzers quadrupole mass spectrometer. To calibrate the system, specifically the orifice radius, a sample of known vapor pressure is placed in the temperature controlled Knudsen cell. The molecular beam consisting of the effusing molecules is ionized in the upper chamber by 70 eV electron impact, then sampled by the mass spectrometer. After accounting for the ionization cross section of the calibration compound,[35a] this produces a signal proportional to the equilibrium vapor pressure of the calibration compound. Calibration compounds used[35] include benzophenone, ferrocene and stilbene, with saturation vapor pressures of the order of 0.1 to 1 Pa at room temperature.

After calibration, the saturation vapor pressure of a compound can be determined from the intensity of its mass spectrometer signal as compared with the calibration compound. The radius of the effusing orifice is selected to be roughly one tenth of the mean free path of the effusing compound to ensure that the orifice does not disturb the thermodynamic equilibrium of the lower cell. Consequently, the sizes of the orifices deployed have ranged from a few hundred micrometers for vapor pressures in the 0.1 to 1 Pa range, to a few millimeters in diameter for

lower volatility compounds.[35] The detection limit is determined by the sensitivity of the mass spectrometer. As with the Knudsen mass loss methods, measurements can be made at higher temperature and extrapolated to atmospherically relevant temperatures. Typical problems with the technique are the need for reference compounds with well-defined vapor pressures and that the ionization cross sections are needed for concentration calibrations; the latter are typically well-known for organic compounds ionized using 70 eV electron impact ionization.

3.2 Single particle methods

If the gas-phase partial pressure of a specific compound deviates from the corresponding equilibrium vapor pressure over the surface of an aerosol particle, the particle will evaporate or grow until equilibrium is reached (see Section 2). Values for the equilibrium vapor pressures can thus be inferred by following the evaporation or condensational growth of individual aerosol particles at controlled conditions, as long as the gas phase composition is known. Solid and/or subcooled liquid saturation vapor pressures of dicarboxylic acids have been determined in this way.[33f,g,37] The methods used in these studies vary in terms of methods for holding the particle in place, particle generation and particle size detection. What is common for all of them is the trapping of single aerosol particles and optical monitoring of changes in their size, based on the light scattered by the particle.[21] The wavelength of the light source sets the lower limit for the particle size that can be investigated with these methods. Consequently, particle sizes investigated with these techniques are typically in the range of 2-20 μm. The optical methods often allow for simultaneous detection of the size change and morphology, and thus the phase of the particle, assuming that crystalline particles tend to have non-spherical morphologies whereas

amorphous particles are spherical. In some instances also the refractive index, providing a direct measure of the evolving composition can be detected. The basic principles of the single particle methods that have been used for measuring the saturation vapor pressures of dicarboxylic acids are summarized in Figure 1B and Table 1. In the following, these methods are divided into two classes according to the method used for holding the particles in place: the methods applying an Electrodynamic Balance (EDB), [33f,g,37-38] and the methods using optical tweezers.[33g,39] Because of symmetry requirements, the optical tweezer technique is applicable for measurements of liquid droplets or amorphous solid particles that are approximately spherical, while the EDB can be applied on both liquid and non-spherical crystalline samples.

3.2.1 Electrodynamic Balance (EDB)

As has been first demonstrated by Davis and Ray[40] measurements of diffusion-controlled evaporation rates of single, micron-size particles suspended in an electrodynamic balance can be used to yield saturation vapor pressures for low-volatility organics. The basic idea of an EDB is to balance the gravitational force acting on the particle with a force induced by an electric field. The gaseous environment surrounding the particle is continually flushed with humidified and temperature-controlled air, to sweep away the gas phase organic molecules from the EDB chamber. It is assumed that the EDB chamber has a negligible concentration of organic gas phase molecules, and hence there is only a flux of organic material from the particle to gas phase, and not vice versa. During evaporation the change in particle size is observed as a function of time, and the saturation vapor pressure of the organic molecule is determined as described in section 2.4. Experiments are performed at a variety of relative humidities to obtain a range of concentrations of the organic molecule in the particle phase. To calculate equilibrium vapor

pressures of the organic compound in the liquid state from evaporation rates, the composition of the particle, the density of the particle, the molar mass of the organic compound, and the diffusivity in the buffer gas need to be known accurately. Importantly, assuming the mass accommodation coefficient to be unity leads to negligible errors in vapor pressure estimates, as long as the actual value of the accommodation coefficient is larger than approximately 0.1, because the levitated particles are well within the continuum regime.

Two electrodynamic balances have been applied to measure solid and subcooled liquid phase saturation vapor pressures of dicarboxylic acids; the EDB setup at ETH, Zurich and the EDB setup at the University of Cambridge (this has now been moved to University of Birmingham). Both setups are based on the double-ring electrode configuration.[41] The ring electrodes generate a superposed DC and AC field. Levitation is achieved because the weight of the particle, and any other vertical net force, is balanced by an electrostatic DC force. The AC field acts to focus the particle in the null point of the AC field. Of course this requires the particle to have a net charge. The charge is assumed to have no effect on the evaporation kinetics or thermodynamics of the investigated particles. This has been shown to be a well justified assumption for the typical net charging states and particle sizes (roughly 5 – 20 μm in diameter).[42]

The main difference between the two setups is the technique to measure the size of the particle. Details of the two setups are given briefly below.

The setup at ETH Zurich[33f,37,43] allows for measurement of the evaporation rate of aqueous, liquid particles as well as non-spherical, solid particles. A single liquid, aqueous aerosol particle is inductively charged and injected into the EDB using an ink jet single particle generator filled

with a diluted aqueous solution, and then levitated by the electric field in the EDB. Solid particles are either injected directly into the EDB by contact charging, or aqueous solution particles are transformed to solids by efflorescence through drying. Temperature (with stability better than 0.1 K and an accuracy of ±0.5 K), relative humidity (RH, with accuracy within ±1.5% between 10% and 90%) and total pressure are adjusted. The evaporation of the particle is monitored by precision sizing (with an accuracy in evaporation rate of $\pm 1 \cdot 10^{-6}$ μm^2 s^{-1}), using optical resonance spectroscopy with a white light source, and applying Mie theory.[33f] For solid particles, which are in general non-spherical, the actual non-spherical particle shape needs to be considered. Using an equivalent sphere radius approximation, one can still deduce evaporation rates from optical resonance spectroscopy by assigning a size parameter to a specific resonance in the spectra, and following its temporal evolution.[37a] To distinguish unambiguously liquid (spherical) particles from solid (non-spherical) particles, the two-dimensional angular scattering pattern is monitored continuously using a CCD camera.[44] Equilibrium vapor pressures between 10^{-6} Pa and 10^{-1} Pa can be measured with this technique, the relative humidity ranging from dry (<0.5%) to about 98% with a relative error in vapor pressure in the liquid state estimated to be of the order of 30% plus an absolute error of $\pm 0.4 \times 10^{-6}$ Pa for an evaporation experiments lasting 24 hours.[43]

In the setup at the University of Cambridge,[33g,38] a continuous-wave HeNe laser is directed at the particle within the EDB. The resulting angularly resolved fringe pattern, of the elastic Mie scattered light, is used to estimate the changing particle size. The absolute uncertainty in the particle size from this technique is ~ ±1 μm. However, the relative size of the particle can be measured to ~ 100 nm on a per particle basis. A geometric optics method is used to analyze the scattering patterns.[45] It is important to note that experiments on the dicarboxylic acids using this

EDB setup have only been performed on particles that are aqueous solution droplets generated from atomized solutions. The variation in RH and temperature around the set point in these experiments were approximately ±1% and ±0.2 K, respectively.

3.2.2 Optical tweezers

Optical tweezers represent another type of particle trap. The details of the optical tweezers technique are described elsewhere,[46] and only its use for measuring evaporation of atmospherically relevant organic compounds from single aerosol particles will be highlighted here. Optical tweezers use a tightly focused laser beam to trap a single aerosol particle with sizes ranging from 4 to 16 μm.[47] The particle is confined in three dimensions, and can be held indefinitely by the optical forces. Optical tweezers can be used to trap liquid particles and spherical amorphous particles, but not crystalline materials due to the lack of spherical symmetry. As a consequence, the evaporation of organic substances can only be measured from particles that are liquid mixtures, aqueous solutions, or amorphous solids. In the following, the optical tweezers at Bristol University[33g] where a single beam gradient force optical trap combined with Raman spectroscopy and bright field microscopy to probe single aerosol particles are described.

The trapped particle is held at the focal point of the trapping laser within a custom-fabricated cell, through which a flow of gas passes allowing control of the local environment experienced by the particle *e.g.* RH. The RH can be controlled and measured within ±1% for an extended time period of several hours. A single aerosol particle is randomly captured from a cloud of aerosol, generated using a medical nebulizer, flowed through the trapping cell. A light emitting diode (LED) provides illumination for conventional bright field microscopy allowing the morphology

of the trapped particle to be observed in real time. Inelastically back-scattered Raman light from the particle is collected using a spectrograph and CCD detector with a time resolution of 1 s. The observed Raman scatter is composed both of spontaneous Raman scattering that is dependent on the frequency of vibrational modes of chemical species in the particle, and stimulated Raman scattering that is superimposed on the spontaneous band and occurs at wavelengths commensurate with Whispering Gallery Modes (WGMs). WGMs are sharp features in the Raman spectrum that occur with wavelength spacing and position related to the particle size. By comparing the wavelengths at which WGMs are observed, with predictions from Mie scattering theory, the droplet size can be determined with nanometer accuracy.[46a] In the early vapor pressure measurements using optical tweezers,[33g] a volume fraction mixing rule was used to estimate the dependence of the droplet refractive index on the RH of the measurement using the equilibrium composition estimated from the Extended Aerosol Inorganic Model (E-AIM),[48] and the pure component refractive indices. This approach allows an accurate determination of droplet radius from the WGM fingerprint. Measuring the change in particle radius whilst the particle is held at constant RH (within 1%) for a time, typically in excess of 10 hours, then allows the equilibrium vapor pressure of the evaporating organic to be determined from the calculated mass flux of the volatile organic from the evaporating particle using a similar approach to the corresponding measurements with the EDB.[33g] The uncertainties in the equilibrium vapor pressure values depend on the compound in question, but the largest sources of uncertainties are estimated to be lack of knowledge about mass accommodation coefficients, and lack of knowledge about the potential fluctuation of RH during the course of the experiment. As an example, the uncertainty

in the glutaric acid equilibrium vapor pressure resulting from ±2% variations in RH over the course of 5 hours is estimated to be of the order of ±70% to 80%.

More recently, a refined approach has resulted from the capability of simultaneously determining the droplet radius and refractive index from the fingerprint of WGMs[49] recorded from an optically tweezed droplet. Fluctuations in RH drive changes in the refractive index of a particle, whereas the evaporation of a semi-volatile component carries with it the solvating water, leading to no change in refractive index for a binary component droplet. Thus, by examining the correlation between the instantaneous fluctuations in particle size and refractive index, the hygroscopic response can be separated from the change in gas-particle partitioning of the organic component, allowing simultaneous retrievals of the hygroscopicity of the aerosol (solute concentration as a function of RH) and pure component equilibrium vapor pressures.[39] No active control over RH is required and, indeed, it has been shown that RH fluctuation is desirable as it allows the determination of both hygrsocopicity and equilibrium vapor pressures. These studies provided the first clear demonstration of the value in measuring both the composition (through refractive index), and size of the particle if accurate measurements of vapor pressures are to be made, rather than simply measuring the droplet size as a function of time. However, the approach is dependent on extremely accurate measurements of size and refractive index with accuracies of better than ±2 nm and ±0.00065, respectively.

3.3 Particle size distribution methods

In addition to using observations of size changes of trapped individual, micron-sized, particles, equilibrium vapor pressures of low-volatility compounds can be determined by observing the

change of the mean or modal size or total mass of a population of airborne particles in a non-equilibrium situation. Such methods include: 1) the modified Tandem Differential Mobility Analyzer (FT-TDMA) system including a laminar flow tube for studies of the equilibrium vapor pressure over dry particles and aqueous solution droplets at ambient conditions;[33a,33c-e,33h,50] 2) the Volatility-TDMA (V-TDMA) system[31d] for measurements of the equilibrium vapor pressures of dry dicarboxylic acid particles over a large temperature range; 3) the Integrated Volume Method[31e,f,51] (IVM) for studies on the equilibrium vapor pressures and evaporation kinetics of dry and aqueous dicarboxylic acid particles.

The techniques described in this section share a common foundation based on the aerosol mobility chromatograph (TDMA) first presented by Liu et al.[52] for studies of hygroscopic growth and suggested by Rader and McMurry[33a] for studies of saturation vapor pressures of aerosol components.

The use of particle populations instead of single particle samples permits studies of smaller (sub-micrometer sized) particles, and smaller changes in their absolute mass for a detectable change in their diameter, assuming that variations in the gas phase composition are known. Consequently, much shorter experimental time scales of evaporation can be used to observe similar relative change in the volume of the particles compared to the single particle methods. On the other hand, at the smaller sizes the evaporation process becomes more sensitive to additional properties of the evaporating species, such as the mass accommodation coefficients and surface tensions. The techniques described in this section differ in terms of the particle sizes and concentrations, the temperature range, and the sample phase (liquid or solid) that can be probed. The common factors between all of them are 1) the generation of an aerosol population, either by atomization of liquid

solutions or nucleation (followed by diffusion drying, if needed), or nucleation from a super-saturated vapor and size selection and measurement with a differential mobility analyzer; 2) the evaporation of these particles in a temperature- and/or RH-controlled environment; 3) measurement of any change in the size or total volume of the aerosol population as a function of time, temperature and/or RH. In all of these techniques the measured particle size is the mobility size and the particles are assumed to be spherical. The basic principles of the methods using aerosol size distributions are outlined in Figure 1C (see also Table 1).

3.3.1 Flow-Tube Tandem Differential Mobility Analyzer (FT-TDMA)

The TDMA system including a laminar flow tube was developed by Rader and McMurry.[33a] It was first used for organic aerosol droplets[33h,50a,53] and later modified[33c,d,50b,c,50e] for studies of solid state saturation vapor pressures over a range of temperatures under dry conditions. The FT-TDMA system at Aarhus University (until 2013 at University of Copenhagen), described in more detail here, also allow for determination of solid state and subcooled liquid state saturation vapor pressures from evaporation of aqueous solution droplets at a controlled relative humidity and temperature,[33d,e,33h,54] as well as studies of equilibrium vapor pressures of low-volatility organic molecules over aqueous solution droplets containing also an inorganic salt.[50g,h] The general scheme is to let monodisperse particles, selected with a Differential Mobility Analyzer (DMA), evaporate in a laminar flow-tube and measure changes in size using a Scanning Mobility Analyzer System (SMPS). Typical particle sizes used in the dicarboxylic acid experiments[33d,e,33h,54] ranged from some tens to hundreds of nanometers, and typical timescales of evaporation for these particles were in the range seconds to minutes. The aerosol is generated by

atomizing an aqueous solution of the compound(s) of interest in a constant output atomizer. Depending on the scope of the experiment, the droplets can be dried by passing through a series of silica gel driers followed by dilution with dry air, or remain as aqueous solution droplets in equilibrium with surrounding air at a controlled relative humidity.

A nearly monodisperse size fraction is selected with a DMA and allowed to evaporate while flowing through a 3.5 m long laminar flow-tube (26 mm inner diameter) under controlled conditions of temperature and relative humidity. Sheath air in the flow tube minimizes loss of particles to the walls and dilutes the gas phase. To avoid recondensation of organic vapors in the DMA columns, the organic vapors can be removed by passing the DMA sheath air through activated charcoal followed by particle filters, or the DMA can be operated in non-recirculating mode.

Typical particle number concentrations used in these studies are of the order of some hundreds to thousands of particles per cm^3. The flow-tube has four sampling ports along its length, and the change in particle size is monitored with a SMPS. Only particle sizes measured using the second DMA column are compared with each other. The equilibrium vapor pressures over the evaporating particles or droplets are inferred from the evaporation rates of the particles – in a similar manner and using similar equations as in the case of the single particle methods (see Section 2). This requires knowledge of (or assumptions regarding) the diffusivity, activity coefficient (in the case of an aqueous solution), the accommodation coefficient of the evaporating compound, and surface tension or free energy, and density of the (mixed) particles. It is also typically assumed that the gas phase remains far below saturation with the evaporating compounds, which is usually reasonable given the relatively low particle mass concentrations

used in the TDMA studies.[33e] At high aerosol loadings and low equilibrium vapor pressures, however, this assumption might become problematic.[50g]

3.3.2 Volatility Tandem Differential Mobility Analyzer (V-TDMA)

The Gothenburg V-TDMA setup[31d] used to obtain saturation vapor pressures of C_4-C_{10} dicarboxylic acids consists of four major parts that represents; generation, size selection, heating and size change analysis. The aerosol particles were generated by atomization followed by drying in silica diffusion dryers (RH<5%). From the generated, dry aerosol, a narrow size range was selected using DMA operated in a re-circulating mode where the sheath air flow was conditioned using charcoal and silica scrubbers. A sample:sheath air ratio of 1:20 was used to ensure a narrow size distribution. The initial mean particle diameters selected were between 80 and 110 nm. The mass concentration of the selection was in the range of 0.1 to 1 μg m^{-3}, depending on the compound, with a typical number concentration of 50-500 cm^{-3}. The size selected aerosol was subsequently directed through one of several ovens. The heated part of each of the ovens consists of a 50 cm stainless steel tube mounted in an aluminum block with a heating element. The oven temperature was controlled and monitored, where the temperatures of each of the ovens can be set and measured independently from 298 to 573 K with a variability of ± 1 K from the set value. The availability of several ovens at different temperatures allows swift changes in evaporative temperatures by switching the flow between the ovens. With a sample flow of 0.3 LPM, and assuming plug flow, the residence time in the heated part of the oven was 2.8 s. At the exit of the heated part, the flow was directed to activated charcoal diffusion scrubbers in order to absorb the evaporated gas and prevent re-condensation onto the particles upon cooling. The resulting aerosol

was classified using a SMPS-system. The change in the particle mode diameter from the evaporation was monitored for each temperature and normalized to the diameter determined at the reference temperature (298 K). The VTDMA works under non-equilibrium conditions, so the equilibrium vapor pressure values were determined from the evaporation rates at selected temperatures. Similar dynamic evaporation calculation was done as in the case of the FT-TDMA and the single aerosol particle methods, and therefore requiring assumptions on the diffusion coefficients, accommodation coefficients, densities, and surface tensions of the evaporated compounds (see Section 2). The derived saturation vapor pressures corresponds to the temperature of the corresponding oven, and the data requires extrapolation to room temperature using the Clausius-Clapeyron assumption.

3.3.3 The Integrated Volume Method (IVM)

Different to the FT-TDMA and V-TDMA methods which work under non-equilibrium conditions, the Integrated Volume Method (IVM)[31e,f,51] is based on observing integrated volume changes of aerosol particle size distribution as a function of temperature under quasi-equilibrium conditions. The integrated volume change is obtained by comparing aerosol size distributions measured with two SMPS systems. One is measuring at room temperature and the other through a thermodenuder, which is operated at an elevated temperature (typically 300 to 330 K).[31e,51] Both temperatures are constantly monitored and recorded. The SMPS measurements are corrected for temperature-dependent particle losses, which are less than 5% below 330 K. The IVM denuder does not use any absorbing material in its heated and cooling sections, such that the aerosol passing through the denuder evaporates, ideally saturating the gas phase. Residence times

longer than 20 s and relatively high aerosol concentrations (around 500 μg m^{-3}) are used to achieve equilibration of the aerosol with the surrounding air at the new temperature, within the residence time in the denuder. The equilibrium condition is verified by performing the measurements at a two times shorter residence time in the denuder or two times lower aerosol concentration. The measurements are performed at several thermodenuder temperatures and the change in particle volume is observed. Since the measurements are performed at equilibrium conditions, no assumptions are required on the value of the accommodation coefficient of the species. The equilibrium vapor pressures and vaporization enthalpies are determined from a fit of the Clausius-Clapeyron equation to the temperature-dependent data of aerosol volume concentrations.[31e] The wall losses of the gaseous species in the heated section of the thermodenuder have been shown to be negligible, while re-condensation of the gaseous material to the particles in the cooling section is generally small (less than 5%).[55] The only direct assumption that the data interpretation method uses is that the particles are spherical, which is needed to translate the SMPS measurements to aerosol volume and mass concentration. Based on the SEM images of adipic and azelaic aerosol particles, this assumption could result in an overestimation of saturation vapor pressures by 15–30%.[31f] Noise in experimental data is the main source of uncertainty in the derived thermodynamic properties, which is estimated to be about 30% for the vapor pressure and 10% for the enthalpy of vaporization. The method is limited to compounds that are chemically inert to the wall material of the thermodenuder, as any chemical reaction with the walls would make achieving thermodynamic equilibrium impossible.

3.4 Thermal desorption methods

Temperature Programmed Desorption (TPD) methods are used to determine compound vapor pressures from the measurement of temperature-dependent evaporation rates from compounds collected on a temperature-controlled surface at low total pressures.[28b,31b,c,56] So far two somewhat similar, yet different setups utilizing TPD have been applied for measurements of the equilibrium vapor pressures and vaporization enthalpies of solid phase dicarboxylic acids, namely Thermal Desorption Particle Beam Mass Spectrometry (TDPB-MS)[31b,56a] and Thermal Desorption Proton Transfer Chemical Ionization Mass Spectrometry (TPD-PT-CIMS).[28b,31c,56b] The basic principles of these methods are outlined in Figure 1D (see also Table 1). In both methods, aerosol particles are generated by atomizing liquid solutions of the investigated organic compounds, dried with diffusion dryers and collected onto a cooled plate. After sufficient time to collect enough material, the time dependent change in the gas-phase concentrations due to evaporation are monitored using mass spectrometry as the sample is heated. The observed evaporation rates of the samples are converted to molecular evaporation flux densities (molecules s^{-1} m^{-2}), which can be compared directly to a model of the evaporation process using the kinetic regime equations for molecular transport (see Section 2). In the following the main differences of the two methods will be summarized.

3.4.1 Thermal Desorption Particle Beam Mass Spectrometry (TDPB-MS)

The Thermal Desorption Particle Beam Mass Spectrometry (TDPB-MS) in the Ziemann Group[31b,56a] has been applied for measurements of saturation vapor pressures of dicarboxylic acids. A monodisperse fraction (roughly 100 to 300 nm in diameter) of the atomized and dried

aerosol particles is selected with a DMA. It is assumed that these monodisperse particles are deposited on the collection surface as non-interacting individual spheres. Initial particle collection takes place onto a plate at a temperature sufficiently low (typically around 223 K)[31b] such that evaporation is negligible during collection. The collected sample of roughly 1 μg in mass is then heated to temperatures up to 373 K, and electron impact ionization with a quadrupole mass spectrometer is used to detect the evaporating molecules. Evaporation rates of the sample are quantified by multiplying the observed instantaneous signal intensity (counts s^{-1}) of a characteristic ion by a calibration factor (molecules $particle^{-1}$ $counts^{-1}$), that is equal to the initial number of molecules in a single particle divided by the total counts of the characteristic ion signal measured during evaporation. Results are plotted as a normalized mass thermogram, which is a graph of the evaporation rate versus desorption temperature. The measured normalized mass thermogram is then compared to the predicted evaporation in the kinetic regime (see Section 2.4), which is appropriate given that the evaporation is taking place at very low pressures. The temperature dependence of the equilibrium vapor pressure is characterized through the Clausius-Clapeyron equation (Equation 4), where the enthalpy of sublimation for solid particles is determined from a fit to the measured evaporation rate versus temperature.[31b]

3.4.2 Temperature Programmed Desorption Proton Transfer Chemical Ionization Mass Spectrometry (TDP-PT-CIMS)

In the Temperature Programmed Desorption Proton Transfer Chemical Ionization Mass Spectrometry (TPD-PT-CIMS) technique,[28b,31c,56b] particles generated from atomization and drying are collected into a pile (~1 mm, typically conical or half spherical in shape), on a plate at

temperatures that can be cooled down to 250 K and heated up to > 430 K, and from which evaporation occurs. In the TPD-PT-CIMS the collected sample is pre-heated to ensure that residual solvent molecules from the atomization process are removed. Although pre-heating leads to some evaporation of the organic material, this does not influence the subsequent measurements. Following collection, the sample is heated using a linear temperature ramp (typically a few K min^{-1}) and the evaporation rate is measured. Temperature-dependent evaporation rates (molecules s^{-1}), are directly quantified from the measured gas-phase concentrations, determined using proton transfer chemical ionization with a quadrupole mass spectrometer, and the known PT-CIMS flow rate. As with the TDPB-MS, the observed mass thermograms are compared to an evaporation model to allow for quantitative determination of temperature dependent vapor pressures. The initial surface area of the sample, which is needed for calculating the molecular flux densities, is determined from visual observation of the deposited sample.

It is important to note that, as with the single particle measurements and most of the TDMA methods, neither of the TPD methods directly measure equilibrium vapor pressures, but actually evaporation rates. Thus, the determination of equilibrium vapor pressures requires an assumption about the mass accommodation coefficient for the compound of interest. For the TPD experiments, it has been assumed that it is unity, which means that the derived vapor pressures are lower limits.

3.4.3 Atmospheric Solids Analysis Probe Mass Spectrometry (ASAP-MS)

Vapor pressures for low-volatility compounds can also be measured using Atmospheric Solids Analysis Probe Mass Spectrometry (ASAP-MS), as recently applied at the University of California, Irvine.[57] ASAP-MS is also a thermal desorption technique that determines evaporation rates from samples that are deposited on a probe tip. Samples of the organic molecule of interest can be deposited on the ASAP tip by one of several methods. For the measurement of vapor pressures of pure compounds such as the dicarboxylic acids, the analyte was dissolved in a solvent and a small volume (typically 5 μL) was placed on the probe tip. For ASAP-MS measurements of secondary organic aerosol, the sample is transferred directly by drawing the tip across the sample collected on an impactor in order to avoid biasing due to the use of solvents. Most of the solvent quickly evaporates,[58] and any remaining solvent is removed when the the probe is placed into the ionization region of an atmospheric pressure mass spectrometer where the initial temperature is 313 K. A corona discharge probe provides the ionization source. In the negative ion mode, $O_2(H_2O)_n^-$ ions are the ionizing agent. A small vial containing water is located in the source region to provide protonated water clusters as the ionizing agent for the positive ion mode. Knowledge of the shape of the dried sample is necessary to allow for conversion of observed evaporation rates to evaporation fluxes. It was observed[57] that the samples typically dried with a disc-like shape with diameters of 0.5-1.5 mm, corresponding to heights of only 10^{-4}-10^{-3} mm based on the amount of deposited material. Dry N_2 gas is passed over the probe tip at atmospheric pressure as the temperature of the gas is increased from 313K at a rate of 8 K min^{-1}. As molecules evaporate, they are ionized and carried into the mass spectrometer where they are detected. The probe material can affect the measurement

through adsorption of the sample on the surface. Uncoated PEEK tubing was found to give desorption profiles with the least amount of broadening and with the peak at the lowest temperature, and thus was used for the reported dicarboxylic vapor pressure measurements. Similar to the TDPB-MS, temperature-dependent absolute evaporation rates are determined from the known deposited sample amount, and the ratio of the instantaneous ion current to the total integrated ion current measured over the course of the desorption. The measured evaporation rates are converted to saturation vapor pressures,[57] using a modified form of the Langmuir's model of evaporation, assuming an accommodation coefficient of unity and accounting for time and temperature-dependent variations in the sample dimensions as evaporation proceeded. This is essentially the evaporation flux equation for the kinetic regime, and this should be kept in mind when considering the results from the ASAP-MS as the measurements are made at atmospheric pressure.

4. Experimentally determined saturation vapor pressures and transition enthalpies of dicarboxylic acids

In this section, current saturation vapor pressures and sublimation/vaporization enthalpies of dicarboxylic acids as determined from experiments are reviewed.

4.1 Straight chain dicarboxylic acids

Straight chain dicarboxylic acids of the general formula $HOOC(CH_2)_{n-2}COOH$ have emerged as a standard set of molecules for comparison of methods for measurement of saturation vapor pressures within atmospheric science.

Dicarboxylic acids are water soluble molecules which have been identified in aerosol samples from numerous places around the globe including polar,[59] rainforest,[60] urban,[61] rural,[61a,62] and marine[63] environments. Long term observations of the concentration of dicarboxylic acids in ambient aerosol samples show variation with temperature, season, time of day, and points to photochemical oxidation of VOCs[64] as an important source of dicarboxylic acids. Consistent with this interpretation, dicarboxylic acids have been identified in smog chamber experiments simulating such processes.[65] Other sources of dicarboxylic acids in the atmosphere include biomass burning,[66] motor exhaust,[67] and potentially aqueous phase chemistry.[68] The shorter acids (C_2-C_7) have been attributed to stem mainly from anthropogenic emissions and/or oxidation of VOCs of anthropogenic origin, while the longer chain (C_8-C_{11}) dicarboxylic acids largely stem from biogenic emissions and/or oxidation of biogenic VOCs.[69]

All of the experimental techniques described in Section 3 have been used to determine the saturation vapor pressure of one or more straight chain dicarboxylic acids at one or several temperatures. Here the acids where the number of carbons is n=2 to 10, for which most data are available are considered in detail. Most studies report a characteristic alternation of the vapor pressures with the number of carbon atoms in the chain (odd – even alternation), which has been related to solid state structure.[33d] This is consistent with the previous finding[70] that dicarboxylic acids (>C_5) with an odd number of carbon atoms have lower melting points and sublimation enthalpies, compared to dicarboxylic acids with an even number of carbon atoms.

Figure 2 shows a summary of solid state vapor pressures of C_2-C_{12} dicarboxylic acids at 298 K based on the discussion in Sections 4.1.2-4.1.8. Results are color coded according to the experimental method used. Results from Knudsen based methods are in black color tone, from

single particle methods in green color tone, from particle size distribution methods (TDMA methods) are in blue color tone, and from thermal desorption methods in red color tone. Measurements were in many cases not performed at 298 K, thus the values at 298 K shown in Figure 2 were obtained using the Clausius-Clapeyron equation and the value of ΔH_{fus} provided in each study. In some cases extrapolation was made outside the range of experimental temperatures. Figure 3 shows the enthalpies of sublimation. It is less clear if an odd-even alternation exists for the enthalpy.

It is evident from Figures 2 and 3 that there is a large spread in reported solid state vapor pressures and enthalpies of sublimation, with a variation between one and four orders of magnitude between the lowest and highest solid state vapor pressure reported for an individual acid. The variation is far beyond error bars of the experiments. Figure 4 shows a summary of subcooled liquid vapor pressures for dicarboxylic acids based in discussion in Sections 4.1.2-4.1.8. Figure 5 shows the corresponding reported enthalpies of vaporization. Results from different methods are in agreement within error bars, but it should be noticed that there are fewer data available, and only from the TDMA and EDB techniques.

It has been discussed in the literature[31c,31f] that different preparation methods and pre-treatments of particles can lead to a difference in the physical state of the particles. It will be shown below that some of the datasets from particle size distribution methods, in which test aerosols were produced by atomization and quick drying of dicarboxylic acids with odd carbon number smaller than 9, could be representative of the subcooled state, rather than the reported solid state. Therefore, in the following analysis (and in Figures 2-5), such datasets will be assumed to represent the subcooled state. Whether or not such an assumption is fully justified remains an

open question, which will be discussed in the following sections, along with a detailed look at each of the dicarboxylic acids.

4.1.1 General fitting procedure

The procedure used to obtain vapor pressures and transition enthalpies from combined datasets is described in the following. Figures 7-15 show reported saturation vapor pressures versus inverse temperature for C_2-C_{10} dicarboxylic acids. Filled symbols indicate saturation vapor pressure measurements taken in a state assumed to be solid crystalline, while open symbols present measurements assumed to represent the subcooled, liquid state. The lines are fits to the data using Equation 4. To avoid overemphasis of a single dataset with a large number of data taken within a small temperature range, all data within a dataset are assigned to a regular grid in inverse temperature space with a resolution of 100 K/T. To calculate the data for each grid point, a linear regression using Equation 4 with all the data within the temperature range of the particular grid cell was performed. If there was only one data point within a grid cell, this data point was used at its measured temperature for the grid-based dataset. This does not completely eliminate weighting towards measurements that were carried out over larger temperature ranges, which consequently have more data points, but helps to minimize differences. Please note that this procedure does not lead to the same regression as if all data points were used as given. Hence the saturation vapor pressure at 298 K may deviate significantly from the mean of the published data points. The lines shown in the Figures 7-15 are fits to all data after assigning them to this grid as described. Figure 6 illustrates the procedure for the data of oxalic acid shown in Figure 7 in the crystalline state. The black symbols are the data compiled on the grid, the red line is the fit to Equation 4, the dark shaded region the 95% confidence interval of the linear regression, and the

light shaded area the 95% prediction interval. This fit yields the saturation vapor pressure estimate for 298 K as shown in the lower panel of Figures 7-15, with the uncertainty given by the 95% confidence interval.

4.1.2 Oxalic acid ($C_2H_2O_4$)

Reported solid and liquid state vapor pressures for oxalic acid are shown in Figure 7.[32,37b,71] Oxalic acid is the shortest of the dicarboxylic acids and presents special challenges. The anhydrous solid shows polymorphism[72] and different saturation vapor pressures have been reported for the anhydrous α-orthorhombic and β-monoclinic forms.[71b]

Figure 7 shows the saturation vapor pressures reported in the literature for oxalic acid, versus inverse temperature. Here, as in all figures showing the data of the individual acids (Figures 7-15), filled symbols indicate saturation vapor pressure measurements taken in a state assumed to be the solid crystalline state, while open symbols represent measurements in subcooled, liquid state.

Three data points (green open circles) are available for the saturation vapor pressure of sub-cooled oxalic acid, based on measurements of evaporation of aqueous solution droplets.[37b] As discussed by Soonsin et al.[37b] these data agree with the saturation vapor pressures reported by Noyes & Wobbe[71a] for anhydrous oxalic acid formed by condensation from the gas phase. Noyes and Wobbe describe their oxalic acid as being "quite lumpy" which could be indicative that it was an amorphous solid, and as such has a vapor pressure similar to that of the subcooled liquid. Fitting the subcooled liquid saturation vapor pressures reported by Soonsin et al.[37b] as described in section 4.1.1 yields log $p^0_{l,oxalic,\alpha}$= - (4128±3)K/T + (12.31±0.01) where uncertainties

represent one standard error. The pressure of the subcooled liquid at 298 K is $p^0_{l,oxalic}(298K) = \left(2.9^{+0.1}_{-0.1}\right)\cdot 10^{-2}$ Pa and the enthalpy change of vaporization is $\Delta H_{vap,oxalic}$ = (79±15) kJ mol^{-1}.

The saturation vapor pressures of the α-form of anhydrous oxalic acid reported are slightly lower,[71b-d] but close to the saturation vapor pressures of the subcooled liquid.[37b] The saturation vapor pressures reported by Booth et al.[35c] for anhydrous oxalic acid fall in the same range. Differential scanning calorimetry (DSC) was used to verify that it was a solid. The data by Booth et al. [35c] are assumed to represent the α-form as are the data by Noyes & Wobbe.[71a]

From a fit to the α-form data by Noyes & Wobbe,[71a] de Wit et al.,[71d] Booth et al.,[35b] de Kruif et al.,[71c] and Bradley & Cotson[71b] (following the grid procedure outlined above) log $p^0_{s,oxalic,\alpha}$= -(5221±217)K/T + (15.7±0.7) is obtained where uncertainties represent one standard error. This fit corresponds to $p^0_{s,oxalic,\alpha}(298K) = \left(1.4^{+0.6}_{-0.4}\right)\cdot 10^{-2}$ Pa and $\Delta H_{sub,oxalic,\alpha}$= (100±4) kJ mol^{-1} where uncertainties on vapor pressure and enthalpy includes upper and lower 95% confidence interval. The mean of the published sublimation enthalpies is $\Delta H_{sub,oxalic,\alpha}$= (91±9) kJ mol^{-1}.

The β-form of the anhydrous oxalic acid reported by Bradley & Cotson[71b] has a significantly lower saturation vapor pressure than the subcooled liquid and the α-form of the anhydrous oxalic acid. Hence, the β-form is not included in the fit.

Soonsin et al.[37b] also inferred solid state saturation vapor pressures of oxalic acid based on measurements of evaporation rates of effloresced particles in the EDB. The particles were spectroscopically shown to be dehydrated solids, but their polymorphic forms remained unclear. These solid-state saturation vapor pressures are the lowest reported. They are in good agreement

with saturation vapor pressures estimated from a solution that is saturated with respect to the dihydrate. Again, because these solid data clearly do not represent the data of the α-form crystal, they were not included in the fit.

Figure 7 demonstrates that the solid state saturation vapor pressure of oxalic acid depends both strongly, and in a complex, way on the polymorphic form of the acid. Another thing to consider in the discussion of oxalic acid is that it forms dihydrates in aqueous solution. The solid oxalic acid dihydrate can exist as α- or β- dihydrates. Only vapor pressures (sum of equilibrium vapor pressures of water and oxalic acid) for the α form have been reported[71d] since a stable β-form of the dihydrate could not be obtained.

No attempt to derive further information from the multifaceted dataset presented in Figure 7 is made herein. Instead, it is recommended that additional studies of the saturation vapor pressure of oxalic acid are performed, paying careful attention to the phase, polymorphic form, and hydration state of the particle or sample studied.

4.1.3 Malonic acid ($C_3H_4O_4$)

Figure 8 shows solid and subcooled liquid saturation vapor pressures for malonic acid.[31c,31g,32,33d,33f-h,37b,54] The subcooled liquid saturation vapor pressure of malonic acid has been inferred from measurements of evaporation rates of aqueous solution droplets at ambient temperatures in a number of studies.[33g,37,50f] The size of these droplets ranged from submicro-meter size in the TDMA system,[33h,50f] to micrometer size using the EDB.[33g,37b] The reported subcooled liquid saturation vapor pressures versus inverse temperature are shown with open

symbols in Figure 8. The vapor pressures obtained from measurements of evaporation rates of dried sub-micron sized malonic acid particles reported by Bilde et al.[33d] have been suggested to represent the subcooled liquid state.[33f] This seems reasonable based on the good agreement with the other subcooled liquid values[33f,33h,54] and thus the saturation vapor pressure of malonic acid reported by Bilde et al.[33d] is therefore treated as a subcooled liquid vapor pressure. This is further supported by electrodynamic balance experiments of micrometer sized malonic acid particles that were found to show reversible and continuous water sorption, with no deliquescence or crystallization.[73]

The subcooled liquid saturation vapor pressures from the different techniques are in good agreement. Following the gridded approach outlined in section 4.1.1, log $p^0_{l,malonic}$= -(6451±689)K/T + (18.4±2.4) corresponding to $p^{0}_{\mathrm{l,malonic}}(298K) = \left(6.2^{+3.2}_{-2.1}\right)\cdot 10^{-4}$ Pa and $\Delta H_{vap,malonic}$=(123±13) kJ mol^{-1} are obtained. The mean of the published vaporization enthalpies is $\Delta H_{vap,,malonic}$=(115±22) kJ mol^{-1}.

Solid state saturation vapor pressures for malonic[31c,31g,32,37b] acid versus inverse temperature are shown in Figure 8 (filled symbols). Malonic acid has three crystal structures: α (> 352 K), β (352 – 47 K) and γ (< 47 K).[74] It is thus possible that the data above 352 K do not represent the same phase as the rest of the solid data, or even a subcooled phase as speculated by Soonsin et al.[37b] No transitions before the melting point were observed by Booth et al.[35b]

Using all the solid state data gives log $p^0_{s,malonic}$= - (6832±331) K/T + (19.1±1.0) corresponding to $p^{0}_{\mathrm{s,malonic}}(298K) = \left(1.7^{+1.1}_{-0.7}\right)\cdot 10^{-4}$ Pa and $\Delta H_{sub,malonic}$ = (131±6) kJ mol^{-1}. The mean of the published sublimation enthalpies is $\Delta H_{sub,malonic}$ = (111±15) kJ mol^{-1}.

4.1.4 Succinic acid ($C_4H_6O_4$)

Figure 9 shows solid and subcooled liquid saturation vapor pressures for succinic acid.[23,31b-d,31g,32,33d,33h,37b,57,75] Electrodynamic balance experiments[73] for succinic acid show clear deliquescence (RH=98.8%) and efflorescence (RH=55.2-59.3%) behavior.

Analysis of the subcooled values gives log $p^0_{l,succinic}$ = - (5037±747) K/T + (14.0±2.6) corresponding to $p^{0}_{\mathrm{l,succinic}}(298K) = \left(1.3^{+1.5}_{-0.7}\right)\cdot 10^{-3}$ Pa and $\Delta H_{vap,succinic}$ = (96±14) kJ mol^{-1}. The mean of the published vaporization enthalpies is $\Delta H_{vap,succinic}$ = (105±1) kJ mol^{-1}.

The solid state data from different techniques are in good agreement, but with the data reported by Saleh et al.[23] being higher than the others, and the data reported by Bruns et al.[57] being lower. Soonsin et al.[37b] report two values for the saturation vapor pressure for a crystallized succinic acid particle at 298 K in the electrodynamic balance: the higher value measured directly after efflorescence, the lower value one day later. Particle rearrangements and collapse, loss of enclosed water, and further crystallization of liquid or/and amorphous portions may explain this behavior.

Linear least squares analysis following the gridded approach described in section 4.1.1, of all the solid data gives log $p^0_{s,succinic}$ = - (5432±251) K/T + (14.1±0.8) corresponding to

$p^{0}_{\mathrm{s,succinic}}(298K) = \left(7.7^{+5.0}_{-3.0}\right)\cdot 10^{-5}$ Pa and $\Delta H_{sub,succinic}$ = (104±5) kJ mol^{-1}. The mean of the published sublimation enthalpies is $\Delta H_{sub,succinic}$ = (115±15) kJ mol^{-1}.

4.1.5 Glutaric acid ($C_5H_8O_4$)

Figure 10 shows reported solid state and subcooled liquid state saturation vapor pressures for glutaric acid.[31b-d,31g,32,33d,33g,h,37b,57,76] Glutaric acid shows deliquescence (83.5-85% RH) and efflorescence (29-33% RH)[73] and should thus be solid in the TDMA experiments performed at RH<29%. It is however striking that the TDMA measurements reported as solid[31d,33d] seem to agree with the subcooled liquid saturation vapor pressures. Soonsin et al.[37b] observed that after efflorescence, glutaric acid particles levitated by the electric field of the EDB at 291 K evaporated with a rate corresponding to that of the subcooled liquid for the first hours. After a day, the saturation vapor pressure inferred from measured evaporation rates dropped to a value corresponding to the value obtained from saturated solution measurements, which should be equivalent to the solid state value. Soonsin et al.[37b] suggest that effloresced glutaric acid particles initially are only partly crystalline, and contain aqueous inclusions. In typical TDMA experiments particles are dried rather quickly in diffusion dryers and/or by dilution with dry air, and although the particles (nm scale) are much smaller than the particles studied in the EDB (micrometer scale) it cannot be excluded that aqueous inclusions exist. The TDMA results are thus treated as representing the subcooled liquid state in the following. The data reported by Booth et al.[35b] seem to fit with other solid state values at high temperatures, but then tend towards the subcooled liquid values at lower temperatures. The reason for this is unclear, since the

samples were inserted into the instrument in their crystalline state, and the phase state was confirmed to be solid by DSC.

Analysis of the subcooled vapor pressure data, gives log $p^0_{l,glutaric}$ = - (6175±394) K/T + (17.7±1.3) corresponding to $p^0_{\mathrm{l,glutaric}}(298K) = \left(1.0^{+0.3}_{-0.2}\right)\cdot 10^{-3}$ Pa and $\Delta H_{vap,glutaric}$ = (118±8) kJ mol^{-1}. The mean of the published vaporization enthalpies is $\Delta H_{vap,glutaric}$ = (100±5) kJ mol^{-1}.

A fit to the solid data using the procedure outlined in section 4.1.1 yields log $p^0_{s,glutaric}$ = -(5742±414)K/T + (15.5±1.3) corresponding to $p^0_{\mathrm{s,glutaric}}(298K) = \left(1.7^{+1.5}_{-0.8}\right)\cdot 10^{-4}$ Pa and $\Delta H_{sub,glutaric}$ = (110±8) kJ mol^{-1}. The mean of the published sublimation enthalpies is $\Delta H_{sub,glutaric}$ = (130±11) kJ mol^{-1}.

4.1.6 Adipic acid ($C_6H_{10}O_4$)

Figure 11 shows reported solid state and subcooled liquid state saturation vapor pressures for adipic acid.[23,31b-f,32,33d,54,57,75-76] Adipic acid shows deliquescence (RH > 99%) and efflorescence (RH >85%).[77] Only one set of liquid state values have been provided so far from TDMA experiments[50f] reporting $\Delta H_{vap,adipic}$ = (113±22) kJ mol^{-1} over a temperature range of 293-298 K and $p^0_{\mathrm{l,adipic}}(298K) = \left(1.8^{+1.0}_{-0.7}\right)\cdot 10^{-4}$ Pa. Due to the limited temperature range of the subcooled liquid values, no further calculations of enthalpy of fusion are done at this point. Subcooled liquid values over a larger temperature interval are desirable.

There is large scatter in the solid state data at the temperatures relevant in the atmosphere. Fitting all reported solid state saturation vapor pressures results in log $p^0_{s,adipic}$ = -(6128±292) K/T +

(15.8±0.9) giving $p^{0}_{\mathrm{s,adipic}}(298K) = \left(1.9^{+1.4}_{-0.8}\right)\cdot 10^{-5}$ and $\Delta H_{sub,adipic}$ = (117±6) kJ mol^{-1}. The mean of the published sublimation enthalpies is $\Delta H_{sub,adipic}$ = (131±18) kJ mol^{-1}.

Further information, in particular on the phase state of dried adipic acid particles, is needed to resolve the scatter in the solid state data.

4.1.7 Pimelic acid ($C_7H_{12}O_4$)

Figure 12 shows reported saturation vapor pressures for pimelic acid.[23,31b-e,31g,33d,57] No subcooled liquid values have been derived from evaporation rates of aqueous solution droplets, but Salo et al.[31d] report the presence of two types of particles with different volatilities, and suggests the co-existence of crystalline (type 1) and liquid (type 2) particles. Chattopadhyay & Ziemann[31b] reported two distinct desorption profiles in their thermal desorption experiments, indicative of two different types of particles, but they attributed those to two polymorphic forms of the crystal. The lower panel of Figure 12 shows significant disagreement, close to three orders of magnitude, between the reported vapor pressures at 298 K. As for glutaric acid, we here proceed on the interpretation that due to the particle drying method the data of Bilde et al.,[33d] the type 2 data of Salo et al.[31d] and the data by Saleh et al.[31e] are representative for the vapor pressure of the subcooled liquid (or amorphous solid).

For the subcooled liquid the chosen subset of the data gives log $p^{0}_{l,pimelic}$ = - (5669±868) K/T+(15.3±2.8) yielding $p^{0}_{l,pimelic}(298K) = \left(2.2^{+1.9}_{-1.0}\right)\cdot 10^{-4}$ Pa and $\Delta H_{vap,pimelic}$ = (108 ±17) kJ mol^{-1}. The mean of the published sublimation enthalpies is $\Delta H_{vap,pimelic}$ = (141±12) kJ mol^{-1}.

The data by Cappa et al.,[31c] Salo et al.[31d] type I, Bruns et al.,[57] and Chattopadhyay & Zieman[31b] are all treated as representative for the saturation vapor pressure of the crystalline material. The dataset chosen to represent the solid (crystalline) state yields log $p^0_{s,pimelic}$ = -(6769±575) K/T + (17.8±1.7) corresponding to $p^0_{s,pimelic}(298K) = \left(1.1^{+2.7}_{-0.8}\right)\cdot 10^{-5}$ Pa and $\Delta H_{vap,pimelic}$ = (108 ±17) kJ mol^{-1}. The mean of the published sublimation enthalpies is $\Delta H_{sub,pimelic}$ = (148±16) kJ mol^{-1}. Given the large discrepancies between the reported solid state vapor pressures of pimelic acid it is clear that the understanding of pimelic acid is poor, and illustrates the need for understanding what contributes to the variability between, and overall accuracy of, the various techniques.

4.1.8 C_8-C_{10} acids

For the C_8-C_{10} acids fewer data are available, and no subcooled liquid saturation vapor pressures have been derived from evaporation rates of aqueous solution droplets. Data from thermal desorption and from TDMA techniques are available.[31b,31g,56b,57,75]

The data for suberic acid $C_8H_{14}O_4$ are shown in Figure 13.[31b-d,33d,57,75] Fitting all reported solid state saturation vapor pressures results in log $p^0_{s,suberic}$= - (6308±276) K/T + (15.7±0.8) giving $p^0_{s,sub}(298K) = \left(3.3^{+2.4}_{-1.4}\right)\cdot 10^{-6}$ and $\Delta H_{sub,adipic}$ = (121±5) kJ mol^{-1}. The mean of the published sublimation enthalpies is $\Delta H_{sub,suberic}$ = (148±28) kJ mol^{-1}.

Figure 14 shows the data for azelaic acid, $C_9H_{16}O_4$,. [31b-d,31f,33d,57] Here, the solid state saturation vapor pressure fit yields log $p^0_{s,azelaic}$= - (5169±479) K/T + (12.6±1.4) giving $p^0_{s,azelaic}(298K) = \left(1.7^{+2.7}_{-1.0}\right)\cdot 10^{-5}$ Pa and $\Delta H_{sup,azelaic}$ = (99±10) kJ mol^{-1}. The mean of the published sublimation enthalpies is $\Delta H_{sub,azelaic}$ = (146±26) kJ mol^{-1}.

The data for sebacic acid $C_{10}H_{18}O_4$, are shown in Figure 15.[31b-d,57,75] The regression yields log $p^0_{s,sebacic}$ = - (6895±470) K/T + (16.8±1.4) giving $p^0_{s,sebac}(298K) = \left(4.8^{+11.5}_{-3.4}\right)\cdot 10^{-7}$ Pa and $\Delta H_{sup,sebacic}$ = (132±9) kJ mol^{-1}. The mean of the published sublimation enthalpies is $\Delta H_{sub,sebacic}$ = (148±30) kJ mol^{-1}.

4.2 Conclusions on straight chain dicarboxylic acids

Looking at all data for the individual dicarboxylic acids (Figures 7-15), it becomes obvious that the differences between saturation vapor pressures obtained by the different techniques are sometimes very large, particularly for the longer chain dicarboxylic acids. As an example, azelaic acid is used, where the solid state saturation vapor pressures at 298 K obtained by different methods cover four orders of magnitude, strikingly larger than the error estimate of the individual datasets. Another remarkable observation is that subcooled liquid saturation vapor pressures from different techniques typically are in reasonable agreement.

A good example is glutaric acid, which is the acid studied by almost all techniques. Here, all the reported data for the saturation vapor pressure in the liquid state agree within error, and the deviation from the lowest to the highest pressure is only 35%. The solid state vapor pressures in contrast deviate by two orders of magnitude between lowest and highest reported pressure, and only few agree with each other within the reported error.

Another interesting observation is that the temperature dependence of saturation vapor pressure, *i.e.* the slopes of the individual datasets (the enthalpies of sublimation and vaporization), agree almost always better with each other than the reported saturation vapor pressures themselves. As example, again azelaic and glutaric acid are used, see the upper panel of Figure 14 and 10,

respectively. This is, however, perhaps not surprising since the range of physically plausible enthalpies is quite narrow compared to the range of physically plausible saturation vapor pressures.

Hence, the saturation vapor pressures at 298 K for the combined dataset are derived using a regression, taking all datasets into account as described in detail in section 4.1.1. For the sublimation and vaporization enthalpies the mean of all reported values are used. These are given in Table 2.

From analyzing the combined dataset, it remains difficult to identify the reason or reasons for the discrepancies observed. It seems however clear that part of it is related to the physical state of the compounds studied, since there is better agreement of the data taken in the subcooled state compared to those measured in the solid state. If the physical state cannot be directly determined by a measurement technique, it needs to be inferred by additional information obtained from bulk experiments or single particle techniques. While this may give clear directions for one compound (*e.g.* malonic acid, which has never been observed to crystallize in single particle experiments) the assignment of physical state might remain ambiguous for other compounds (*e.g.* pimelic acid). Moreover, crystallization of a sample is not necessarily complete. If a crystalline sample contains small liquid or amorphous shares, the measured vapor pressure will represent rather the value of the subcooled liquid than the one of the crystallized fraction. The large scatter of vapor pressures reported for pimelic acid might be due to ambiguities of its physical state. This illustrates that for reliable saturation vapor pressure values full control of the physical state is needed. This might also involve recrystallization of the purchased materials and determination of amorphous shares prior to bulk saturation vapor pressure measurements.

For the techniques relying on measurement of evaporation rates, the obtained saturation vapor pressure relies on having knowledge of the accommodation coefficient, which is often assumed to be unity. As discussed in section 2.4 there is a large uncertainty in the value of the accommodation coefficient that can significantly influence the obtained saturation vapor pressure. This is particularly true for those techniques studying small particles.[21] The vapor pressure derived from measured evaporation rates will be too small if the accommodation coefficient used is too high. The physical state and the degree of crystallization could affect the value of the accommodation coefficient. This could be one of the reasons why the reported enthalpies tend to agree better with each other than the reported saturation vapor pressures.

Yet another potential reason for the discrepancies in the reported solid state vapor pressures is if some solvent molecules are trapped within the solid, and mass loss or evaporation rate is wrongly attributed to solute vapor pressure. This effect had been investigated by Saleh et al.,[31e,f,55] for adipic- and azelaic acids, and found not to cause systematic errors, at least not in the IVM technique, although the presence of residual solvent was found to influence the measurements from the TPD-PT-CIMS.[31c] The interactions of the evaporating compounds with the walls of the different experimental setups presents another topic that deserves further attention.[78]

Since atmospheric models (see section 7) need the subcooled saturation vapor pressure values for partitioning predictions, it is recommended that subcooled saturation vapor pressures are measured whenever possible. The data taken in the solid form needs to be converted according to Equation 6, which may introduce additional uncertainty if the enthalpy of fusion or the heat capacity are not well determined.

4.3 Related dicarboxylic acids

In addition to the straight chain dicarboxylic acids discussed in detail above, experimentally obtained saturation vapor pressures have been reported for a number of related secondary organic aerosol components containing two carboxylic acid groups. They can broadly be divided into two types; carbon backbone variants, and dicarboxylic acids with additional substitutions. The carbon backbone variants include branched diacids and cyclic diacids (*e.g.* from sesquiterpene oxidation). The other type consists of straight chain dicarboxylic acids with hydroxy- and amino-groups substituted onto the carbon backbone. Table 3 shows solid and liquid state saturation vapor pressures at 298 K along with enthalpies of sublimation and vaporization for the two types of substituted dicarboxylic acids.

4.3.1 Solid state saturation vapor pressures

For the branched di-acids (2-methyl-malonic, 2-methyl-succinic and 2-methyl-glutaric acid) where data from the two different bulk Knudsen cell systems[34,35b] are available, agreement between the obtained solid state saturation vapor pressures is within reported error bars.

Effects of amino substituents ($-NH_2$) have only been studied by Booth et al.[35b] using a Knudcen cell; they find that the amino group increases the solid state saturation vapor pressure in the case of succinic acid as parent molecule, but lowers the saturation vapor pressure of glutaric acid in the 2-position.

The reported saturation vapor pressures for the oxo-substituted diacids are difficult to reconcile and there are few overlapping datasets. For 2-oxo glutaric acid both the the Knudsen cell

technique[35b] and the Thermal Desorption technique[31b] yield higher solid state vapor pressures than the vapor pressure obtained from the TDMA technique[50c] which is likely representative of the liquid state. The Thermal Desorption technique[31b] result in a very pronounced difference in solid state vapor pressure going from the 2 to 3 position for the oxo substitution: the vapor pressures of 2-oxo glutaric and adipic acids are higher than the vapor pressure of the parent acid, while the vapor pressures of the corresponding oxo-acids with the oxo-group in the 3 position are up to almost two orders of magnitude lower.

Using the Knudcen cell technique [35b] a hydroxy group (-OH) results in a slight decrease in the solid state saturation vapor pressure of the dicarboxylic acid. For comparison, a series of monocarboxylic acids were studied using the Thermal Desorption Technique[31b] and it was also found that the solid state saturation vapor pressure is reduced by the presence of a hydroxy group, and that the effect increases with distance between the carboxylic acid and the hydroxy group. The results on hydroxy group substitutions are however very difficult to reconcile. In particular the saturation vapor pressures obtained from the Using the Knudcen cell technique[35b] which by the nature of the sample and method are inherently solid state, are around 3-5 orders of magnitude higher than the subcooled liquid state values obtained from the EDB technique.[43]

For cyclic di-acids there is no overlap between measured compounds, and saturation vapor pressures have only been reported from two laboratories using the Knudsen cell[35c] and TDMA techniques[33c], respectively.

4.3.2 Subcooled liquid state saturation vapor pressures

Very few subcooled liquid state vapor pressures have been reported in the literature for substituted dicarboxylic acids. Subcooled liquid saturation vapor pressures for a series of substituted dicarboxylic acids have been reported[43] from measurements of evaporation rates of aqueous solution droplets using the EDB (2-methylmalonic acid, 2-hydroxymalonic (tartronic) acid, 2-methylglutaric acid, citric acid and DL-tartaric) acid.

Based on the discussions in Sections 4.1 and 4.2, the dried particles of dicarboxylic acids ($< C_9$) with an odd number of carbon atoms studied with the FT-TDMA technique are likely to be in the liquid state. It is thus assumed that also the methyl- and oxo- substituted dried particles of the odd-numbered (malonic-, glutaric- and pimelic-) dicarboxylic acids studied with the TDMA technique[50c-e] are in the liquid state. This is further supported by the results and discussion in Huisman et al.[43] who did not observe crystallization of 2-methyl malonic acid particles (micrometer scale) after several days at RH<3% in the EDB. If this assumption is correct, there is good agreement between the liquid state saturation vapor pressures obtained using the EDB and TDMA techniques.

Carboxylic acids with an oxo (=O) group in the β (3) position to a carboxylic acid group can decarboxylate in aqueous solution, potentially followed by chemical reactions such as aldol condensation. When particles are generated from bulk aqueous solutions the possibility of such reactions should thus be considered. Such reactions were confirmed for 2-oxo-succinic and 3-oxo-glutaric acids, and the vapor pressures from the FT-TDMA technique for these acids

represent the reaction products formed in the atomized solution.[50c] These multicomponent dried organic particles are likely to be liquid. [28a,56b]

Liquid state saturation vapor pressures (subcooled if at temperatures below the melting point) can be obtained from solid state vapor pressures using Equation 6. Given the large deviations and inconsistencies between the solid state vapor pressures in Table 3, the resulting subcooled liquid saturation vapor pressures must be interpreted and compared with caution. Even so, the solid state saturation vapor pressures in Table 3 have been converted to subcooled liquid vapor pressures using experimental values for ΔH_{fus} and T_m from Booth et al.[35b] assuming $\Delta C_p = \Delta S$.

Figure 16 shows the effect of different groups on the liquid state saturation vapor pressure of the parent dicarboxylic acid at 298 K. The overall trends seem to be the following: i) All measurement techniques agree that a methyl group does not lower or increase the vapor pressure by more than a factor of ten. The effect of two methyl groups seems to be of similar order of magnitude. ii) The figure suggests, that the substitution of hydroxyl (-OH) and oxo (=O) can lead to a stronger reduction in saturation vapor pressure than CH_3 substitution. iii) For addition of several functional groups there is strong disagreement between results from different methods. Based on the EDB measurements, the addition of two polar groups, such as for citric acid and tartaric acids, has a very large (several orders of magnitude) lowering effect on saturation vapor pressure. In contrast the Knudsen cell data[35b] show no change or increase in saturation vapor pressure with the addition of two polar groups.

The available dataset on substituted dicarboxylic acids suffers from lack of overlapping data, disagreement between overall tendencies, and inconsistencies between the few datasets that do

overlap. Detailed quantification of the effects of different substituents and their interactions is thus not possible. Table 3 and Figure 16 demonstrate the challenge in finding a basis set of well determined saturation vapor pressures for model development. Clearly, there is a strong need for additional studies and measurements of vapor pressures in general, and subcooled liquid saturation vapor pressures specifically, of organic molecules of atmospheric relevance.

5. Saturation vapor pressure estimation methods

To review the current understanding of the relationship between structure and saturation vapor pressure highlighted by the experimental data, and to assess the effects of propagating that understanding to a wider set of molecules, available predictive techniques can be compared with one another and with experimental data. However, this is not a straightforward task. Numerous estimation methods are available in the literature for predicting saturation vapor pressures of organic molecules. Most of these techniques were developed for the chemical industry and are typically constrained by databases heavily biased toward monofunctional compounds with saturation vapor pressures in the range ~10^3 – 10^5 Pa.[30c] Few of the estimation methods derived from these data claim to have much accuracy below ~10^2 Pa. Thus, these vapor pressure estimations methods derived from chemical industry databases are not necessarily applicable to the often multifunctional atmospheric compounds,[30c] and use of them can lead to significant errors in atmospheric modelling studies.[7a,30b,c] Nonetheless, estimation methods are widely used in atmospheric studies since, as has been previously discussed, measured thermodynamic property data are not available for most atmospherically relevant compounds. In this section we: 1) summarize saturation vapor pressure estimation methods, 2) perform a comparison of

measured and predicted property values for dicarboxylic acids using a subset of available methods, 3) review published pure-component sensitivity studies, and 4) provide suggestions for data needs required to improve current predictive techniques.

Measuring the saturation vapor pressure of all atmospherically relevant compounds is not practical or feasible. Methods that rely on existing data and allow extrapolation to a wider range of compounds can mitigate such limitations, but require thorough review and evaluation of the structural and parametric uncertainties associated with each method. Group contribution methods (GCMs) are an important type of model used for estimating thermodynamic properties of organic molecules. GCMs are based on the principle that functional groups in a molecule contribute additively to the property of interest, and are the main focus of the proceeding discussion. The pure component saturation vapor pressure of compounds in the liquid and subcooled liquid state can be calculated using GCMs. It is worthwhile noting that computational quantum mechanics models are in principle able to predict physical properties without experimental data. The COSMO-RS model (conductor-like screening model- real solvents) is an example.[79] Whilst the absolute accuracy of such models remains largely unassessed, their ability to predict certain vapor pressures of compounds with varying structures and functionality has been demonstrated.[80] The ability of such models to predict saturation vapor pressures of atmospherically important compounds with desired accuracy is largely unexplored. Alternatively, in support of GCM development and testing, application of models like COSMO-RS might enable qualitative probing of relationships between molecular structure and saturation vapor pressure; and provide data for compounds which cannot be synthesized, are dangerous to study or are for other reasons not feasible for experimental studies.

5.1 Group Contribution Methods (GCMs)

Group contribution methods (GCMs) are developed from base molecules with known properties, *e.g.* the n-alkane series. Adding a functional group to the base molecule (*e.g.* OH bonded to one aliphatic carbon atom in an n-alkane) will alter the property of the n-alkane and the contribution of this new group (OH) can be back-calculated from the experimental values of the n-alkane, and the substituted n-alkane. If the group contribution concept holds, the contribution of the -OH group should not depend on the n-alkane from which it was derived. While this is true in many cases, there are also numerous exceptions. Deviations from additivity should be understandable on a molecular basis, and be described by a physically realistic correction term. These corrections are typically capturing so called proximity effects, *e.g.* the influence of two neighboring groups on each other, or effects on a mesomeric system. Once the functional form of the predictive equation has been determined, parameters are derived using experimental data. Given the sparsity of atmospherically relevant data available, careful weighting needs to be given to specific groups to avoid the problems of under- or over-fitting. In the case of available but limited data, existing predictive techniques may not have appropriate representation of specific groups. For example, parameters for groups such as hydroperoxide, peroxyacid and peroxy acetyl nitrate (PAN) only have been obtained from small sets of experimental data.[81] When functional groups are not explicitly accounted for in a predictive technique, an alternative approach is to break them down into subsidiary groups with known contributions. This is usually done in a way that conserves the number of heavy atoms: nitrate group = ether group + nitro group; hydroperoxide group = ether group + alcohol group; peroxyacid group = ether group + carboxylic acid group, and PAN = ester group + ether group + nitro group. Whilst this method has been used in some vapor pressure

GCMs,[82] it is not obvious that the interactions of a hydroperoxide group (for example) with other groups in a liquid mixture can be accurately modeled as an ether plus an alcohol group.

Saturation vapor pressure estimation methods must be able to account for the fact that temperatures are variable in the atmosphere, and saturation vapor pressure has a non-linear temperature dependency. Measurements are typically made at a specific temperature that can be higher (or lower) than ambient, such that the GCMs must extrapolate from the experimental temperature to ambient temperature(s). For the estimation of vapor pressures as function of temperature, both an absolute vapor pressure value at a specific temperature, and the slope of the logarithm of vapor pressure with reciprocal temperature are therefore required. This slope can be calculated from the heat and volume change of vaporization, using the Clausius-Clapeyron equation (Equation 1). The available temperature correction methods are split into two categories. The majority of methods rely on extrapolation from the boiling point T_b at a pressure of 1 atmosphere, to the vapor pressure at the temperature of interest (*i.e.*, ambient). These are discussed in section 5.1.1. Predictive techniques also exist which do not require a boiling point; these are discussed in section 5.1.2.

5.1.1 Temperature-dependent GCMs requiring boiling point

Methods for obtaining saturation vapor pressures by extrapolating from T_b include Myrdal & Yalkowsky[83] and Nannoolal et al.[84] The latter utilizes the same complex group-contribution structure as the T_b estimation method of Nannoolal et al.[85] A refinement of Nannoolal et al.[84] was published by Moller et al.,[86] featuring an additional term aimed at improving predictions for aliphatic alcohols and carboxylic acids, new size dependent groups to improve predictions for

several functional groups, and additional hydrocarbon groups. For some of the compounds of atmospheric interest, the boiling point is high (>700 K) and thus a relatively small error in the slope of the extrapolation-line between T_b and ambient temperature (typically ~298 K) can make a large difference in the predicted saturation vapor pressure.[30c] Similarly to the T_b extrapolation methods, the corresponding states method of Lee-Kesler [87] uses critical temperature T_c.

As is often the case for atmospherically-relevant compounds, if T_b is not known experimentally, it has to be estimated. Approaches for estimating T_b include the group contribution method of Stein and Brown,[88] used in both the Extended AIM Thermodynamics model (E-AIM)[48b,89] and EPI-Suite[90], and the more recent method of Nannoolal et al.[85] The method of Stein & Brown[88] is a modification of the simple Joback & Reid method[91] (which tends to overpredict T_b), to which Stein & Brown[88] added 44 groups (to total 85) and a correction for high T_b values. The method of Nannoolal et al.[85] includes both primary and secondary groups (>130 depending on the functionalities covered), along with group interaction terms (207 terms in total). The use of secondary groups (*e.g.* -CHO connected to aromatic C, and -CHO connected to a non-aromatic C), allows consideration of proximity effects through corresponding group interaction or correction terms. Models such as Lee-Kesler that require T_c, typically use the group contribution method of Ambrose.[87]

5.1.2 Temperature-dependent GCMs not requiring boiling point

Predictive techniques also exist which do not require estimation of T_b or T_c. The method of Capouet & Muller[92] for complex organic molecules uses the saturation vapor pressure of the parent hydrocarbon as a primary parameter from which additional functional group increments

are added. Additional methods that fall in this category are the SIMPOL method[93] and the EVAPORATION method.[81]

5.1.3 Application and assessment of GCMs for dicarboxylic acids

In this section liquid state saturation vapor pressures of straight chain dicarboxylic acids estimated from GCMs are compared with the saturation vapor pressures derived from experiments described in Section 4. The estimated saturation vapor pressures for glutaric-, adipic-, pimelic- and suberic acid in Figure 17 were published by Booth et al.,[35c] while the other values have been calculated for this comparison. Some general observations can be made that have been confirmed in other studies.[30c,d] Most estimation methods over predict the experimentally based recommended values derived herein for dicarboxylic acids with $\leq C_8$. Moller et al.[86] overestimates vapor pressures for $< C_7$. The exceptions are the estimated values obtained from the EVAPORATION method[81] and from the Nannoolal et al.[84] vapor pressure prediction method using boiling points estimated with the Joback & Reid method.[91]

Saturation vapor pressures for dicarboxylic acids with $> C_6$ were under predicted using the methods by Nannoolal et al.[84] and Joback & Reid.[91] The EVAPORATION method[81] showed the best agreement with measurements; however, the model was developed using many of the same compounds, thus this measurement to model comparison does not satisfactorily test the predictive capability of this estimation method. Predictions by the Moller et al.[86] vapor pressure extrapolation method are closer to measurements than those using Nanoolal et al.[84] with boiling points estimated with the Stein & Brown method[88] or the Nannolal et al. method.[85] This is to be expected given the method was designed to improve predictions for compounds with such

functionality. Unlike EVAPORATION[81] however, the more recent data derived from instruments described in Section 3, and represented by the measurement data in Figure 17, was not used for parameter fitting.

This raises an important aspect of testing group contribution methods. Evaluating both structural and parametric uncertainty should be done using compounds both internal and external to the training basis set, with the external compounds being the more critical test.

5.2 Review of prior pure component sensitivity studies

The ability of GCMs to replicate measured pure-component saturation vapor pressures for other atmospherically relevant compounds has been sporadically studied in the literature. Clegg et al.[89b] reviewed the predictions made by a wide range of vapor pressure estimation methods for a limited number of surrogate compounds, and showed that the methods could give very divergent predictions for the same compound. Barley & McFiggans[30c] compared the performance of a selection of methods against experimental data for 45 multifunctional compounds. Whilst these compounds were more volatile than compounds expected to contribute significantly to organic aerosol particle mass in the atmosphere, they found that the vapor pressure extrapolation method of Nannoolal et al.[84] and the method of Moller et al.[86] compared better with experimental data than the other vapor-pressure methods studied when used with the Nannoolal et al.[85] T_b estimation method. O'Meara et al.[30d] followed the study of Barley & McFiggans[30c] and expanded the experimental basis set for predictive technique evaluation from 45 to 90 compounds with emphasis on compounds with lower volatilities than the previous study. For pure component vapor pressures, they found EVAPORATION[81] (applicable to 46 of the 90 test compounds) to be

the most accurate. However, of the vapor pressure estimation methods that were applicable to all the test set compounds, the Lee–Kesler[87] method showed the lowest mean absolute error, and the Nannoolal et al.[84] method showed the lowest mean bias error, when both used normal boiling points estimated using the Nannoolal et al.[85] method. The authors recommended EVAPORATION[81] to be extended to cover all functionalities composing SVOCs. However, comparison of all available models currently can only be done for a small subset of molecules,[30c,d] as the individual methods do not account for the same functional groups. For example, in the study of O'Meara et al.,[30d] the methods of Nannoolal et al.,[84] Moller et al.,[86] Myrdal & Yalkowsky[83] and Lee-Kesler[87] were able to cover all 90 compounds of the testset, whereas the methods of Capouet & Muller,[92] EVAPORATION[81] and Pankow & Asher[93] covered 42, 46 and 81 compounds, respectively. As independent data become available against which to test the model formulations, the comparison of individual models should be repeated.

5.2.1 Recommendations based on pure component studies

The discussion up to this point largely has been focused on the limitations of GCMs due to lack of available experimental data for organic molecules and moieties of importance in the atmosphere. However, also of importance is the potential for over fitting.[30c,d] When data for an insufficient number of compounds or functionalities are used to fit a large number of functional group parameters and to develop correction terms, the resultant parameterizations may simply be fitting the noise or fluctuations in the data rather than the trends.[30c] The resultant GCMs reproduce the property values of the training set well, but perform poorly when applied to compounds outside of the training set. Examples have been given by Topping et al.[94] and Zuend et al.[95] for activity coefficient estimation methods, and Booth et al.[35c] for vapor pressure

estimation methods. O'Meara et al.[30d] suggested the potential for over fitting in comparing SIMPOL[93] with EVAPORATION.[81] In order to better represent structural effects in GCMs and the functional groups most relevant in the atmosphere, better understanding of the role of molecular structure on saturation vapor pressure must be achieved and improved mathematical functions must be developed. This will require high quality experimental data allowing exploration of the effects of functionalization, molecular structure and phase on saturation vapor pressure.

An ideal experimental basis set would fulfill the following criteria: 1) encompass atmospherically relevant molecules and functional groups; 2) include a wide variety of chemical structures and combinations of relevant functional groups; and 3) represent well-defined phase states (crystalline, amorphous solid, (subcooled) liquid). With respect to the development of GCMs, data are needed to address the following key limitations and uncertainties: underrepresented molecules and functional groups; inter- and intramolecular bonding; and temperature dependence. Important aspects of each are discussed in more detail below.

Underrepresented molecules, longer chain (> C_{18}) hydrocarbons: Alkanes have been widely studied due to their importance in many areas of industrial processing, especially distillation. There is however considerable uncertainty in the vapor pressures of very high chain length hydrocarbons[96] (*e.g.* C_{18}-C_{28}). Accurate saturation vapor pressures for the carbon chain backbone is essential to many types of structure-activity relationships (SARs), and data are both sparse and unreliable in the pressure ranges of interest to atmospheric scientists.[96] Macknick & Prausnitz[97] report the liquid state saturation vapor pressure of n-octadecane at 298 K to be $2.5 \cdot 10^{-6}$ Pa. This molecule thus seems to be a good candidate as a reference molecule of well-defined state at

ambient conditions (liquid) for measurements using several of the methods described in Section 3. The addition of alcohol functional groups leads to a decrease in saturation vapor pressure of approximately two orders of magnitude, which suggests that investigation of monofunctional alcohols from C_{18}-C_{25} would also prove beneficial. There have been a number of previous studies that have investigated the saturation vapor pressures of various monocarboxylic acids with low vapor pressures.[31b,c,76,98] Applying that suite of techniques to an expanded set of compounds, particularly > C_{12}, is suggested so that broader comparisons can be made.

Underrepresented functional groups, nitro and nitrate containing compounds: Reactions of volatile organic precursors with NO_x lead to formation of nitro and nitrate groups. There exists some data in the literature for polynitrates, but few data are available for compounds with combinations of nitro and/or nitrate with -COOH and -OH groups. However, using such compounds may raise significant safety issues. There is also a very limited amount of data on these groups included in estimation methods, for example the widely used Nannoolal[84] method has 13 aromatic nitro compounds, and just three aliphatic nitro compounds and four nitrate compounds. The status for intra-molecular interactions is similarly poor with just two nitro-nitro interactions and two nitro-amino interactions being included.

Molecular bonding: Intra-molecular interactions, such as hydrogen bonding between neighboring -OH and -COOH groups is highly dependent on the positions of the interacting groups. Hydroxy groups have in some cases been shown to substantially raise the solid state vapor pressure of a carboxylic acid,[35b] and in other cases to lower it.[43]

Some polar groups (*e.g.* ketones, aldehydes, esters and ethers) are known to have a limited impact upon volatility in their own right, but may be able to participate in intramolecular hydrogen bonding and thus significantly modify the effect of -OH and -COOH groups on volatility. These effects must be clarified and accounted for to improve saturation vapor pressure estimation methods for compounds in the atmosphere.

*Temperature dependen*ce: At the present time, there is little possibility of being able to measure accurate T_b values (due to decomposition) for a wide range of multifunctional compounds, particularly compounds with multiple groups that greatly reduce volatility. Hence, vapor pressure data collected at ambient temperatures (after correction to subcooled liquid vapor pressure values if required) would need to be extrapolated up to T_b, *i.e.* a process that is likely to give significant error in the experimentally derived T_b value because of the length of extrapolation. An alternative approach could be to use a different reference pressure (T_b is the reference temperature at a pressure of 1 atmosphere); a pressure of 1 Pa has been suggested. This would have the advantage of reducing the extrapolation required from experimental data to the reference pressure, but might mean that a lot of data for more volatile compounds *(e.g.* monofunctional compounds) would not be included in the final model because of large uncertainties in their vapor pressures at 1 Pa. Hence, a model developed using a reference pressure of 1 Pa would be a very narrow model based on a relatively small set of data for specific use by the atmospheric community. However, the data on which it was based would be predominantly from multifunctional compounds, and though it might be initially restricted to a few functional groups (*e.g.* -OH and -COOH), it could be expanded as data for multifunctional compounds with additional groups (*e.g.* ketones, aldehydes, nitrate, and nitro) in multiple mixed combinations become available.

6. Well-defined mixtures containing dicarboxylic acids

Atmospheric aerosol particles rarely consist of single organic species, but instead of complex mixtures of organics, water and inorganic compounds. The equilibrium vapor pressure of an organic molecule over a mixed particle is influenced by deviations from ideality and potential chemical reactions in the mixed particle, as well as the phase state of the particle. In this section, a brief overview of what is known about the detailed thermodynamics of well-defined mixtures of dicarboxylic acids with water, inorganic salts and each other is presented. The knowledge gained about these simple mixtures is the first step towards a mechanistic picture of the complex mixtures present in the atmosphere.

6.1 Mixtures of dicarboxylic acids with water and common inorganic aerosol constituents

As described by Raoult's law (Equation 7), the equilibrium vapor pressure of component *i* over a mixture is obtained from the saturation vapor pressure by scaling by the mole fraction of *i* in the mixture (particle phase). Non-ideality is taken into account through the non-unity activity coefficient that depends on the mixture composition and temperature. Activity coefficients can be predicted using thermodynamic models and group contribution techniques.[95,99]

In Section 4 it was discussed how subcooled liquid saturation vapor pressures of individual dicarboxylic acids are derived from studies of the evaporation of aqueous solution droplets containing a single dicarboxylic acid.[33e,f,33h,37b,43,50f] In these aqueous two-component systems, the phase is liquid and the description of the activity coefficients is considerably simplified by thermodynamic consistency requirements,[12] which link the activity coefficients of individual components in the mixture to each other. At equilibrium the water activity in an aqueous solution

droplet is equal to the relative humidity of the surrounding gas. The equilibrium, relative humidity can often be reliably measured over a range of aqueous mixture compositions and temperatures, and activities of the dicarboxylic acids can thus be directly inferred and used to constrain activity models. This was for example done for C_2-C_5 dicarboxylic acids using an EDB setup.[73] Comparison of activity coefficients derived from experimental results with those predicted using GCMs led to suggested modifications of the group contribution parameters. A compilation of experimental data from bulk solutions and from suspended particles have been used to constrain the E-AIM model.[48a] While some differences in activity coefficients of dicarboxylic acids and water in aqueous solution predicted by different models exist, the uncertainty related to the activity coefficient predictions is considerably smaller than the uncertainty related to prediction and measurement of pure component saturation vapor pressures.[33g,43,50g] Also, the deviations from ideality for aqueous solutions of C_2-C_5 dicarboxylic acids seem to be relatively small.[48a,48c]

We now proceed to discuss mixed particles containing dicarboxylic acids, water and inorganic salts. While activity coefficients of water have been derived from experimental studies of aqueous mixtures of dicarboxylic acids and common inorganic salts such as sodium chloride and ammonium sulphate,[38,100] only a few studies have targeted the activity coefficients and equilibrium vapor pressures of the organic species in/over ternary particles.[33g,50g,h,101] The quantification of the dicarboxylic acid activity over a ternary mixture is complicated compared to the binary mixture discussed above. Measurements of water activity (*i.e.* relative humidity) are insufficient to constrain the thermodynamics of the system, and independent quantification of the equilibrium vapor pressures of the organic species is often needed. Furthermore, the dissociation

and chemical interactions between the ions in the particle phase (*e.g.* organic salt formation) can complicate the picture considerably.

The evaporation of succinic acid from an aqueous solution in a FT-TDMA setup has been found to be decreased by the presence of sodium chloride and ammonium sulphate much more than predicted by the E-AIM model.[50g,h] The same phenomenon was recently reported[20] for a series of dried particles containing dicarboxylic acids (oxalic-, succinic-, acetic- and citric acids respectively) and chloride- or ammonium sulphate. The formation of practically non-volatile organic salts in the particle phase, as has been previously reported,[100b,102] was suggested as the reason for this behavior. The effect is stronger for ammonium sulphate than sodium chloride, and increases with decreasing pure-component saturation vapor pressure of the acid. On the contrary, Pope et al.[33g] found no clear effect of sodium chloride on the evaporation of malonic acid or glutaric acid from aqueous solution droplets. Furthermore, Yli-Juuti et al.[50g] searched for potential reaction products in bulk solutions and atomized droplets containing succinic acid and ammonium sulfate using offline analysis and identified no reaction products.

6.2 Mixtures of multiple dicarboxylic acids

Several studies have addressed the thermodynamics of bulk mixtures or particles containing several dicarboxylic acids.[28,51,103] Marcolli et al.[28a] theoretically showed that the liquid (or amorphous) phase is the thermodynamically stable phase for a large number of miscible components. Furthermore, they experimentally studied the hygroscopic behavior of mixed particles containing malonic-, malic-, maleic-, glutaric- and methyl-succinic acids, and found the deliquescence relative humidity to decrease with increasing number of components in the

mixture. Cappa et al.[28b] have studied an equimolar mixture of nine straight-chain dicarboxylic acids (C_3-C_{10}+C_{12}), and observed that the different components evaporated with unique desorption profiles, which was interpreted as the mixture having been well-mixed even at low RHs, potentially indicating liquid-like behavior. However, the derived saturation vapor pressures for these individual compounds differed somewhat from their pure component values, which were interpreted as deviations from ideality. The addition of $NaNO_3$ salt to this organic mixture did not lead to changes in the general behavior, although it did lead to changes in the estimated activity coefficients of the individual compounds. Booth et al.,[104] directly measured the viscosity of these same mixtures in macroscopic bulk samples and found values much larger (10^6 – 10^7 Pa s) than those for typical liquids (< 10^2 Pa s), thus indicating a solid, semi-solid or amorphous phase of dry mixtures at temperatures below 330-350 K. At room temperature, water mole fractions of about 0.8 and larger were required for the mixture to show clearly liquid-like viscosities. It should be noted however, that the viscosity measurements were conducted at macroscopic bulk samples instead of small airborne particles whose phase might depend on particle size.[105]

It has become evident that the phase state of mixed particles is critical for estimating the equilibrium vapor pressures of organic compounds above these particles. Thus, knowledge on the phase state of dicarboxylic acids and other organic molecules in the ambient particles is needed.

7. Bridging the gap between saturation vapor pressures of individual organic molecules and atmospheric aerosol volatility

A major objective of knowing the thermodynamic properties of the molecules in the atmosphere is to understand and predict the partitioning of these molecules between the condensed and vapor phases. However, to describe and predict gas to particle partitioning of organic molecules in the atmosphere, scientists face two major (and related) challenges: first, the solvent into which a molecule partitions (*i.e.* the particle) is not precisely specified, and second, the mole fractions and even molecular identity of the partitioning molecules are often unknown or very uncertain.

Discussed in this section are the relevance of saturation vapor pressures and properties of mixed inorganic and organic particles for predicting partitioning of organic compounds in the atmosphere. Three general approaches for predicting atmospheric partitioning are discussed:

The *bottom up* method for atmospheric partitioning is to predict as explicitly as possible the full composition of organic aerosol (gas + particle), including the thermodynamic properties (Section 7.1).

The *molecular probes* method involves measuring the partitioning behavior f_i^{cond} of selected compounds and comparing that to predictions in order to assess the behavior of ambient aerosols even when their exact composition is unknown (Section 7.2).

The *top down* methods for atmospheric partitioning are empirical, based on observation of bulk gas to particle partitioning as a function of total organic aerosol particle mass and subsequent description of the mixture through a set of surrogate compounds with a best-fit distribution of thermodynamic properties (Section 7.3).

All three approaches can be tested using data from smog-chamber experiments, which constitute controlled subsets of atmospherically relevant conditions. They can also be implemented in chemical transport models and compared against field data. Figure 18 illustrates the different approaches used to understand evaporation and condensation of organic compounds in the atmosphere.

7.1 Bottom up: explicit prediction of secondary organic aerosol partitioning

In recent years there have been some efforts to predict ambient and chamber particulate mass loadings from explicit consideration of individual molecules. This has coincided with the maturation and use of explicit (*e.g.* GECKO[106]) and near explicit, (*e.g.* the Master Chemical Mechanism MCM[107]) or quasi explicit (*e.g.* BOREAM[108]) models of gas-phase VOC oxidation. These models differ in terms of the number of species and chemical reactions considered, and in terms of the method of mechanism generation. These models have been tested against smog-chamber SOA formation data with mixed results. It is in general difficult to establish whether model to measurement discrepancies are caused by incomplete chemical mechanisms, missing chemical processes, inaccurate vapor pressure estimation, or some combination of these.

Jenkin et al.[109] found that a two-order of magnitude decrease in vapor pressure over the GCM-predicted values was required to reproduce the observed SOA mass concentration for experiments using SOA formed from the α-pinene + O_3 reaction from MCM. Camredon et al.[110] suggested that the choice of saturation vapor pressure estimation method was responsible for some of this discrepancy. When no condensed phase reactions were allowed, they found that the use of a vapor pressure estimation scheme, that is thought to systematically under predict the

compound saturation vapor pressures, was required to give the best agreement for the α-pinene + O_3 system. However, if they allowed for condensed phase reactions, which were found necessary to better represent the mass spectral fingerprints of the particles, then they were able to utilize what is thought to be a more realistic vapor pressure estimation scheme. Chen et al.[111] reported good agreement between predicted and observed SOA mass distributions using a combination of the MCM[107] and SIMPOL[93] vapor pressure prediction scheme, but disagreement between measured and modeled O:C and H:C ratios, which they suggested was due to lack of consideration of condensed-phase peroxide decomposition and subsequent oligomerization.

Using BOREAM, Capouet et al.[108] simulated SOA mass within a factor of two of the measured values for many α-pinene + O_3 chamber oxidation experiments. The difference between their results and those of Jenkin,[109] was again attributable largely to differences in vapor pressure prediction techniques, since little consideration of condensed phase reactions was made (though sensitivities to peroxyhemiacetal formation at reasonable rate estimates were investigated). Still, in order to replicate the SOA yield from some ozonolysis experiments, the BOREAM oxidation scheme required modification to produce greater amounts of low vapor pressure products (pinic- and hydroxy-pinonic acid), which indicates that deficiencies in the gas-phase mechanism can also be important.

More recent investigations suggest that chemically explicit approaches may overpredict atmospheric and chamber loadings. For example, simulations using the GECKO model systematically overestimate SOA production.[8c] Sensitivity analyses suggest missing gas-phase processes that break the carbon skeleton of the parent compound *i.e.*, underrepresentation of fragmentation vs. functionalization; although it is possible that unaccounted losses of gaseous

vapors to the chamber walls may play some role in the overprediction.[78a] The increased mass produced by this explicit approach is attributable to the formation of later generation oxidation products with increased functionality, and hence lower vapor pressures compared to quasi-explicit approaches,[8c] indicating that gas phase processes may be largely responsible for the missing mass in the earlier simulations. These studies were less sensitive to the vapor pressure prediction method because of the large contribution of very low volatility, multi-generational oxidation products to the SOA particle mass. Very recent experimental studies suggest that some extremely low volatility products may be formed via novel auto-oxidation processes that are not in the current mechanisms.[9,112]

7.2 Molecular probes of physical-chemical properties of complex organic aerosols

Molecular probes, if carefully selected, can help to understand the distribution of material between the vapor and condensed phases in the atmosphere. The parameter of interest in this approach is the gas-particle partitioning coefficient of compound *i,* $K_{p,i}$.

The extent to which a particle is in equilibrium with the surrounding gas phase, has been ascertained by measuring C_i^{cond}, C_i^{vap} and *TSP,* which together yield $K_{p,i}$, for a selection of compounds (often a homologous series), and then plotting log $K_{p,i}$ vs. log $p_{l,i}^0$, with $p_{l,i}^0$ values taken from the literature or calculated using estimation methods. For equilibrium partitioning the slope of the line should be –1, and for absorptive partitioning the intercept is equal to $b = \log\left(\frac{R \cdot T \cdot f_{OM}}{M_{OM} \cdot \gamma_{x,i}}\right)$ (see Equation 15). Examples of this approach have been reported in studies

for a variety of compounds.[113] C_i^{cond} and C_i^{vap} have most often been determined using chromatographic methods, and TSP has been measured using gravimetric methods or online particle sizing instruments.

Analyses of simple hydrocarbons such as alkanes and polycyclic aromatic hydrocarbons (PAHs) are among the easiest, and provide a relatively direct indication of gas to particle partitioning equilibrium. This is because they are inert and thermally stable, so measurements of C_i^{cond} and C_i^{vap} are straightforward, and reported values of $p_{l,i}^0$ are expected to be accurate.

The gas to particle distributions of smaller oxygenated species, especially carbonyls, has also been investigated. Some studies have found slopes of log $K_{p,i}$ vs. $\log \gamma_{x,i} \cdot p_{l,i}^0$ plots close to –1, indicative of equilibrium, but substantial discrepancies are also common and have been attributed to adsorption-desorption kinetics, non-exchangeable material, variations in compound and *TSP* concentrations and temperature during sampling, and measurement artifacts.[113a-d,114] However, in some cases laboratory studies of SOA formation have observed values of $K_{p,i}$ measured for oxygenated reaction products that are orders of magnitude larger than those predicted using Equation 15.[113h-k,115] The most plausible explanation for this is that these compounds are not present in the particle phase as single molecules, but instead exist as covalently bound species or oligomers formed through heterogeneous and/or multiphase reactions with other compounds.

Recent advances in instrumentation for semi-continuous analysis of gas- and particle-phase organics, including advances in Gas Chromatography -MS[116] and CIMS[117] enable higher time resolution measurements and consequently tracking dynamical variation in partitioning.

Available comparisons between ambient measurements and theoretical calculations suggest levoglucosan[114b] and *n*-alkanes[116a] partition roughly according to equilibrium partitioning theory. Good agreement (within one order of magnitude) between measured and modeled $K_{p,i}$ values for C_{15}-C_{23} alkanes has been reported[114a]; slopes of measured vs. predicted log $K_{p,i}$ were 0.8-0.9 for docosane and 0.7-0.8 for tricosane. For C_6-C_{12} alkanoic acids measured particle-phase concentrations higher than predicted values have been reported,[116a] with phase transitions occurring ~2-4 carbons lower than expected. Some of these differences may be due to incomplete collection of the gas phase. Measurements of the partitioning of C_1-C_{18} alkanoic mono acids on relatively short timescales (~1 h) , using acid-specific (acetate anion) CIMS, are in reasonable agreement with equilibrium partitioning theory.[118] The level of agreement is however, dependent on the vapor pressure dataset used for comparison. Further, the uncertainty in the measured f_i^{cond} increased substantially above C_{16}, making quantitative comparison difficult. Nonetheless CIMS measurements are especially sensitive to acids and can extend to very low vapor pressure compounds,[119] thus potentially enabling the use of the diacids reviewed here as molecular partitioning probes. Ambient measurements of the gas to particle distribution of alkyl-nitrates can also be fitted according to partitioning theory, although the derived effective alkyl-nitrate vapor pressures are substantially lower than expected for first-generation oxidation products.[120] Overall, currently available ambient measurements generally indicate that the partitioning of organics is often describable by absorptive partitioning theory. Analyses such as those presented above will be greatly enhanced with the ability to uniquely identify the marker species and improvement in the accuracy of vapor pressure predictions.

Two of the most pressing needs for measuring and modeling gas-particle partitioning are: 1) greater understanding of the factors that determine the phase of organic aerosol particles[113b,c,121] and 2) the role of oligomers in aerosol chemistry.[8b,113h-k,122] Both of these topics can be investigated using appropriate nonreactive and reactive molecular probes. Ideally, the compounds should be commercially available or easily synthesized, easily measured, have a wide range of saturation vapor pressures (from volatile to nonvolatile), and be characteristic of specific heterogeneous and/or multiphase reactions. When possible, it would also be beneficial to employ compounds that are characteristic of specific POA or SOA sources. For example, nonreactive compounds from combustion sources include alkanes, PAHs, steranes, and hopanes,[123] and reactive compounds formed by VOC oxidation include pinonaldehyde, pinonic acid, and pinic acid for monoterpenes,[113i] and alkylnitrates and hydroxynitrates for alkanes.[124] Analyses of simple monofunctional aldehydes, alcohols, and carboxylic acids (regardless of their source), which can react on or in particles to form hemiacetals and esters, could provide useful information on oligomer formation.[122a] It is also important that methods that can quantitatively determine the concentrations of species in their oligomerized forms (*i.e.* that do not reduce compounds to their monomeric components during analysis) are used and further developed. Comparisons between the oligomeric content estimated between different methods will be important. Studies conducted to explore correlations of K_p with atmospheric variables such as relative humidity, temperature, NO_x- O_3- and CO-concentrations, particle properties such as particle acidity and O:C ratio, and others would also be especially valuable. In addition, new data on the vapor pressures and activity coefficients of molecular probes, and the identification and characterization of new such compounds are needed.

7.3 Top down: volatility distributions of complex organic mixtures and atmospheric impact

In the bottom-up approaches, the mole fraction of compound *i* is simulated or measured, and the equilibrium vapor pressure and activity coefficient is calculated or inferred from measurements. In the top-down approaches however, the molecular composition, individual molar masses, and hence the mole fractions of individual components are not known. Instead, the total mass concentrations of organic particles and the mass fractions of its components are generally better accessible from experimental data. Therefore, top-down approaches are best formulated using Equation 17 adjusted to a mass fraction based scale as described in Section2.5.[29] Many chemical transport models represent the organic gas to particle distribution as a mixture of surrogate compounds described by their C_i^* (or $K_{p,i}$). One common formulation reduces the system to two surrogate compounds with variable C_i^* (the 2-product approach);[121] while a second formulation, (the Volatility Basis Set (VBS))[29,96,125] uses a greater number of surrogate compounds (commonly 4 to 8) and with the C_i^* values specified to vary by factors of 10 at 300 K. These applications often make a pseudo-ideal solution approximation, where $\gamma_{mass,i}$ and thus C_i^* are approximately constant under atmospheric conditions (although in the top-down approaches $\gamma_{mass,i}$ and C_i^* are not truly separable).[126]

Equation 19 shows that as the concentration of the absorbing organic phase C_{OA} increases, the fraction f_i^{cond} will also increase. Likewise, relatively less volatile constituents (lower C_i^*) will be more abundant in the condensed phase, and the scale concentration for a constituent with f_i^{cond}

=0.5in equilibrium is found at $C_i^* = C_{OA}$. Because organic aerosol concentrations are frequently a few μg m^{-3}, this means that the scale saturation concentration for semi-volatile organics in the atmosphere is of order 1 μg m^{-3}, or $p_i^{eq} \sim 10^{-5}$ Pa. Furthermore, studies analyzing the growth of the smallest atmospheric nanoparticles indicate a significant presence of ELVOC compounds ($C_i^* <$ 10^{-3} μg m^{-3}) with even considerably lower equilibrium vapor pressures.[26,127]

7.3.1 Empirical determination of volatility distributions of complex aerosols

Most top-down empirical approaches to volatility determination depend on experimental observations of the equilibrium behavior predicted by Equations 17-19 and/or their combinations with the dynamic condensation and/or evaporation equations (see Section 2.4). Specifically[122a,128], f_i^{cond} is expected to increase as the aerosol loading C_{OA} increases, and consequently the aerosol particle mass yields should rise. The reverse should occur upon dilution. Conversely, when primary aerosol emissions are isothermally diluted through the atmospherically relevant range of particle mass concentrations, the particles are generally observed to shrink toward a new equilibrium state.[129] The extent of mass loss as a function of C_{OA} can be inverted to determine a volatility distribution. It should, however, be noted that such interpretations typically assume that monomers dominate the condensed phase, although recent efforts have attempted to account for the influence of oligomers on the observed evaporation.[130] Further, it can be difficult to fully separate the influence of increasing C_{OA} from the continuous production of new condensable material in laboratory chamber SOA growth experiments.[131]

In addition to formation and dilution experiments, the volatility of aerosol particles can be measured by similar methods to those described for single compound vapor pressures, often relying on measuring dynamic changes of the aerosol size distribution upon heating[132] similar in concept to isothermal dilution experiments, though there are difficulties with such retrievals.[133]

There are several potential pitfalls to these empirical methods for inferring the volatility of the complex mixtures. These pitfalls are not unique to the empirical approach however, and most apply to the bottom up and molecular probe approaches as well.

First, laboratory studies are often conducted in a chamber – in many cases a large Teflon® bag – that includes walls. The role of those walls, whether simply as sinks for particle deposition[134] with or without attendant particle-vapor interactions[135] or potentially as sinks for vapors through irreversible deposition,[136] or reversible adsorption or absorption[78,137] can confound interpretation of chamber experiments.

Second, data interpretation is often based on an assumption that the aerosol suspension has reached equilibrium – both in terms of the internal mixing as well as the gas-particle equilibrium. Potential deviations from equilibrium cause the residence time of the aerosol in the system to influence the results, as the equilibrating time for complex mixtures can be longer than for simpler mixtures.[138] The equilibration timescale for an aerosol suspension depends on the aerosol surface area (really the timescale for vapor collisions with particles, known as the condensation sink), which can range from seconds at high concentration to many minutes at low concentrations typical of the atmosphere.[139] Mass accommodation coefficients less than unity can

also increase equilibration timescales.[78a,133a,137b,139] Furthermore, condensed-phase diffusion in highly viscous glassy particles may further delay equilibration.[121b,131,140]

Third, the partitioning calculations of smog chamber experiments often assume that the overall composition of the organic mixture (including both phases) remains constant during an experiment. During dilution experiments with primary emissions, the more highly volatile compounds evaporate before the lower volatility compounds; secondary organic aerosol formation experiments involve chemical production of secondary species with varying volatilities.[96] As such, in both types of experiments the composition may change continuously throughout. The decomposition or formation of oligomers during dilution or production experiments can also lead to complications regarding assumptions of constant composition.

Fourth, the presence of water also affects the volatility measurements of organic mixtures, but has been somewhat difficult to establish and calls for accurate thermodynamics describing the water activity in these mixtures.[30a,95,141] The same holds for other inorganic aerosol constituents as well.

Fifth, there may be more than one phase containing organic mixtures. The thermodynamic principles described above apply to any single condensed phase. However, several separate condensed phases can potentially co-exist in complex atmospheric particles, and thus identifying the proper value for C_{OA} based only on observations of the total aerosol particle mass concentration can be a challenge. One common assumption is that the organic molecules form a single mixture and the inorganic molecules form another, but that is far from the only possibility. Recent work[141b,142] has shown that mixtures of organics and inorganic salts can form either one or two condensed phases, depending on both the relative humidity and the degree of

oxidation of the organic compounds. As organic molecules themselves will also tend to phase separate based on polarity,[113f] it is entirely possible that typical atmospheric particles contain three condensed phases at low RH – a non-polar organic phase, a polar organic phase, and a crystalline inorganic phase – and two phases at high RH – an aqueous phase and a non-polar organic phase. Real systems will dynamically evolve between these extremes. Knowing the representative phase of the atmospheric organic mixtures is critical for understanding the partitioning behavior of atmospheric organic molecules – as the saturation vapor pressures over different physical phases can differ drastically as shown in Section4. As RH approaches 100%, a dilute aqueous phase develops and water solubility becomes a critical property. Solubility estimation is however beyond the scope of this work.

The shapes and C_i^* ranges of the volatility distributions derived for complex OA mixtures vary with the aerosol source and atmospheric aging.[129c,132b,132h] The challenges in fully reconciling volatility distributions from growth, dilution and thermodenuder experiments have not been fully resolved. A number of recent experiments indicate there may be a significant amount of material comprising OA that has exceptionally low effective saturation concentrations.[9,26,127a,132b,143] These ELVOC compounds may be formed directly in the gas-phase[9] or from condensed phase reactions.[144] The saturation concentrations of ELVOCs are close to (or even below) the lower detection limit of the present experimental techniques for measuring well-defined equilibrium vapor pressures of specific components. Quantifying these extremely low values is, however, needed on one hand for predicting the evolution of OA loadings at clean environments, and on the other hand for predicting their participation in new particle growth.

This presents a challenge to improve the sensitivity of the experimental techniques to determine saturation vapor pressures of extremely low volatility compounds.

8. Summary and conclusion

Accurate measurement of the equilibrium vapor pressures for low saturation vapor pressure organics ($p_{sat} < 10^{-2}$ Pa) remains challenging. There exist a number of techniques that can be used, that differ in terms of whether they fundamentally probe the equilibrium (or quasi-equilibrium) state or evaporation rates, and the temperature range over which they can be applied. The series of homologous, straight-chain dicarboxylic acids have received much attention over the past decade given their atmospheric relevance, commercial availability and low saturation vapor pressures, thus making them ideal test compounds. An additional reason that these compounds continue to receive attention, is the large discrepancies between the absolute values of their equilibrium vapor pressures at room temperature and their phase-transition enthalpies obtained from different experimental techniques. Uncertainties in the solid state saturation vapor pressures obtained from individual methodologies are typically of the order of 50-100%, but the differences between saturation vapor pressures obtained with different methods are approximately 1-4 orders of magnitude, with the spread tending to increase as saturation vapor pressure decreases. There are similar issues associated with measured values for the enthalpy of sublimation, with the spread between experiments being ~60-80 kJ mol^{-1} (compared to absolute values of ~130 kJ mol^{-1}), yet typical reported uncertainties being only ±10 kJ mol^{-1}.

Some of these differences may be attributable to methodological differences. For example, methods that probe evaporation rates to determine saturation vapor pressures rely on knowledge

of the mass accommodation coefficient. However, differences persist even between different evaporation-based methods, which suggest that there may be more fundamental issues at play. One such issue is that some of the dicarboxylic acids can exist with multiple solid state structures that have distinct saturation vapor pressures. Further, the samples on which measurements are performed may actually exist as amorphous subcooled liquids rather than solid crystalline compounds, again with consequences for the measured saturation vapor pressures, since the subcooled liquid phase will have a higher saturation vapor pressure than the crystalline solid phase. Although it seems reasonable that such phase issues can explain some of the differences between techniques, perhaps up to an order of magnitude in saturation vapor pressure, phase differences are unlikely to explain differences as large as 3-4 orders of magnitude. Furthermore, the losses of vapor molecules within the respective instrumental setups remain to be exactly quantified as long as direct measurements of the low gas-phase concentrations are not available. Empirical and semi-empirical equilibrium vapor pressure estimation methods rely on fitting to experimental data. Such persistent disparities in the measurements of dicarboxylic acid vapor pressures represent a key limitation for estimation method development, because these compounds tend to have some of the lowest saturation vapor pressures for organic compounds that have been measured. Further, the approximate saturation vapor pressures of the dicarboxylic acids fall right in the range of typical organic mass loadings in the atmosphere (0.1 – 10 $\mu g\ m^{-3}$, corresponding approximately to 10^{-6} – 10^{-4} Pa). Compounds with equilibrium vapor pressures in this range will exhibit the greatest sensitivities in terms of their gas to particle partitioning to uncertainties in their saturation vapor pressures, with consequent impacts on the ability of explicit and semi-explicit chemical models to simulate secondary organic aerosol formation.

There is clearly a need for further investigation of equilibrium vapor pressures of compounds that are present in atmospheric aerosol particles, both for the sake of providing the estimation methods with new data and to ultimately understand what contributes to the variability between, and overall accuracy of the various techniques that provide bottom up information. It is suggested that an expansion beyond the dicarboxylic acids to both simpler compounds (such as long chain alkanes or compounds with single functional groups) and more complex compounds (*i.e.* multi-functional compounds) is needed. Near-term focus should be on simpler compounds, as there is concern about decomposition upon heating of more complex compounds. The saturation vapor pressure of several longer n-alkanes is of the order of 10^{-6} Pa, which suggests that characterization of the saturation vapor pressures of alkanes in the range C_{10}-C_{30} would prove beneficial. To share samples between laboratories is also recommended, to ensure that differences between starting material are not responsible for differences in results. The influence of sample generation and preparation should continue to be explored. If possible, raw data should be reported in tables as supplementary material to facilitate direct comparison between techniques at the actual measurement temperature.

The current state of predictive technique evaluation has raised several important issues. Whilst it could be that model structural uncertainty is low, based on some pure component studies, there is a definite need for high quality experimental data that will allow exploration of both structural and parametric uncertainty, the effects of functionalization on vapor pressure, as well as molecular structure including relative positions and inter- and intramolecular interactions, and phase. As to how this data should be constructed, an ideal experimental basis set would fulfill the following criteria: 1) encompass atmospherically relevant molecules and functional groups; 2)

include a wide variety of chemical structures and combinations of relevant functional groups; and 3) represent well-defined phase states (crystalline, amorphous, (subcooled) liquid). Implicit in this requirement, there are currently underrepresented molecules and functional groups, as well as problems such as accurately measuring and/or predicting the boiling point. The latter point might force a change in the reference pressure at which data for the atmospheric community is retrieved.

The greatest need to successfully bridge the gap between systems of a few components and systems approaching atmospheric complexity, is to develop a succession of model mixtures that extend complexity in controlled ways while remaining well characterized. For example, one or more mixtures of constituents spanning a wide volatility range that remain liquid and miscible over the full composition range could simultaneously challenge all three bridging the gap methods discussed: the bottom up, the molecular probes as well as the top down methods.

To understand the role of aerosols in air quality and climate it is necessary to quantify the partitioning of organic molecules between the gas and particle phase in the atmosphere. During the last decade a substantial scientific effort has been dedicated to develop instrumentation and model frameworks for doing so. This has improved our knowledge but also pointed to major open scientific questions. In particular, this review demonstrates the strong need for further investigation of the equilibrium vapor pressures and transition enthalpies of individual compounds that are present in atmospheric aerosol particles.

9. Nomenclature

Symbol	Explanation	Unit
A_0	Orifice area	m^2
a	Subscript referring to particle surface	
α_m	Mass accommodation coefficient	
β	Transition regime correction factor	
C	Mass concentration	kg m^{-3}
C^*	Effective saturation concentration	kg m^{-3}
c	Molar concentration, subscript referring to continuum regime	mol m^{-3}
c_p	Molar heat capacity at constant pressure	J mol^{-1} K^{-1}
D_{vap}	Diffusion coefficient	m^2 s^{-1}
D_p	Particle diameter	M
f_i^{cond}	The fraction of molecule *i* residing in condensed phase	
g	Subscript referring to gas	
φ	Mass fraction	
γ_x	Mole fraction based activity coefficient	
γ_{mass}	Mass-based activity coefficient	
ΔH_{fus}	Enthalpy of fusion (solid to liquid)	J mol^{-1}
ΔH_{sub}	Enthalpy of sublimation (solid to gas)	J mol^{-1}
ΔH_{vap}	Enthalpy of vaporization (liquid to gas)	J mol^{-1}

ΔG_{vap}	Gibbs free energy change upon vaporization	J mol^{-1}
ΔG_{fus}	Gibbs free energy change upon fusion	J mol^{-1}
ΔS_{vap}	Entropy of vaporization	J mol^{-1} K^{-1}
I	Mass flux	kg s^{-1}
i	Subscript referring to chemical component	
k	Subscript referring to kinetic regime	
trs	Subscript referring to transition regime	
Kn	Knudsen number	
l	Subscript referring to liquid	
l_0	Orifice length	m
λ	Mean free path	m
M	Molar mass	mol kg^{-1}
m	Sample mass	kg
ω_0	Clausing probability factor	
OA	Subscript referring to condensed organic aerosol	
p	Pressure	Pa
p^{eq}	Equilibrium vapor pressure	Pa
p^0	Saturation vapor pressure	Pa
R	Molar gas constant	J mol^{-1} K^{-1}
RH	Relative humidity	%
r_0	Orifice radius	m
r_p	Particle radius	m

s	Subscript referring to solid	
ss	Subscript referring to saturated solution	
σ	Surface tension	N m^{-1}
T	Temperature	K
T_b	Boiling point temperature	K
T_t	Triple point temperature	K
T_g	Glas transition temperature	K
T_c	Critical temperature	K
t	Time	s
‹v›	Mean thermal speed	m s^{-1}
v_m	Molar volume	m^3
X	Mole fraction	
w	Mass fraction	
∞	Subscript referring to a distance far away from particle surface	

Acknowledgements

We acknowledge Nordforsk (NCoE BACCI) and The Electric Power Research Institute (EPRI) for support for travel and workshop participation. We thank Doc. Theo Kurten for discussions and Professor Barbara Finlayson-Pitts for input on the Analysis Probe Mass Spectrometry technique. IR acknowledges the European Research Council (ERC-StG-ATMOGAIN, grant n:o 278277) and Vetenskapsrådet (grant n:o 2011-5120) for financial support.

Figure captions

Figure 1: The basic principles of the experimental techniques described in section 3 used to determine saturation vapor pressures of dicarboxylic acids. A dashed line indicates a step that is not included in all methods.

1A: Knudsen cell based methods. Top right: Knudsen Effusion Mass Spectrometry (KEMS).[35b,c] Bottom right: Knudsen mass loss methods.[31a,31g,34]

1B: Single particle methods. Electrodynamic balance (EDB)[33f,g,37-38] and optical tweezers.[33g]

1C: Particle size distribution methods. FT-TDMA refers to the Flow Tube -TDMA;[33c-e,50b,50h,54,145] V-TDMA refers to the Gothenburg Volatility TDMA [31d] and IVM to the Integrated Volume Method.[31e,f,51,146]

1D: Thermal desorption methods: Thermal Desorption Particle Beam Mass Spectrometry TDPB-MS[31b,56a] and Temperature Programmed Desorption Proton Transfer Chemical Ionization Mass Spectrometry (TD-PT-CIMS).[28b,31c,56b] Atmospheric solids analysis probe mass spectrometry (ASAP-MS).[57-58]

Figure 2: Solid state saturation vapor pressures ($p_{s,i}^0$) at 298 K for straight chain dicarboxylic acids as a function of the number of carbon atoms: Noyes & Wobbe (1926),[71a] Bradley & Cotson (1953),[71b] Davies & Thomas(1960),[75] de Kruif et al. (1975),[71c] de Wit et al. (1983),[71d] Ribeiro da Silva et al. (1999),[31g] Booth et al. (2010),[35b] Soonsin et al. (2010),[37b] Tao & McMurry (1989),[76] Bilde et al. (2003),[33d] Saleh et al. (2008),[31e] Saleh et al. (2009),[23] Saleh et al. (2010),[31f] Salo et al. (2010),[31d] Chattopadhyay & Ziemann (2005),[31b] Cappa et al. (2007),[31c] Bruns et al. (2012).[57] The

combined values are best estimates obtained from the datasets for each acid (Figures 7-15) as described in section 4.

Figure 3: Enthalpies of sublimation (ΔH_{sub}) for straight chain dicarboxylic acids as a function of the number of carbon atoms: Noyes & Wobbe (1926),[71a] Bradley & Cotson (1953),[71b] Davies & Thomas (1960),[75] de Kruif et al. (1975),[71c] de Wit et al. (1983),[71d] Ribeiro da Silva et al. (1999),[31g] Booth et al. (2010),[35b] Soonsin et al. (2010),[37b] Tao & McMurry (1989),[76] Bilde et al. (2003),[33d] Saleh et al. (2008),[31e] Saleh et al. (2009),[23] Saleh et al. (2010).[31f] Salo et al. (2010).[31d] Chattopadhyay & Ziemann (2005).[31b] Cappa et al. (2007),[31c] Bruns et al. (2012).[57]

Figure 4: Subcooled liquid saturation vapor pressures ($p_{l,i}^0$) at 298 K for straight chain dicarboxylic acids. Values from TDMA studies were reported as solid state vapor pressures but likely represent the subcooled liquid state and are shown as such here (see text for details). Tao & McMurry (1989),[76] Bilde et al. (2003),[33d] Koponen et al. (2007),[33h] Riipinen et al. (2007),[54] Saleh et al. (2008),[31e] Saleh et al. (2009),[23] Salo et al. (2010),[31d] Zardini et al. (2006),[33f] Soonsin et al. (2010),[37b] Pope et al. (2010).[33g] The combined values are best estimates obtained from the datasets for each acid (Figures 7-15) as described in section 4.

Figure 5: Enthalpies of vaporization (ΔH_{vap}) for straight chain dicarboxylic acids reported in the literature as a function of the number of carbon atoms. The phase state studied in the TDMA studies is assumed to be the subcooled liquid state. See text for details: Tao & McMurry (1989),[76] Bilde et al. (2003),[33d] Koponen et al. (2007),[33h] Riipinen et al. (2007),[54] Saleh et al. (2008),[31e] Saleh et al. (2009),[23] Salo et al. (2010),[31d] Zardini et al. (2006),[33f] Soonsin et al. (2010),[37b] Pope et al. (2010).[33g]

Figure 6: Illustration of how data for oxalic acid, $C_2H_2O_4$, vapor pressure in the solid state were assigned to a regular grid in inverse temperature space (resolution of 100 K/T). See text for details. The black symbols are the data compiled on the grid, the red line is the fit to Equation 4, the dark shaded region the 95% confidence interval of the linear regression and the light shaded area the 95% prediction interval.

Figure 7. Upper panel: Saturation vapor pressure of the solid (filled symbols) and the subcooled liquid state (open symbols) of oxalic acid, $C_2H_2O_4$, versus inverse temperature reported in the literature: Noyes & Wobbe (1926),[71a] Bradley & Cotson (1953),[71b] de Kruif et al. (1975),[71c] de Wit et al. (1983),[71d] Booth et al. (2009)[32] and Soonsin et al. (2010).[37b] The lines represent a linear least squares fit using the gridded approach as described in Section 4.1.1. The crystalline state α-form (black solid line) and the subcooled liquid state (black dashed line). Lower panel: Best estimates (based on the fit) for the vapor pressure in the solid state at 298 K (black filled circle) and for the vapor pressure in the subcooled liquid state state at 298 K (black open symbol) together with the reported vapor pressures at 298 K by the individual experiments shown in the upper panel.

Figure 8: Upper panel: Saturation vapor pressure of the solid state (filled symbols) and the subcooled liquid state (open symbols) of malonic acid, $C_3H_4O_4$, versus inverse temperature reported in the literature: Riberio da Silva et al. (1999),[31g] Booth et al. (2009),[32] Soonsin et al. (2010), [37b] Cappa et al. (2007),[31c] Bilde et al. (2003),[33d] Koponen et al. (2007),[33h] Riipinen (2007),[54] Zardini et al. (2006)[33f] and Pope et al. (2010).[33g] The vapor pressures from Bilde et al. (2003) are assumed to represent the subcooled liquid state. The lines represent a linear least squares fit using the gridded approach as described in Section 4.1.1. The solid state (black solid

line) and the subcooled liquid state (black dashed line). Lower panel: Best estimates (based on the fit) for the vapor pressure in the solid state at 298 K (black filled circle) and for the vapor pressure in the subcooled liquid state (black open symbol) together with the reported vapor pressures at 298 K by the individual experiments shown in the upper panel.

Figure 9: Upper panel: Saturation vapor pressure of the solid (filled symbols) and the subcooled liquid state (open symbols) of succinic acid, $C_4H_6O_4$, versus inverse temperature reported in the literature: Davies and Thomas (1960),[75] Ribeiro da Silva et al. (1999),[31g] Booth et al. (2009),[32] Bilde et al. (2003),[33d] Saleh et al. (2009),[23] Salo et al. (2010),[31d] Soonsin et al. (2010),[37b] Chattopadhyay & Ziemann (2005),[31b] Cappa et al. (2007),[31c] Bruns et al. (2012)[57] and Koponen et al. (2007).[33h] The lines represent a linear least squares fit using the gridded approach as described in Section 4.1.1. The solid state (black solid line) and the subcooled liquid state (black dashed line). Lower panel: Best estimates (based on the fit) for the vapor pressure in the solid state at 298 K (black filled circle) and for the vapor pressure in the subcooled liquid state state at 298 K (black open symbol) together with the reported vapor pressures at 298 K by the individual experiments shown in the upper panel.

Figure 10: Upper panel: Saturation vapor pressure of the solid state (filled symbols) and the subcooled liquid state (open symbols) of glutaric acid $C_5H_8O_4$ versus inverse temperature reported in the literature: Ribeiro da Silva et al. (1999),[31g] Booth et al. (2009),[32] Soonsin et al. (2010),[37b] Chattopadhyay & Ziemann (2005),[31b] Cappa et al. (2007),[31c] Bruns et al. (2012),[57] Tao & McMurry (1989),[76] Bilde et al. (2003),[33d] Koponen et al. (2007),[33h] Salo et al. (2010),[31d] Soonsin et al. (2010)[37b] and Pope et al. 2010.[33g] The vapor pressures from Bilde et al. (2003) are assumed to represent the subcooled liquid state. The lines represent a linear least squares fit using

the gridded approach as described in Section 4.1.1. Lower panel: Best estimates (based on the fit) for the vapor pressure in the solid state at 298 K (black filled circle) and for the vapor pressure in the subcooled liquid state state at 298 K (black open symbol) together with the reported vapor pressures at 298 K by the individual experiments shown in the upper panel.

Figure 11: Upper panel: Saturation vapor pressure of the solid state (filled symbols) and the subcooled liquid state (open symbols) of adipic acid, $C_6H_{10}O_4$, versus inverse temperature reported in the literature: Davies & Thomas (1960),[75] Booth et al. (2009),[32] Tao & McMurry (1989),[76] Bilde et al. (2003),[33d] Saleh et al. (2008),[31e] Saleh et al. (2009),[23] Saleh et al. (2010),[31f] Salo et al. (2010),[31d] Chattopadhyay & Ziemann (2005),[31b] Cappa et al. (2007),[31c] Bruns et al. (2012)[57] and Riipinen et al. (2007).[54] The lines represent a linear least squares fit using the gridded approach as described in Section 4.1.1. The solid state (black solid line) and the subcooled liquid state (black dashed line). Lower panel: Best estimates (based on the fit) for the vapor pressure in the solid state at 298 K (black filled circle) and for the vapor pressure in the subcooled liquid state state at 298 K (black open symbol) together with the reported vapor pressures at 298 K by the individual experiments shown in the upper panel.

Figure 12: Upper panel: Saturation vapor pressure of the solid state (filled symbols) and the subcooled liquid state (open symbols) of pimelic acid $C_7H_{12}O_4$,versus inverse temperature reported in the literature: Ribeiro da Silva et al. (1999),[31g] Salo et al. (2010),[31d] Chattopadhyay & Ziemann (2005),[31b] Cappa et al. (2007),[31c] Bruns et al. (2012),[57] Bilde et al. (2003),[33d] Saleh et al. (2008),[31e] Saleh et al. (2009),[23] Salo et al. (2010).[31d] The vapor pressures from Bilde et al. (2003), the type 2 data of Salo et al. (2010) and the data by Saleh et al. (2009) are assumed to represent the subcooled liquid state, see text for details. The lines represent a linear least squares fit using

the gridded approach as described in Section 4.1.1. The solid state (black solid line) and the subcooled liquid state (black dashed line). Lower panel: Best estimates (based on the fit) for the vapor pressure in the solid state at 298 K (black filled circle) and for the vapor pressure in the subcooled liquid state at 298 K (black open symbol) together with the reported vapor pressures at 298 K by the individual experiments shown in the upper panel.

Figure 13:

Upper panel: Saturation vapor pressure of the solid state (filled symbols) of suberic acid, $C_8H_{14}O_4$, versus inverse temperature reported in the literature: Davies & Thomas (1960),[75] Bilde et al. (2003),[33d] Salo et al. (2010),[31d] Chattopadhyay & Ziemann (2005),[31b] Cappa et al. (2007),[31c] and Bruns et al. (2012).[57] The line represents a linear least squares fit using the gridded approach as described in Section 4.1.1. Lower panel: Best estimates (based on the fit) for the vapor pressure in the solid state at 298 K (black filled circle) together with the reported vapor pressures at 298 K by the individual experiments shown in the upper panel.

Figure 14

Upper panel: Saturation vapor pressure of the solid state (filled symbols) of azelaic acid, $C_9H_{16}O_4$, versus inverse temperature reported in the literature: Ribeiro da Silva et al. (1999),[31g] Bilde et al. (2003),[33d] Cappa et al. (2007),[31c] Salo et al. (2010),[31d] Saleh et al. (2010),[31f] Bruns et al. (2012)[57] and Chattopadhyay & Ziemann (2005).[31b] The line represents a linear least squares fit using the gridded approach as described in Section 4.1.1. Lower panel: Best estimates (based on the fit) for the vapor pressure in the solid state at 298 K (black filled circle) together with the reported vapor pressures at 298 K by the individual experiments shown in the upper panel.

Figure 15: Upper panel: Saturation vapor pressure of the solid state (filled symbols) of sebacic acid ($C_{10}H_{18}O_4$) versus inverse temperature reported in the literature: Davies & Thomas (1960),[75] Salo et al. (2010),[31d] Chattopadhyay & Ziemann (2005),[31b] Cappa et al. (2007)[31c] and Bruns et al. (2012).[57] The line represents a linear least square fit using the gridded approach as described in Section 4.1.1. Lower panel: Best estimates (based on the fit) for the vapor pressure in the solid state at 298 K (black filled circle) together with the reported vapor pressures at 298 K by the individual experiments shown in the upper panel.

Figure 16: Subcooled liquid vapor pressure for the substituted dicarboxylic acids in Table 3 relative to the subcooled liquid vapor pressure of the parent acid (obtained using the same technique) at 298 K. The x-axis gives the substituent(s) present in the dicarboxylic acid. The parent acids are distinguished by color, the measurement techniques by the different symbols. The grey shaded markers refer to the oxo-group in the 3-position. An arrow associated with a data point indicates an upper limit.

Figure 17: Comparison of experimental subcooled liquid saturation vapor pressures (combined experimental) (Section 4, Table 3) with the subcooled saturation vapor pressures obtained from a series of estimation methods for straight chain dicarboxylic acids. For the C_2-C_7 dicarboxylic acids the experimental liquid state values from Table 3 were used. For the $>C_7$ dicarboxylic acids, the current best estimate solid state saturation vapor pressures were converted to subcooled liquid values using Equation 6 with melting points and enthalpies of fusion as reported by Roux et al. (2005).[147] VP refers to vapor pressures and Tb to boiling points. Estimation methods used: Nannoolal et al. (2008)[84] (VP)/Joback & Reid (1987)[91] (Tb), Nannoolal et al. (2008)[84] (VP)/Stein & Brown (1994)[88] (Tb), Nannoolal et al. (2008)[84] (VP)/Nannoolal et al. (2004)[85] (Tb), Myrdal &

Yalkowsky (1997),[83] (VP)/Joback & Reid (1987)[91] (Tb), Myrdal & Yalkowsky (1997)[83] (VP)/Stein & Brown (1994)[88] (Tb), Myrdal & Yalkowsky (1997)[83] (VP)/Nannoolal et al. (2004)[85] (Tb), Moller et al. (2008),[86] EVAPORATION,[81] and SIMPOL.[93]

Figure 18: Three different methods to constrain phase partitioning in complex mixtures that should converge, both for complex atmospheric samples and more constrained smog-chamber studies. Top-down methods involve predicting a distribution of compounds, saturation vapor pressures, and activity coefficients from first-principles chemical reaction mechanisms and thermodynamic relations. Molecular probes involve comparing predictions and observations of partitioning for a subset of molecules that can be measured in both phases and whose thermodynamics are well known. Bottom up methods involve empirically establishing the volatility distribution of a sample and perturbing the sample out of equilibrium via compression, dilution, or temperature change.

Table 1. A summary of conditions and key features of the experimental systems that have been applied for measurements of saturation vapor pressures and sublimation and vaporization enthalpies of C_2-C_{12} dicarboxylic acids. The systems are explained in more detail in Section 3.

Method	**Knudsen cell methods**		**Single particle methods**		**Particle size distribution methods**			**Thermal desorption methods**		
	Mass loss	KEMS	EDB	Optical tweezers	FT-TDMA	V-TDMA	IVM	TDPB-MS	TPD-PT-CIMS	ASAP-MS
Sample phase	Solid		Solid and liquid	Liquid	Solid and liquid	Solid and liquid	Solid	Solid		
Sample size	Bulk (few mg)		~Particles of diameter 5-20 µm		~Particles of diameter 10-600 nm			~µg of particles with diameter 100-300 nm	Macroscopic deposits of accumulation mode particles	Sample left after evaporation of solvent
Sample generation	Used as received		Flicking solid/droplet injection	Atomization	Atomization (+ drying), For IVM also dry condensation			Atomization + drying		Deposit sample on probe tip
Observable(s)	Δm(t)	Gas phase mass spectrum, relative gas phase concentration	D_p(t), particle morphology Tweezers: refractive index		Particle size distribution: TDMA + flowtube: D_p as a function of time VTDMA: D_p before and after heating IVM: Total aerosol volume before and after heating (obtained from D_p)			Gas phase mass spectrum, gas phase concentration as a function of time. Visual monitoring of sample		
Temperature [K]	253-543	298-338	248-315	280-304	288-333	298-573	298-333	271-333	290-385	327-389
RH [%]	Not applicable (dry)		0-95%	0-99%	0-95%	< 5%	< 10%	Not applicable (dry)		
Gas phase pressure [Pa]	$<10^{-2}$	$<10^{-3}$–10^{-5}	Atmospheric		Atmospheric			$6 \cdot 10^{-6}$	10^{-1}	Atmospheric

Table 2: A summary of experimentally derived solid, $p_s^0(298K)$, and subcooled liquid, $p_l^0(298K)$, saturation vapor pressures at 298 K along with enthalpies of sublimation, ΔH_{sub}, and vaporization, ΔH_{vap}, for C_2-C_{10} straight chain dicarboxylic acids. For each acid, the vapor pressure obtained from fitting the combined set of literature data as described in Section 4.1.1 is given in the first line, together with enthalpies of transition obtained as the average of the reported literature values. See also Figures 2-15. Best estimates are reported with uncertainties representing one standard deviation. See section 4.2 for the reasoning for providing these values as current best estimates. For each acid also the saturation vapor pressures at 298 K along with enthalpies of transition obtained from the individual studies is provided. If an asymmetric uncertainty was reported in the original study the largest value is reported herein.

References: Bilde et al. (2003),[33d] Booth et al. (2010),[35b] Bradley & Cotson (1953),[71b] Bruns et al. (2012),[57] Cappa et al. (2007),[31c] Cappa et al. (2008),[56b] Chattopadhyay & Ziemann (2005),[31b] Davies & Thomas (1960),[75] de Kruif et al. (1975),[71c] de Wit et al. (1983),[71d] Koponen et al. (2007),[33h] Noyes & Wobbe (1926),[71a] Pope et al. (2010),[33g] Ribeiro da Silva et al. (1999), [31g] Ribeiro da Silva et al. (2001),[34] Riipinen et al. (2007),[54] Saleh et al. (2008),[25] Saleh et al. (2009),[23] Saleh et al. (2010)[31f], Salo et al. (2010),[31d] Soonsin et al. (2010),[37b] Tao & McMurry (1989),[76] and Zardini et al. (2006).[33f]

Molecule	$p_s^0(298K)$ [Pa]	ΔH_{sub} [kJ mol^{-1}]	Reference	$p_l^0(298K)$ [Pa]	ΔH_{vap} [kJ mol^{-1}]	Reference
Oxalic acid $C_2H_2O_4$ 	$\left(1.4^{+0.6}_{-0.4}\right)\cdot10^{-2}$	91± 9		$\left(2.9^{+0.1}_{-0.1}\right)\cdot10^{-2}$	79 ± 15	
	(2.15±0.9)×10^{-2}	75 ± 11	Booth et al. (2010)	(2.9±1.5)×10^{-2}	79 ± 15	Soonsin et al. (2010)
	(3.1±0.1)×10^{-2}	90.6	Noyes & Wobbe (1926)			
	1.15×10^{-2}	98.2 ± 1.3	Bradley & Cotson (1953)			
	1.10×10^{-2}	93.7 ± 1.3	de Kruif et al. (1975)			
	1.8×10^{-2}	97.1	de Wit et al. (1983)			
	(2.5±0.9)×10^{-4}	n.a.	Soonsin et al. (2010)			
Malonic acid $C_3H_4O_4$ 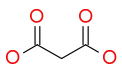	$\left(1.7^{+1.1}_{-0.7}\right)\cdot10^{-4}$	111± 15		$\left(6.2^{+3.2}_{-2.1}\right)\cdot10^{-4}$	115± 22	
	(5.73±2.29)×10^{-4}	92 ± 13	Booth et al. (2010)	(5.3±2.7)×10^{-4}	92 ± 15	Bilde et al. (2003)#
	(8.0±2.9)×10^{-5}	107 ± 4	Soonsin et al. (2010)	(4.9±1.0)×10^{-4}	122.1 ± 24.8	Riipinen et al. (2007)
	(6.7±2.6)×10^{-4}	111.4 ± 0.7	Ribeiro da Silva et al. (1999)	(9.0±4.4)×10^{-4}	137 ± 16	Pope et al. (2010), EDB
	(2.2±0.5)×10^{-4}	132.1 ± 5	Cappa et al. (2008)	(4.5±2.8)×10^{-4}	n.a.	Pope et al. (2010), Tweezers
				(6.7±2.6)×10^{-4}	141.9 ± 19.9	Pope et al. (2010)
				(4.3±1.5)×10^{-4}	96 ± 11	Soonsin et al. (2010)
				(3.2±1.2)×10^{-4}	100 ± 17	Zardini et al. (2006)
Succinic acid $C_4H_6O_4$ 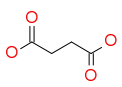	$\left(7.7^{+5.0}_{-3.0}\right)\cdot10^{-5}$	115± 15		$\left(1.3^{+1.5}_{-0.7}\right)\cdot10^{-3}$	105 ± 1	
	(1.13±0.45)×10^{-4}	93 ± 14	Booth et al. (2010)	(1.7±0.5)×10^{-3}	106 ± 8	Soonsin et al. (2010)
	(6.0±2.1)×10^{-6}	125 ± 8	Soonsin et al. (2010)	(9.9±2.4)×10^{-4}	104.1 ± 23.1	Koponen et al. (2007)
	(3.6±1.5)×10^{-5}	123.2 ± 2.6	Ribeiro da Silva et al. (2001)			
	(3.2±0.6)×10^{-5}	128 ± 2	Cappa et al. (2007)			
	(4.6±2.3)×10^{-5}	138 ± 11	Bilde et al. (2003)			
	(6.4±2.0)×10^{-5}	112 ± 12	Salo et al. (2010)			
	(3.7±1.1)×10^{-4}	88 ± 3	Saleh et al. (2009)			
	4.2×10^{-5}	118 ± 3	Davies & Thomas (1960)			
	1.37×10^{-4}	119.5	Chattopadhyay & Ziemann (2005)			
	(2.5±0.7)×10^{-5}	107 ± 2	Bruns et al. (2012)*			
Glutaric acid	$\left(1.7^{+1.5}_{-0.8}\right)\cdot10^{-4}$	130 ± 11		$\left(1.0^{+0.3}_{-0.2}\right)\cdot10^{-3}$	100 ± 5	

$C_5H_8O_4$ 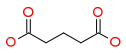	$(4.2\pm1.7)\times10^{-4}$ $(4.8\pm1.6)\times10^{-5}$ $(2.5\pm1.6)\times10^{-4}$ $(1.2\pm0.6)\times10^{-4}$ 4.04×10^{-4} $(4.1\pm2.9)\times10^{-6}$	123 ± 18 122± 8 119.8 ± 1.2 134 ± 4 132.3 149 ± 10	Booth et al. (2010) Soonsin et al. (2010) Ribeiro da Silva et al. (1999) Cappa et al. (2007) Chattopadhyay & Ziemann (2005) Bruns et al. (2012)*	$(9.3\pm2.8)\times10^{-4}$ $(9.2\pm4.6)\times10^{-4}$ $(7.1\pm2.2)\times10^{-4}$ $11.2\pm9.6)\times10^{-4}$ $(8.5\pm3.1)\times10^{-4}$ $(1.0\pm0.2)\times10^{-3}$	99 ± 8 91 ± 7 106.1 ± 23.2 100.8 ± 23.9 101 ± 20 102	Soonsin et al. (2010) Bilde et al. (2003)# Koponen et al. (2007) Pope et al. (2010) Salo et al. (2010)# Tao & McMurry (1989)#
Adipic acid $C_6H_{10}O_4$	$\left(1.9^{+1.4}_{-0.8}\right)\cdot10^{-5}$	131 ± 18		$\left(1.8^{+1.0}_{-0.7}\right)\cdot10^{-4}$	113 ± 22	
	$(6.00\pm2.4)\times10^{-6}$ $(2.6\pm1.0)\times10^{-6}$ $(1.4\pm0.7)\times10^{-5}$ $(5.8\pm1.8)\times10^{-5}$ $(3.4\pm1.2)\times10^{-5}$ 8.4×10^{-6} 3.02×10^{-5} $(1.3\pm1.0)\times10^{-6}$ $(1.5\pm0.2)\times10^{-5}$	119 ± 18 145 ± 5 154 ± 6 97 ± 8 135 ± 13 129 ± 1 146.2 136 ± 10 118	Booth et al. (2010) Cappa et al. (2007) Bilde et al. (2003) Salo et al. (2010) Saleh et al. (2008) Davies & Thomas (1960) Chattopadhyay & Ziemann (2005) Bruns et al. (2012)* Tao & McMurry (1989)	$(1.7\pm0.3)\times10^{-4}$	113.2 ± 21.8	Riipinen et al. (2007)
Pimelic acid $C_7H_{12}O_4$ 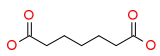	$\left(1.1^{+2.7}_{-0.8}\right)\cdot10^{-5}$	148 ± 16		$\left(2.2^{+1.9}_{-1.0}\right)\cdot10^{-4}$	141 ± 12	
	$(3.9\pm0.6)\times10^{-6}$ $(1.8\pm6.0)\times10^{-5}$ 2.47×10^{-5} 6.54×10^{-6} $(6.0\pm3.3)\times10^{-7}$ $(1.2\pm0.5)\times10^{-5}$	153 ± 4 161 ± 50 124.0 80.0 162 ± 19 139.9 ± 1.0	Cappa et al. (2007) Salo et al. (2010) Chattopadhyay & Ziemann (2005) Chattopadhyay & Ziemann (2005) Bruns et al. (2012)* Ribeiro da Silva et al. (1999)	$(1.0\pm0.5)\times10^{-4}$ $(1.7\pm0.8)\times10^{-4}$ $(7.2\pm1.7)\times10^{-5}$	147 ± 11 127 ± 20 149 ± 10	Bilde et al. (2003)# Salo et al. (2010) Saleh et al. (2008)#
Suberic acid $C_8H_{14}O_4$ 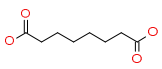	$\left(3.3^{+2.4}_{-1.4}\right)\cdot10^{-6}$	148 ± 28				
	$(1.8\pm1.2)\times10^{-7}$ $(1.6\pm0.8)\times10^{-6}$ $(1.4\pm0.6)\times10^{-5}$ 1.0×10^{-6} 3.29×10^{-6} $(4.0\pm1.8)\times10^{-7}$	168 ± 7 184 ± 12 101 ± 10 143 ± 4 148.0 144 ± 10	Cappa et al. (2007) Bilde et al. (2003) Salo et al. (2010) Davies & Thomas (1960) Chattopadhyay & Ziemann (2005) Bruns et al. (2012)*			
Azelaic acid $C_9H_{16}O_4$ 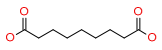	$\left(1.7^{+2.7}_{-1.0}\right)\cdot10^{-5}$	146 ± 26				
	$(1.0\pm0.6)\times10^{-8}$ $(9.4\pm4.7)\times10^{-6}$ $(4.7\pm0.8)\times10^{-5}$ $(1.4\pm0.5)\times10^{-5}$ 7.41×10^{-6} $(6.9\pm4.2)\times10^{-8}$ $(6.3\pm5.0)\times10^{-7}$	178 ± 5 153 ± 24 96 ± 5 145 ± 15 138.0 155 ± 13 159.9 ± 1.6	Cappa et al. (2007) Bilde et al. (2003) Salo et al. (2010) Saleh et al. (2010), atomization Chattopadhyay & Ziemann (2005) Bruns et al. (2012)* Ribeiro da Silva et al. (1999)			
Sebacic acid $C_{10}H_{18}O_4$ 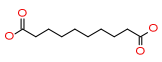	$\left(4.8^{+11.5}_{-3.4}\right)\cdot10^{-7}$	148 ± 30				
	$(1.6\pm0.8)\times10^{-8}$ $(9\pm5)\times10^{-6}$ 7.6×10^{-8} 1.47×10^{-6} $(7.8\pm3.2)\times10^{-8}$	181 ± 8 100 ± 12 161 ± 3 146.5 152 ± 3	Cappa et al. (2007) Salo et al. (2010) Davies and Thomas (1960) Chattopadhyay & Ziemann (2005) Bruns et al. (2012)*			
Undecanedioic acid $C_{11}H_{20}O_4$ 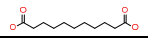		152 ± 15				
	$(1.9\pm1.8)\times10^{-7}$ 3.25×10^{-6}	162.5 ± 1.9 141.5	Ribeiro da Silva et al. (1999) Chattopadhyay & Ziemann (2005)			
Dodecanedioic		157 ± 8				

acid $C_{12}H_{22}O_4$ 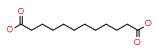	$(3.4\pm1.1)\times10^{-8}$ 1.0×10^{-7} 2.42×10^{-6} $(4.7\pm3.3)\times10^{-8}$	169 ± 4 153 ± 3 156.0 150 ± 36	Cappa et al. (2007) Davies & Thomas (1960) Chattopadhyay & Ziemann (2005) Bruns et al. (2012)*			

Reported as p_s^0, but likely p_l^0, see text

* to obtain the values and uncertainties at 298 K, a linear regression to the reported temperature dependent vapor pressures was performed, and the uncertainty given here is the 95% confidence interval

Table 3: Experimentally derived solid state, $p_s^0(298K)$, and subcooled liquid, $p_l^0(298K)$, saturation vapor pressures at 298 K and enthalpies of sublimation, ΔH_{sub}, and vaporization, ΔH_{vap}, for substituted dicarboxylic acids. The saturation vapor pressures and transition enthalpies for the phase state studied (or most likely studied) in a given experiment are highlighted as bold. The number of significant figures and the uncertainties are reported as quoted in the individual studies. If the solid state was the one studied experimentally the liquid state saturation vapor pressure and enthalpy of sublimation was obtained using Equation 6 with melting points and Enthalpies of fusion as reported by Booth et al. 2010. The ratios $\frac{p^0_{s,i}}{p^0_{s,parent\ acid}}$ and $\frac{p^0_{l,i}}{p^0_{l,parent\ acid}}$ were calculated as the ratios between the saturation vapor pressure of the substituted dicarboxylic acid and the vapor pressure of the parent dicarboxylic acid obtained using the same measurement method.

References: Bilde et al. (2003),[33d] Bilde & Pandis (2001),[33c] Booth et al. (2010),[35b] Chattopadhyay & Ziemann (2005),[31b] Frosch et al. (2010),[50c] Mønster et al. (2004 and 2006),[50d,e] Huisman et al. (2013),[148] Ribeiro da Silva et al. (2000),[149] and Ribeiro da Silva et al. (2001).[34]

Molecule	**Substituent(s) structure** (b)	ΔT [a] [K]	$p^0_{s,i}$ **298 K** [Pa]	$\Delta H_{sub,i}$ [kJ mol^{-1}]	$p^0_{l,i}$ **298 K** [Pa]	$\Delta H_{vap,i}$ [kJ mol^{-1}]	$\frac{p^0_{s,i}}{p^0_{s,parent\ ac}}$ **298 K** (b)	$\frac{p^0_{l,i}}{p^0_{l,parent\ acia}}$ **298 K** (b)	**Method**	**Reference comment**
2-methyl-malonic acid	-CH_3 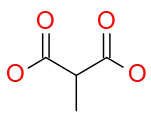	298-318	**(3.34±1.34)×10^{-4}**	**87±13**	(5.34±4.01)×10^{-3}	56	0.6	1.7	Knudsen cell	Booth et al. (2010)
		341-355	**(5.81±2.90)×10^{-4}**	**116.2±0.9**	9.2×10^{-3}	85	0.9	1.7	Knudsen cell	Ribeiro da Silva et al. (2000)
		290-304	See text	See text	**(9.1±3.2)×10^{-4}**	**106±20**	n.a.	1.9	TDMA	Mønster et al. (2004, 2006) #
		270-294			**(1.1±0.3)×10^{-3}**	**89±15**	n.a.	2.6	EDB	Huisman et al. (2013)
2,2-dimethyl-malonic acid	-CH_3, -CH_3 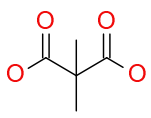	347-363	**(3.32±1.79)×10^{-4}**	**110.2±1.0**	n.a.	n.a.	0.5	n.a.	Knudsen cell	Ribeiro da Silva et al. (2000)
		293-304	See text	See text	**(2.6±0.9)×10^{-4}**	**119±8**	n.a.	0.5	TDMA	Mønster et al. (2004) #
Ethyl-malonic acid	-CH_2CH_3 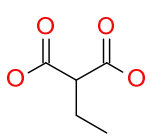	347-362	**(3.14±1.93)×10^{-4}**	**111.2±1.2**	n.a.	n.a.	0.5	n.a.	Knudsen cell	Ribeiro da Silva et al. (2000)
Butyl-malonic acid	- $(CH_2)_3CH_3$ 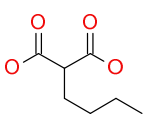	348-362	**(1.55±1.10)×10^{-4}**	**122.5±1.4**	n.a.	n.a.	0.2	n.a.	Knudsen cell	Ribeiro da Silva et al. (2000)
2-methyl-succinic acid	-CH_3 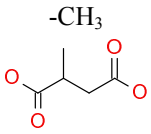	298-318	**(2.54±1.02)×10^{-4}**	**100±15**	(5.58±4.19)×10^{-4}	90	2.2	0.1	Knudsen cell	Booth et al. (2010)
		343-360	**(2.95±1.15)×10^{-4}**	**120.2±0.7**	6.5×10^{-4}	110	8.1	0.5	Knudsen cell	Ribeiro da Silva et al. (2001)
		291-293	**(1.6±0.5)×10^{-3}**	**92±26**	3.5×10^{-3}	n.a.	36	3.5	TDMA	Mønster et al. (2004)
2,2-dimethyl-succinic acid	-CH_3,-CH_3	350-365	**(1.25±0.75)×10^{-4}**	**120.9±1.0**	n.a.	n.a.	3.5	n.a.	Knudsen cell	Ribeiro da Silva et al. (2001)

	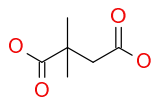	291-300	**(1.5±0.5)×10^{-3}**	**67±10**	n.a.	n.a.	34	n.a.	TDMA	Mønster et al. (2004)
2-methyl-glutaric acid	-CH_3 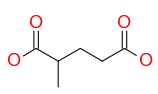	298-318	**(1.85±0.74)×10^{-4}**	**82±12**	(9.63±7.22)×10^{-4}	52	0.4	0.5	Knudsen cell	Booth et al. (2010)
		338-348	**(2.32±1.79)×10^{-4}**	**125.1±1.4**	1.2×10^{-3}	95	0.9	1.0	Knudsen cell	Ribeiro da Silva et al. (2001)
		254-292	n.a.	n.a.	(1.0±0.2)×10^{-3}	97.3±3.5	n.a.	1.1	EDB	Huisman et al. (2013)
2,2-dimethyl-glutaric acid	-CH_3, -CH_3 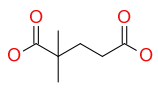	342-353	**(1.68±1.27)×10^{-4}**	**125.1±1.4**	n.a.	n.a.	0.7	n.a.	Knudsen cell	Ribeiro da Silva et al. (2001)
3-methyl-glutaric acid	-CH_3 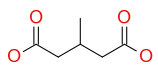	298-318	**(1.77±0.71)×10^{-4}**	**86±13**	(9.19±6.89)×10^{-4}	59	0.4	0.5	Knudsen cell	Booth et al. (2010)
		300-303	See text	See text	(7.3±2.6)×10^{-4}	61±12	n.a.	0.8	TDMA	Mønster et al. (2004)#
3,3-dimethyl-glutaric acid	-CH_3, -CH_3 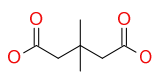	291-300	See text	See text	(2.3±0.8)×10^{-3}	60±16	n.a.	2.6	TDMA	Mønster et al. (2004) #
3-methyl-adipic acid	-CH_3 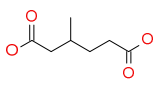	293-304	**(1.3±0.5)×10^{-4}**	**215±16**	n.a.		9.5	n.a.	TDMA	Mønster et al. (2004)
2-amino-succinic (aspartic) acid	-NH_2 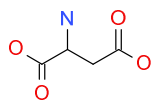	298-318	**(6.71±2.68)×10^{-4}**	**53±8**	(2.56±1.92)×10^{-2}	25	5.9	6.6	Knudsen cell	Booth et al. (2010)
2-amino-glutaric (glutamic) acid	-NH_2 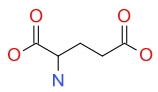	298-318	**(3.60±1.44)×10^{-5}**	**63±9**	(2.05±1.54)×10^{-3}	32	0.1	1.0	Knudsen cell	Booth et al. (2010)
2-oxo-succinic acid	=O 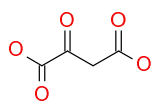	298-318	**(8.23±3.29)×10^{-5}**	**81±12**	(1.67±1.25)×10^{-2}	31	0.7	4.3	Knudsen cell	Booth et al. (2010)
2-oxo-succinic acid oxidation products[c]	n.a.	294	n.a.	n.a.	(1.0±0.3)×10^{-5}	n.a.	n.a.	n.a.	TDMA	Frosch et al. (2010) Phase unknown
2-oxo-glutaric acid	=O 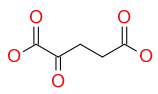	298-318	**(1.23±0.49)×10^{-4}**	**53±8**	(2.02±1.52)×10^{-3}	18	0.3	1.0	Knudsen cell	Booth et al. (2010)
		295			(3.2±0.8)×10^{-5}	n.a.	n.a.	0.05	TDMA	Frosch et al. (2010) assumed liquid
		270-285	**(1.75±0.52)×10^{-3}**	**100.0**	2.9×10^{-2}	n.a.	4.3	15	Thermal desorption	Chattopadhyay & Ziemann (2005)
3-oxo-glutaric acid	=O 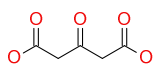	**298-318**	**(5.96±2.38)×10^{-5}**	89±13	(3.22±2.42)×10^{-3}	43	0.1	1.6	Knudsen cell	Booth et al. (2010)
		310-322	**(6.06±1.82)×10^{-6}**	**160.2**	3.2×10^{-4}	n.a.	0.02	0.2	Thermal desorption	Chattopadhyay & Ziemann (2005)
3-oxo-glutaric oxidation producs[c]	n.a.	295	n.a.	n.a.	(1.6±0.4)×10^{-5}	n.a.	n.a.	n.a.	TDMA	Frosch et al. (2010) Phase unknown
2-oxo-adipic acid	=O 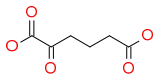	281-301	**(6.29±1.89)×10^{-5}**	**127.0**	n.a.	n.a.	2.1	n.a.	Thermal desorption	Chattopadhyay & Ziemann (2005)
3-oxo-adipic acid	=O 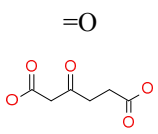	307-329	**(6.89±2.07)×10^{-7}**	**151.0**	n.a.	n.a.	0.02	n.a.	Thermal desorption	Chattopadhyay & Ziemann (2005)

4-oxo-pimelic acid	=O 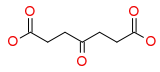	295	n.a.	n.a.	$(3.0\pm0.8)\times10^{-6}$	n.a.	n.a.	0.06	TDMA	Frosch et al. (2010)
5-oxo-azelaic acid	=O 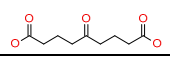	312-330	**$(1.16\pm0.35)\times10^{-6}$**	**118.0**	n.a.	n.a.	0.2	n.a.	Thermal desorption	Chattopadhyay & Ziemann (2005)
2-hydroxy-malonic (tartronic) acid	-OH 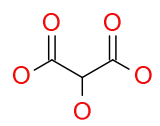	298-318 297-314	**$(2.50\pm1.00)\times10^{-4}$**	**69±10**	$(5.64\pm4.23)\times10^{-3}$ $(4.4\pm1.2)\times10^{-6}$	38 120±19	0.4	1.8 0.01	Knudsen cell EDB	Booth et al. (2010) Huisman et al. (2013)
2-hydrox-succinc (malic) acid	-OH 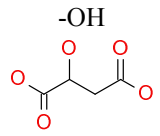	298-318	**$(6.37\pm2.55)\times10^{-5}$**	**81±12**	$(8.72\pm6.54)\times10^{-4}$	52	0.6	0.2	Knudsen cell	Booth et al. (2010)
2,3-dihydroxy-succinic (tartaric) acid	-OH, -OH 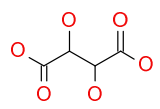	298-318 ~305	**$(1.79\pm0.72)\times10^{-4}$**	**68±10**	$(3.23\pm2.42)\times10^{-1}$ $(3.2\pm1.0)\times10^{-7}$ @~305 K $(1.8-24)\times10^{-8}$ @298 K	5	1.6	84 10^{-5}-10^{-4}	Knudsen cell EDB	Booth et al. (2010) Huisman et al. (2013)
2-hydroxy,2-methyl-succinic acid	-OH, -CH_3 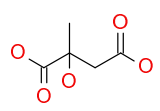	298-318	**$(4.90\pm1.96)\times10^{-4}$**	**104±16**	$(7.48\pm5.61)\times10^{-3}$	68	4.3	1.9	Knudsen cell	Booth et al. (2010)
3-hydroxy,3-carboxyl-glutaric (citric) acid	-COOH, -OH 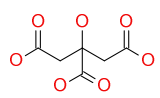	298-318 308-311	**$(3.79\pm1.52)\times10^{-5}$**	**64±10**	$(3.10\pm2.33)\times10^{-3}$ $<1.6\times10^{-7}$ @~311 K $<4.0\times10^{-8}$ @298 K	21	0.1	1.6 $<4\times10^{-5}$	Knudsen cell EDB	Booth et al. (2010) Huisman et al. (2013)
1,1-cyclopropane-dicarboxylic acid	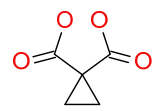	298-318	**$(5.95\pm2.38)\times10^{-4}$**	**126±19**	$(3.10\pm2.33)\times10^{-3}$	n.a.	n.a.	1.6	Knudsen cell	Booth et al. (2011)
1,1-cyclobutane-dicarboxylic acid	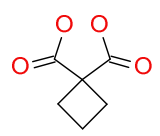	298-318	**$(1.13\pm0.45)\times10^{-4}$**	**84±13**	$(6.47\pm4.85)\times10^{-3}$	n.a.	n.a.	30	Knudsen cell	Booth et al. (2011)
1,2-cyclopentane-diacarboyxlic acid	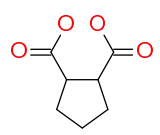	298-318	**$(5.97\pm2.39)\times10^{-5}$**	**66±10**	$(3.47\pm2.60)\times10^{-4}$	n.a.	n.a.	n.a.	Knudsen cell	Booth et al. (2011)
1,3-cyclohexane-dicarboxylic acid	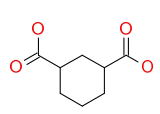	298-318	**$(1.17\pm0.47)\times10^{-4}$**	**67±10**	$(4.60\pm3.45)\times10^{-4}$	n.a.	n.a.	n.a.	Knudsen cell	Booth et al. (2011)
trans-norpinic acid		290-312	**$(1.4\pm0.7C)\times10^{-4}$**	**42±51**	n.a.	n.a.	n.a.	n.a.	TDMA	Bilde & Pandis (2001)
pinic acid	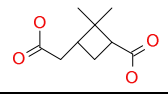	290-323	**$(4.4\pm2.2)\times10^{-5}$**	**109±21**	n.a.	n.a.	n.a.	n.a.	TDMA	Bilde & Pandis (2001)

Reported as p_s^0, but likely p_l^0, see text

References

(1) (a) Watson, J. G. *J. Air Waste Manage. Assoc.* **2002**, *52*, 628. (b) Mazurek, M.; Masonjones, M. C.; Masonjones, H. D.; Salmon, L. G.; Cass, G. R.; Hallock, K. A.; Leach, M. *J. Geophys. Res.: Atmos.* **1997**, *102*, 3779.

(2) (a) Belleudi, V.; Faustini, A.; Stafoggia, M.; Cattani, G.; Marconi, A.; Perucci, C. A.; Forastiere, F. *Epidemiology* **2010**, *21*, 414. (b) Pope, C. A.; Dockery, D. W. *J. Air Waste Manage. Assoc.* **2006**, *56*, 709. (c) Raaschou-Nielsen, O.; Andersen, Z. J.; Beelen, R.; Samoli, E.; Stafoggia, M.; Weinmayr, G.; Hoffmann, B.; Fischer, P.; Nieuwenhuijsen, M. J.; Brunekreef, B.; Xun, W. W.; Katsouyanni, K.; Dimakopoulou, K.; Sommar, J.; Forsberg, B.; Modig, L.; Oudin, A.; Oftedal, B.; Schwarze, P. E.; Nafstad, P.; De Faire, U.; Pedersen, N. L.; Ostenson, C. G.; Fratiglioni, L.; Penell, J.; Korek, M.; Pershagen, G.; Eriksen, K. T.; Sorensen, M.; Tjonneland, A.; Ellermann, T.; Eeftens, M.; Peeters, P. H.; Meliefste, K.; Wang, M.; Bueno-de-Mesquita, B.; Key, T. J.; de Hoogh, K.; Concin, H.; Nagel, G.; Vilier, A.; Grioni, S.; Krogh, V.; Tsai, M. Y.; Ricceri, F.; Sacerdote, C.; Galassi, C.; Migliore, E.; Ranzi, A.; Cesaroni, G.; Badaloni, C.; Forastiere, F.; Tamayo, I.; Amiano, P.; Dorronsoro, M.; Trichopoulou, A.; Bamia, C.; Vineis, P.; Hoek, G. *Lancet Oncology* **2013**, *14*, 813. (d) Loomis, D.; Grosse, Y.; Lauby-Secretan, B.; El Ghissassi, F.; Bouvard, V.; Benbrahim-Tallaa, L.; Guha, N.; Baan, R.; Mattock, H.; Straif, K.; Iarc *Lancet Oncology* **2013**, *14*, 1262. (e) Pope, C. A., III; Ezzati, M.; Dockery, D. W. *New England Journal of Medicine* **2009**, *360*, 376. (f) Chen, Y. Y.; Ebenstein, A.; Greenstone, M.; Li, H. B. *Proc. Natl. Acad. Sci. U. S. A.* **2013**, *110*, 12936. (g) Lim, S. S.; Vos, T.; Flaxman, A. D. *Lancet* **2013**, *381*, 1276.

(3) IPCC *Climate Change 2013: The Physical Science Basis. Contribution of Working Group 1 to the Fifth Assessment Report of the Intergovernmental Panel of Climate Change*; Cambridge University Press: Cambridge, United Kingdom, 2013.

(4) Jimenez, J. L.; Canagaratna, M. R.; Donahue, N. M.; Prevot, A. S. H.; Zhang, Q.; Kroll, J. H.; DeCarlo, P. F.; Allan, J. D.; Coe, H.; Ng, N. L.; Aiken, A. C.; Docherty, K. S.; Ulbrich, I. M.; Grieshop, A. P.; Robinson, A. L.; Duplissy, J.; Smith, J. D.; Wilson, K. R.; Lanz, V. A.; Hueglin, C.; Sun, Y. L.; Tian, J.; Laaksonen, A.; Raatikainen, T.; Rautiainen, J.; Vaattovaara, P.; Ehn, M.; Kulmala, M.; Tomlinson, J. M.; Collins, D. R.; Cubison, M. J.; Dunlea, E. J.; Huffman, J. A.; Onasch, T. B.; Alfarra, M. R.; Williams, P. I.; Bower, K.; Kondo, Y.; Schneider, J.; Drewnick, F.; Borrmann, S.; Weimer, S.; Demerjian, K.; Salcedo, D.; Cottrell, L.; Griffin, R.; Takami, A.; Miyoshi, T.; Hatakeyama, S.; Shimono, A.; Sun, J. Y.; Zhang, Y. M.; Dzepina, K.; Kimmel, J. R.; Sueper, D.; Jayne, J. T.; Herndon, S. C.; Trimborn, A. M.; Williams, L. R.; Wood, E. C.; Middlebrook, A. M.; Kolb, C. E.; Baltensperger, U.; Worsnop, D. R. *Science* **2009**, *326*, 1525.

(5) Hallquist, M.; Wenger, J. C.; Baltensperger, U.; Rudich, Y.; Simpson, D.; Claeys, M.; Dommen, J.; Donahue, N. M.; George, C.; Goldstein, A. H.; Hamilton, J. F.; Herrmann, H.; Hoffmann, T.; Iinuma, Y.; Jang, M.; Jenkin, M. E.; Jimenez, J. L.; Kiendler-Scharr, A.; Maenhaut, W.; McFiggans, G.; Mentel, T. F.; Monod, A.; Prevot, A. S. H.; Seinfeld, J. H.; Surratt, J. D.; Szmigielski, R.; Wildt, J. *Atmos. Chem. Phys.* **2009**, *9*, 5155.

(6) Pankow, J. F. *Atmos. Environ.* **1994**, *28*, 185.

(7) (a) McFiggans, G.; Topping, D. O.; Barley, M. H. *Atmos. Chem. Phys.* **2010**, *10*, 10255. (b) Decesari, S.; Facchini, M. C.; Fuzzi, S.; Tagliavini, E. *J. Geophys. Res.: Atmos.* **2000**, *105*, 1481. (c) Saxena, P.; Hildemann, L. M. *J. Atmos. Chem.* **1996**, *24*, 57.

(8) (a) Donahue, N. M.; Trump, E. R.; Pierce, J. R.; Riipinen, I. *Geophys. Res. Lett.* **2011**, *38*, L16801. (b) Barsanti, K. C.; Pankow, J. F. *Atmos. Environ.* **2004**, *38*, 4371. (c) Valorso, R.; Aumont, B.; Camredon, M.; Raventos-Duran, T.; Mouchel-Vallon, C.; Ng, N. L.; Seinfeld, J. H.; Lee-Taylor, J.; Madronich, S. *Atmos. Chem. Phys.* **2011**, *11*, 6895.

(9) Ehn, M.; Thornton, J. A.; Kleist, E.; Sipila, M.; Junninen, H.; Pullinen, I.; Springer, M.; Rubach, F.; Tillmann, R.; Lee, B.; Lopez-Hilfiker, F.; Andres, S.; Acir, I. H.; Rissanen, M.; Jokinen, T.; Schobesberger, S.; Kangasluoma, J.; Kontkanen, J.; Nieminen, T.; Kurten, T.; Nielsen, L. B.; Jorgensen, S.; Kjaergaard, H. G.; Canagaratna, M.; Dal Maso, M.; Berndt, T.; Petaja, T.; Wahner, A.; Kerminen, V. M.; Kulmala, M.; Worsnop, D. R.; Wildt, J.; Mentel, T. F. *Nature* **2014**, *506*, 476.

(10) Goldstein, A. H.; Galbally, I. E. *Environ. Sci. Technol.* **2007**, *41*, 1514.

(11) Calvert, J. G. *Pure Appl. Chem.* **1990**, *62*, 2167.

(12) Prausnitz, J. M.; Lichtenthaler, R. N.; Azevedo, E. G. d. *Molecular Thermodynamics of Fluid-Phase Equilibria*; Third Edition ed.; Pretentice Hall, Inc. : Upper Saddle River, New Jersey, 1999.

(13) Lienhard, D. M.; Zobrist, B.; Zuend, A.; Krieger, U. K.; Peter, T. *J. Chem. Phys.* **2012**, *136*, 074515.

(14) Seinfeld, J. H.; Pandis, S. N. *Atmospheric Chemistry and Physics: From Air Pollution to Climate Change*; 2nd ed.; John Wiley & Sons Inc.: Hoboken, NY, 2006.

(15) Donahue, N. M.; Trump, E. R.; Pierce, J. R.; Riipinen, I. *Geophys. Res. Lett.* **2011**, *38*.

(16) Hinds, W. C. *Aerosol Technology - Properties, Behaviour and Measurement of Airborne Particles* 2nd revised ed.; John Wiley & Sons, Inc: New York, NY, 1999.

(17) Kulmala, M.; Laaksonen, A. *J. Chem. Phys.* **1990**, *93*, 696.

(18) Pruppacher, H. R.; Klett, J. D. In *Microphysics of Clouds and Precepitiation*; Kluwer Academic Publishers: Dordrecht, The Netherlands, 1998.

(19) (a) Vesala, T.; Kulmala, M.; Rudolf, R.; Vrtala, A.; Wagner, P. E. *J. Aerosol Sci.* **1997**, *28*, 565. (b) Kulmala, M. *Aerosol Sci. Technol.* **1993**, *19*, 381. (c) Davis, E. J. *Aerosol Sci. Technol.* **1983**, *2*, 121. (d) Kolb, C. E.; Cox, R. A.; Abbatt, J. P. D.; Ammann, M.; Davis, E. J.; Donaldson, D. J.; Garrett, B. C.; George, C.; Griffiths, P. T.; Hanson, D. R.; Kulmala, M.; McFiggans, G.; Poeschl, U.; Riipinen, I.; Rossi, M. J.; Rudich, Y.; Wagner, P. E.; Winkler, P. M.; Worsnop, D. R.; O' Dowd, C. D. *Atmos. Chem. Phys.* **2010**, *10*, 10561. (e) Vehkamaki, H.; Riipinen, I. *Chem. Soc. Rev.* **2012**, *41*, 5160.

(20) Julin, J.; Winkler, P. M.; Donahue, N. M.; Wagner, P. E.; Riipinen, I. *Environ. Sci. Technol.* **2014**, *48*, 12083.

(21) Krieger, U. K.; Marcolli, C.; Reid, J. P. *Chem. Soc. Rev.* **2012**, *41*, 6631.

(22) Miles, R. E. H.; Reid, J. P.; Riipinen, I. *J. Phys. Chem. A* **2012**, *116*, 10810.

(23) Saleh, R.; Shihadeh, A.; Khlystov, A. *J. Aerosol Sci.* **2009**, *40*, 1019.

(24) Kroll, J. H.; Donahue, N. M.; Jimenez, J. L.; Kessler, S. H.; Canagaratna, M. R.; Wilson, K. R.; Altieri, K. E.; Mazzoleni, L. R.; Wozniak, A. S.; Bluhm, H.; Mysak, E. R.; Smith, J. D.; Kolb, C. E.; Worsnop, D. R. *Nature Chem.* **2011**, *3*, 133.

(25) Donahue, N. M.; Kroll, J. H.; Pandis, S. N.; Robinson, A. L. *Atmos. Chem. Phys.* **2012**, *12*, 615.

(26) Riipinen, I.; Pierce, J. R.; Yli-Juuti, T.; Nieminen, T.; Hakkinen, S.; Ehn, M.; Junninen, H.; Lehtipalo, K.; Petaja, T.; Slowik, J.; Chang, R.; Shantz, N. C.; Abbatt, J.; Leaitch, W. R.; Kerminen, V. M.; Worsnop, D. R.; Pandis, S. N.; Donahue, N. M.; Kulmala, M. *Atmos. Chem. Phys.* **2011**, *11*, 3865.

(27) Pankow, J. F. *Atmos. Environ.* **1994**, *28*, 189.

(28) (a) Marcolli, C.; Luo, B. P.; Peter, T. *J. Phys. Chem. A* **2004**, *108*, 2216. (b) Cappa, C. D.; Lovejoy, E. R.; Ravishankara, A. R. *Proc. Natl. Acad. Sci. U. S. A.* **2008**, *105*, 18687.

(29) Donahue, N. M.; Robinson, A. L.; Stanier, C. O.; Pandis, S. N. *Environ. Sci. Technol.* **2006**, *40*, 2635.

(30) (a) Barley, M.; Topping, D. O.; Jenkin, M. E.; McFiggans, G. *Atmos. Chem. Phys.* **2009**, *9*, 2919. (b) Barley, M. H.; Topping, D.; Lowe, D.; Utembe, S.; McFiggans, G. *Atmos. Chem. Phys.* **2011**, *11*, 13145. (c) Barley, M. H.; McFiggans, G. *Atmos. Chem. Phys.* **2010**, *10*, 749. (d) O'Meara, S.; Booth, A. M.; Barley, M. H.; Topping, D.; McFiggans, G. *Phys. Chem. Chem. Phys.* **2014**, *16*, 19453. (e) Topping, D. O.; Barley, M. H.; McFiggans, G. *Atmos. Chem. Phys.* **2011**, *11*, 7767. (f) Topping, D.; Barley, M.; McFiggans, G. *Faraday Discuss.* **2013**, *165*, 273.

(31) (a) Ribeiro da Silva, M. A. V.; Monte, M. J. S. *Thermochim. Acta* **1990**, *171*, 169. (b) Chattopadhyay, S.; Ziemann, P. J. *Aerosol Sci. Technol.* **2005**, *39*, 1085. (c) Cappa, C. D.; Lovejoy, E. R.; Ravishankara, A. R. *J. Phys. Chem. A* **2007**, *111*, 3099. (d) Salo, K.; Jonsson, A. M.; Andersson, P. U.; Hallquist, M. *Journal of Physical Chemistry A* **2010**, *114*, 4586. (e) Saleh, R.; Walker, J.; Khlystov, A. *J. Aerosol Sci.* **2008**, *39*, 876. (f) Saleh, R.; Khlystov, A.; Shihadeh, A. *Aerosol Sci. Technol.* **2010**, *44*, 302. (g) Ribeiro da Silva, M. A. V.; Monte, M. J. S.; Ribeiro, J. R. *J. Chem. Thermodyn.* **1999**, *31*, 1093.

(32) Booth, A. M. M., T.; McFiggans, G. ; Percival, C. J.; Mcgillen, M. R.; Topping, D. O. *Atmos. Meas. Tech.* **2009**, *2*, 355.

(33) (a) Rader, D. J.; McMurry, P. H. *J. Aerosol Sci.* **1986**, *17*, 771. (b) Davis, E. J.; Ray, A. K. *J. Colloid Interface Sci.* **1980**, *75*, 566. (c) Bilde, M.; Pandis, S. N. *Environ. Sci. Technol.* **2001**, *35*, 3344. (d) Bilde, M.; Svenningsson, B.; Monster, J.; Rosenorn, T. *Environ. Sci. Technol.* **2003**, *37*, 1371. (e) Riipinen, I.; Svenningsson, B.; Bilde, M.; Gaman, A.; Lehtinen, K. E. J.; Kulmala, M. *Atmospheric Research* **2006**, *82*, 579. (f) Zardini, A. A.; Krieger, U. K.; Marcolli, C. *Optics Express* **2006**, *14*, 6951. (g) Pope, F. D.; Tong, H. J.; Dennis-Smither, B. J.; Griffiths, P. T.; Clegg, S. L.; Reid, J. P.; Cox, R. A. *J. Phys. Chem. A* **2010**, *114*, 10156. (h) Koponen, I. K.; Riipinen, I.; Hienola, A.; Kulmala, M.; Bilde, M. *Environ. Sci. Technol.* **2007**, *41*, 3926.

(34) Ribeiro da Silva, M. A. V.; Monte, M. J. S.; Ribeiro, J. R. *J. Chem. Thermodyn.* **2001**, *33*, 23.

(35) (a) Booth, A. M.; Markus, T.; McFiggans, G.; Percival, C. J.; McGillen, M. R.; Topping, D. O. *Atmos. Meas. Tech.* **2009**, *2*, 355. (b) Booth, A. M.; Barley, M. H.; Topping, D. O.; McFiggans, G.; Garforth, A.; Percival, C. J. *Atmos. Chem. Phys.* **2010**, *10*, 4879. (c) Booth, A. M.; Montague, W. J.; Barley, M. H.; Topping, D. O.; McFiggans, G.; Garforth, A.; Percival, C. J. *Atmos. Chem. Phys.* **2011**, *11*, 655.

(36) (a) Hilpert, K. *Rapid Commun. Mass Spectrom.* **1991**, *5*, 175. (b) Hilpert, K. *Fresenius J. Anal. Chem.* **2001**, *370*, 471.

(37) (a) Zardini, A. A.; Krieger, U. K. *Optics Express* **2009**, *17*, 4659. (b) Soonsin, V.; Zardini, A. A.; Marcolli, C.; Zuend, A.; Krieger, U. K. *Atmos. Chem. Phys.* **2010**, *10*, 11753.

(38) Pope, F. D.; Dennis-Smither, B. J.; Griffiths, P. T.; Clegg, S. L.; Cox, R. A. *J. Phys. Chem. A* **2010**, *114*, 5335.

(39) Cai, C.; Stewart, D. J.; Preston, T. C.; Walker, J. S.; Zhang, Y. H.; Reid, J. P. *Phys. Chem. Chem. Phys.* **2014**, *16*, 3162.

(40) (a) Davis, E. J.; Ray, A. K. *J. Chem. Phys.* **1977**, *67*, 414. (b) Davis, E. J.; Ray, A. K. *J. Aerosol Sci.* **1978**, *9*, 411.

(41) Davis, E. J.; Buehler, M. F.; Ward, T. L. *Rev. Sci. Instrum.* **1990**, *61*, 1281.

(42) Lapshin, V. B.; Yablokov, M. Y.; Palei, A. A. *Russ. J. Phys. Chem.* **2002**, *76*, 1727.

(43) Huisman, A. J.; Krieger, U. K.; Zuend, A.; Marcolli, C.; Peter, T. *Atmos. Chem. Phys.* **2013**, *13*, 6647.

(44) Braun, C.; Krieger, U. K. *Optics Express* **2001**, *8*, 314.

(45) Glantschnig, W. J.; Chen, S. H. *Appl. Opt.* **1981**, *20*, 2499.

(46) (a) Mitchem, L.; Reid, J. P. *Chem. Soc. Rev.* **2008**, *37*, 756. (b) Wills, J. B.; Knox, K. J.; Reid, J. P. *Chem. Phys. Lett.* **2009**, *481*, 153.

(47) Hopkins, R. J.; Mitchem, L.; Ward, A. D.; Reid, J. P. *Phys. Chem. Chem. Phys.* **2004**, *6*, 4924.

(48) (a) Clegg, S. L.; Seinfeld, J. H. *J. Phys. Chem. A* **2006**, *110*, 5718. (b) Wexler, A. S.; Clegg, S. L. *J. Geophys. Res.: Atmos.* **2002**, *107*, ACH 14. (c) Clegg, S. L.; Seinfeld, J. H. *J. Phys. Chem. A* **2006**, *110*, 5692.

(49) Preston, T. C.; Reid, J. P. *J. Opt. Soc. Am. B* **2013**, *30*, 2113.

(50) (a) Rader, D. J.; McMurry, P. H.; Smith, S. *Aerosol Sci. Technol.* **1987**, *6*, 247. (b) Tao, Y.; McMurry, P. H. *Environ. Sci. Technol.* **1989**, *23*, 1519. (c) Frosch, M.; Zardini, A. A.; Platt, S. M.; Mueller, L.; Reinnig, M. C.; Hoffmann, T.; Bilde, M. *Atmos. Chem. Phys.* **2010**, *10*, 5873. (d) Monster, J.; Rosenorn, T.; Svenningsson, B.; Bilde, M. *J. Aerosol Sci.* **2004**, *35*, 1453. (e) Monster, J.; Rosenorn, T.; Svenningsson, B.; Bilde, M. *J. Aerosol Sci.* **2006**, *37*, 1164. (f) Riipinen, I.; Koponen, I. K.; Frank, G. P.; Hyvaerinen, A. P.; Vanhanen, J.; Lihavainen, H.; Lehtinen, K. E. J.; Bilde, M.; Kulmala, M. *Journal of Physical Chemistry A* **2007**, *111*, 12995. (g) Yli-Juuti, T.; Zardini, A. A.; Eriksson, A. C.; Hansen, A. M. K.; Pagels, J. H.; Swietlicki, E.; Svenningsson, B.; Glasius, M.; Worsnop, D. R.; Riipinen, I.; Bilde, M. *Environ. Sci. Technol.* **2013**, *47*, 12123. (h) Zardini, A. A.; Riipinen, I.; Koponen, I. K.; Kulmala, M.; Bilde, M. *J. Aerosol Sci.* **2010**, *41*, 760.

(51) Saleh, R.; Khlystov, A. *Aerosol Sci. Technol.* **2009**, *43*, 838.

(52) Liu, B. Y. H.; Pui, D. Y. H.; Whitby, K. T.; Kittelson, D. B.; Kousaka, Y.; McKenzie, R. L. *Atmos. Environ.* **1978**, *12*, 99.

(53) Zhang, S. H.; Seinfeld, J. H.; Flagan, R. C. *Aerosol Sci. Technol.* **1993**, *19*, 3.

(54) Riipinen, I.; Koponen, I. K.; Frank, G. P.; Hyvaerinen, A.-P.; Vanhanen, J.; Lihavainen, H.; Lehtinen, K. E. J.; Bilde, M.; Kulmala, M. *J. Phys. Chem. A* **2007**, *111*, 12995.

(55) Saleh, R.; Shihadeh, A.; Khlystov, A. *Atmos. Meas. Tech.* **2011**, *4*, 571.

(56) (a) Chattopadhyay, S.; Tobias, H. J.; Ziemann, P. J. *Anal. Chem.* **2001**, *73*, 3797. (b) Cappa, C. D.; Lovejoy, E. R.; Ravishankara, A. R. *J. Phys. Chem. A* **2008**, *112*, 3959.

(57) Bruns, E. A.; Greaves, J.; Finlayson-Pitts, B. J. *J. Phys. Chem. A* **2012**, *116*, 5900.

(58) Bruns, E. A.; Perraud, V.; Greaves, J.; Finlayson-Pitts, B. J. *Anal. Chem.* **2010**, *82*, 5922.

(59) (a) Kawamura, K.; Narukawa, M.; Li, S.-M.; Barrie, L. A. *J. Geophys. Res.: Atmos.* **2007**, *112*, D10307. (b) Kawamura, K.; Kasukabe, H.; Barrie, L. A. *Atmos. Environ.* **1996**, *30*, 1709.

(60) Graham, B.; Mayol-Bracero, O. L.; Guyon, P.; Roberts, G. C.; Decesari, S.; Facchini, M. C.; Artaxo, P.; Maenhaut, W.; Koll, P.; Andreae, M. O. *J. Geophys. Res.: Atmos.* **2002**, *107*, 14.

(61) (a) Limbeck, A.; Puxbaum, H. *Atmos. Environ.* **1999**, *33*, 1847. (b) Stone, E. A.; Hedman, C. J.; Zhou, J. B.; Mieritz, M.; Schauer, J. J. *Atmos. Environ.* **2010**, *44*, 312. (c) Grosjean, D.; Vancauwenberghe, K.; Schmid, J. P.; Kelley, P. E.; Pitts, J. N. *Environ. Sci. Technol.* **1978**, *12*, 313.

(62) Miyazaki, Y.; Kondo, Y.; Shiraiwa, M.; Takegawa, N.; Miyakawa, T.; Han, S.; Kita, K.; Hu, M.; Deng, Z. Q.; Zhao, Y.; Sugimoto, N.; Blake, D. R.; Weber, R. J. *J. Geophys. Res.: Atmos.* **2009**, *114*, D14208.

(63) Kawamura, K.; Sakaguchi, F. *J. Geophys. Res.: Atmos.* **1999**, *104*, 3501.

(64) (a) Kawamura, K.; Yasui, O. *Atmos. Environ.* **2005**, *39*, 1945. (b) Zhang, Y. Y.; Muller, L.; Winterhalter, R.; Moortgat, G. K.; Hoffmann, T.; Poschl, U. *Atmos. Chem. Phys.* **2010**, *10*, 7859.

(65) (a) Ziemann, P. J. *J. Phys. Chem. A* **2002**, *106*, 4390. (b) Borras, E.; Tortajada-Genaro, L. A. *Int. J. Environ. Anal. Chem.* **2012**, *92*, 110. (c) Kalberer, M.; Yu, J.; Cocker, D. R.; Flagan, R. C.; Seinfeld, J. H. *Environ. Sci. Technol.* **2000**, *34*, 4894.

(66) Kundu, S.; Kawamura, K.; Andreae, T. W.; Hoffer, A.; Andreae, M. O. *Atmos. Chem. Phys.* **2010**, *10*, 2209.

(67) (a) Kawamura, K.; Kaplan, I. R. *Environ. Sci. Technol.* **1987**, *21*, 105. (b) Fraser, M. P.; Cass, G. R.; Simoneit, B. R. T. *Environ. Sci. Technol.* **1998**, *32*, 2051.

(68) Blando, J. D.; Turpin, B. J. *Atmos. Environ.* **2000**, *34*, 1623.

(69) Mochida, M.; Kawabata, A.; Kawamura, K.; Hatsushika, H.; Yamazaki, K. *J. Geophys. Res.: Atmos.* **2003**, *108*, 4193.

(70) Thalladi, V. R.; Nusse, M.; Boese, R. *J. Am. Chem. Soc.* **2000**, *122*, 9227.

(71) (a) Noyes, W. A.; Wobbe, D. E. *J. Am. Chem. Soc.* **1926**, *48*, 1882. (b) Bradley, R. S.; Cotson, S. *Journal of the Chemical Society* **1953**, 1684. (c) de Kruif, C. G.; van Ginkel, C. H. D.; Voogd, J. Conf. Inter. Thermo. Chim. , Montpellier, France, 1975; p 11. (d) de Wit, H. G. M.; Bouwstra, J. A.; Blok, J. G.; de Kruif, C. G. *J. Chem. Phys.* **1983**, *78*, 1470.

(72) Devillepin, J.; Novak, A.; Bougeard, D. *Chem. Phys.* **1982**, *73*, 291.

(73) Peng, C.; Chan, M. N.; Chan, C. K. *Environ. Sci. Technol.* **2001**, *35*, 4495.

(74) Fukai, M.; Matsuo, T.; Suga, H. *Thermochim. Acta* **1991**, *183*, 215.

(75) Davies, M.; Thomas, G. H. *Trans. Faraday Soc.* **1960**, *56*, 185.

(76) Tao, Y.; McMurry, P. H. *Environ. Sci. Technol.* **1989**, *23*, 1519.

(77) Chan, M. N.; Kreidenweis, S. M.; Chan, C. K. *Environ. Sci. Technol.* **2008**, *42*, 3602.

(78) (a) Zhang, X.; Cappa, C. D.; Jathar, S. H.; McVay, R. C.; Ensberg, J. J.; Kleeman, M. J.; Seinfeld, J. H. *Proc. Natl. Acad. Sci. U. S. A.* **2014**, *111*, 5802. (b) Kokkola, H.; Yli-Pirilä, P.; Vesterinen, M.; Korhonen, H.; Keskinen, H.; Romakkaniemi, S.; Hao, L.; Kortelainen, A.; Joutsensaari, J.; Worsnop, D. R.; Virtanen, A.; Lehtinen, K. E. J. *Atmos. Chem. Phys.* **2014**, *14*, 1689.

(79) Klamt, A. *J. Phys. Chem.* **1995**, *99*, 2224.

(80) (a) Klamt, A.; Eckert, F. *Fluid Phase Equilib.* **2007**, *260*, 183. (b) Nakajoh, K.; Grabda, M.; Oleszek-Kudlak, S.; Shibata, E.; Eckert, F.; Nakamura, T. *J. Mol. Struct.: Theochem* **2009**, *895*, 9.

(81) Compernolle, S.; Ceulemans, K.; Muller, J. F. *Atmos. Chem. Phys.* **2011**, *11*, 9431.

(82) Camredon, M.; Aumont, B. *Atmos. Environ.* **2006**, *40*, 2105.

(83) Myrdal, P. B.; Yalkowsky, S. H. *Ind. Eng. Chem. Res.* **1997**, *36*, 2494.

(84) Nannoolal, Y.; Rarey, J.; Ramjugernath, D. *Fluid Phase Equilib.* **2008**, *269*, 117.

(85) Nannoolal, Y.; Rarey, J.; Ramjugernath, D.; Cordes, W. *Fluid Phase Equilib.* **2004**, *226*, 45.

(86) Moller, B.; Rarey, J.; Ramjugernath, D. *J. Mol. Liq.* **2008**, *143*, 52.

(87) Reid, R. C., Prausnitz, J. M., and Poling, B. E.: *Properties of gases and liquids*; McGraw-Hill Companies: New York, NY, USA, 1987.

(88) Stein, S. E.; Brown, R. L. *J. Chem. Inf. Comput. Sci.* **1994**, *34*, 581.

(89) (a) Clegg, S. L.; Brimblecombe, P.; Wexler, A. S. In *Extended AIM Aerosol Thermodynamics Model* http://www.aim.env.uea.ac.uk/aim .

(b) Clegg, S. L.; Kleeman, M. J.; Griffin, R. J.; Seinfeld, J. H. *Atmos. Chem. Phys.* **2008**, *8*, 1087.

(90) United States Environmental Protection Agency, W., DC, USA "Estimation Programs Interface Suite for Microsoft Windows. ," 2009.

(91) Joback, K. G.; Reid, R. C. *Chem. Eng. Commun.* **1987**, *57*, 233.

(92) Capouet, M.; Muller, J. F. *Atmos. Chem. Phys.* **2006**, *6*, 1455.

(93) Pankow, J. F.; Asher, W. E. *Atmos. Chem. Phys.* **2008**, *8*, 2773.

(94) Topping, D. O.; McFiggans, G. B.; Coe, H. *Atmos. Chem. Phys.* **2005**, *5*, 1223.

(95) Zuend, A.; Marcolli, C.; Booth, A. M.; Lienhard, D. M.; Soonsin, V.; Krieger, U. K.; Topping, D. O.; McFiggans, G.; Peter, T.; Seinfeld, J. H. *Atmos. Chem. Phys.* **2011**, *11*, 9155.

(96) Donahue, N. M.; Epstein, S. A.; Pandis, S. N.; Robinson, A. L. *Atmos. Chem. Phys.* **2011**, *11*, 3303.

(97) Macknick, A. B.; Prausnitz, J. M. *J. Chem. Eng. Data* **1979**, *24*, 175.

(98) Davies, M.; Malpass, V. E. *J. Chem. Soc.* **1961**, 1048.

(99) (a) Fredenslund, A.; Jones, R. L.; Prausnitz, J. M. *AIChE J.* **1975**, *21*, 1086. (b) Clegg, S. L.; Pitzer, K. S.; Brimblecombe, P. *J. Phys. Chem.* **1992**, *96*, 9470. (c) Clegg, S. L.; Pitzer, K. S.; Brimblecombe, P. *J. Phys. Chem.* **1994**, *98*, 1368. (d) Clegg, S. L.; Pitzer, K. S.; Brimblecombe, P. *J. Phys. Chem.* **1995**, *99*, 6755. (e) Zuend, A.; Marcolli, C.; Luo, B. P.; Peter, T. *Atmos. Chem. Phys.* **2008**, *8*, 4559.

(100) (a) Choi, M. Y.; Chan, C. K. *Environ. Sci. Technol.* **2002**, *36*, 2422. (b) Ma, Q. X.; Ma, J. Z.; Liu, C.; Lai, C. Y.; He, H. *Environ. Sci. Technol.* **2013**, *47*, 10381.

(101) Hakkinen, S. A. K.; McNeill, V. F.; Riipinen, I. *Environ. Sci. Technol.* **2014**, *48*, 13718.

(102) (a) Kerminen, V. M.; Teinila, K.; Hillamo, R.; Pakkanen, T. *J. Aerosol Sci.* **1998**, *29*, 929. (b) Laskin, A.; Moffet, R. C.; Gilles, M. K.; Fast, J. D.; Zaveri, R. A.; Wang, B. B.; Nigge, P.; Shutthanandan, J. *J. Geophys. Res.: Atmos.* **2012**, *117*, D15302.

(103) Choi, M. Y.; Chan, C. K. *J. Phys. Chem. A* **2002**, *106*, 4566.

(104) Booth, A. M.; Murphy, B.; Riipinen, I.; Percival, C. J.; Topping, D. O. *Environ. Sci. Technol.* **2014**, *48*, 9298.

(105) Cheng, Y.; Su, H.; Koop, T.; Mikhailov, E.; Pöschl, U. *Nat Commun* **2015**, *6*.

(106) Aumont, B.; Szopa, S.; Madronich, S. *Atmos. Chem. Phys.* **2005**, *5*, 2497.

(107) (a) Saunders, S. M.; Jenkin, M. E.; Derwent, R. G.; Pilling, M. J. *Atmos. Chem. Phys.* **2003**, *3*, 161. (b) Jenkin, M. E.; Saunders, S. M.; Derwent, R. G.; Pilling, M. J. *Abstr. Pap. Am. Chem. Soc.* **1997**, *214*, 116. (c) Jenkin, M. E.; Saunders, S. M.; Wagner, V.; Pilling, M. J. *Atmos. Chem. Phys.* **2003**, *3*, 181.

(108) Capouet, M.; Mueller, J. F.; Ceulemans, K.; Compernolle, S.; Vereecken, L.; Peeters, J. *J. Geophys. Res.: Atmos.* **2008**, *113*.

(109) Jenkin, M. E. *Atmos. Chem. Phys.* **2004**, *4*, 1741.

(110) Camredon, M.; Hamilton, J. F.; Alam, M. S.; Wyche, K. P.; Carr, T.; White, I. R.; Monks, P. S.; Rickard, A. R.; Bloss, W. J. *Atmos. Chem. Phys.* **2010**, *10*, 2893.

(111) Chen, Q.; Liu, Y. J.; Donahue, N. M.; Shilling, J. E.; Martin, S. T. *Environ. Sci. Technol.* **2011**, *45*, 4763.

(112) (a) Rissanen, M. P.; Kurten, T.; Sipila, M.; Thornton, J. A.; Kangasluoma, J.; Sarnela, N.; Junninen, H.; Jorgensen, S.; Schallhart, S.; Kajos, M. K.; Taipale, R.; Springer, M.; Mentel, T. F.; Ruuskanen, T.; Petaja, T.; Worsnop, D. R.; Kjaergaard, H. G.; Ehn, M. *J. Am. Chem. Soc.* **2014**, *136*, 15596. (b) Crounse, J. D.; Nielsen, L. B.; Jorgensen, S.; Kjaergaard, H. G.; Wennberg, P. O. *Journal of Physical Chemistry Letters* **2013**, *4*, 3513.

(113) (a) Pankow, J. F.; Bidleman, T. F. *Atmos. Environ., Part A* **1992**, *26*, 1071. (b) Rounds, S. A.; Tiffany, B. A.; Pankow, J. F. *Environ. Sci. Technol.* **1993**, *27*, 366. (c) Kamens, R.; Odum, J.; Fan, Z. H. *Environ. Sci. Technol.* **1995**, *29*, 43. (d) Schauer, J. J.; Kleeman, M. J.; Cass, G. R.; Simoneit, B. R. T. *Environ. Sci. Technol.* **2001**, *35*, 1716. (e) Odum, J. R.; Yu, J. Z.; Kamens, R. M. *Environ. Sci. Technol.* **1994**, *28*, 2278. (f) Jang, M.; Kamens, R. M.; Leach, K. B.; Strommen, M. R. *Environ. Sci. Technol.* **1997**, *31*, 2805. (g) Jang, M.; Kamens, R. M. *Environ. Sci. Technol.* **1998**, *32*, 1237. (h) Chandramouli, B.; Jang, M.; Kamens, R. M. *Atmos. Environ.* **2003**, *37*, 853. (i) Yu, J. Z.; Cocker, D. R.; Griffin, R. J.; Flagan, R. C.; Seinfeld, J. H. *J. Atmos. Chem.* **1999**, *34*, 207. (j) Jang, M. S.; Kamens, R. M. *Environ. Sci. Technol.* **2001**, *35*, 3626. (k) Healy, R. M.; Wenger, J. C.; Metzger, A.; Duplissy, J.; Kalberer, M.; Dommen, J. *Atmos. Chem. Phys.* **2008**, *8*, 3215.

(114) (a) Xie, M.; Hannigan, M. P.; Barsanti, K. C. *Atmos. Environ.* **2014**, *95*, 355. (b) Xie, M.; Hannigan, M. P.; Barsanti, K. C. *Environ. Sci. Technol.* **2014**, *48*, 2835.

(115) (a) Saathoff, H.; Naumann, K. H.; Mohler, O.; Jonsson, A. M.; Hallquist, M.; Kiendler-Scharr, A.; Mentel, T. F.; Tillmann, R.; Schurath, U. *Atmos. Chem. Phys.* **2009**, *9*, 1551. (b) Tillmann, R.; Hallquist, M.; Jonsson, A. M.; Kiendler-Scharr, A.; Saathoff, H.; Iinuma, Y.; Mentel, T. F. *Atmos. Chem. Phys.* **2010**, *10*, 7057.

(116) (a) Williams, B. J.; Goldstein, A. H.; Kreisberg, N. M.; Hering, S. V. *Proc. Natl. Acad. Sci. U. S. A.* **2010**, *107*, 6676. (b) Zhao, Y. L.; Kreisberg, N. M.; Worton, D. R.; Isaacman, G.; Weber, R. J.; Liu, S.; Day, D. A.; Russell, L. M.; Markovic, M. Z.; VandenBoer, T. C.; Murphy, J. G.; Hering, S. V.; Goldstein, A. H. *Environ. Sci. Technol.* **2013**, *47*, 3781.

(117) Yatavelli, R. L. N.; Thornton, J. A. *Aerosol Sci. Technol.* **2010**, *44*, 61.

(118) Yatavelli, R. L. N.; Stark, H.; Thompson, S. L.; Kimmel, J. R.; Cubison, M. J.; Day, D. A.; Campuzano-Jost, P.; Palm, B. B.; Hodzic, A.; Thornton, J. A.; Jayne, J. T.; Worsnop, D. R.; Jimenez, J. L. *Atmos. Chem. Phys.* **2014**, *14*, 1527.

(119) Lopez-Hilfiker, F. D.; Mohr, C.; Ehn, M.; Rubach, F.; Kleist, E.; Wildt, J.; Mentel, T. F.; Lutz, A.; Hallquist, M.; Worsnop, D.; Thornton, J. A. *Atmos. Meas. Tech.* **2014**, *7*, 983.

(120) Rollins, A. W.; Pusede, S.; Wooldridge, P.; Min, K. E.; Gentner, D. R.; Goldstein, A. H.; Liu, S.; Day, D. A.; Russell, L. M.; Rubitschun, C. L.; Surratt, J. D.; Cohen, R. C. *J. Geophys. Res.: Atmos.* **2013**, *118*, 6651.

(121) (a) Mikhailov, E.; Vlasenko, S.; Martin, S. T.; Koop, T.; Poschl, U. *Atmos. Chem. Phys.* **2009**, *9*, 9491. (b) Virtanen, A.; Joutsensaari, J.; Koop, T.; Kannosto, J.; Yli-Pirila, P.; Leskinen, J.; Makela, J. M.; Holopainen, J. K.; Poeschl, U.; Kulmala, M.; Worsnop, D. R.; Laaksonen, A. *Nature* **2010**, *467*, 824.

(122) (a) Kroll, J. H.; Seinfeld, J. H. *Atmos. Environ.* **2008**, *42*, 3593. (b) Ziemann, P. J.; Atkinson, R. *Chem. Soc. Rev.* **2012**, *41*, 6582. (c) Barsanti, K. C.; Pankow, J. F. *Atmos. Environ.* **2005**, *39*, 6597. (d) Barsanti, K. C.; Pankow, J. F. *Atmos. Environ.* **2006**, *40*, 6676.

(123) Cass, G. R. *TrAC, Trends Anal. Chem.* **1998**, *17*, 356.

(124) Arey, J.; Aschmann, S. M.; Kwok, E. S. C.; Atkinson, R. *J. Phys. Chem. A* **2001**, *105*, 1020.

(125) Donahue, N. M.; Kroll, J. H.; Pandis, S. N.; Robinson, A. L. *Atmos. Chem. Phys.* **2012**, *12*, 615.

(126) Koo, B. Y.; Ansari, A. S.; Pandis, S. N. *Atmos. Environ.* **2003**, *37*, 4757.

(127) (a) Pierce, J. R.; Riipinen, I.; Kulmala, M.; Ehn, M.; Petaja, T.; Junninen, H.; Worsnop, D. R.; Donahue, N. M. *Atmos. Chem. Phys.* **2011**, *11*, 9019. (b) Riipinen, I.; Yli-Juuti, T.; Pierce, J. R.; Petaja, T.; Worsnop, D. R.; Kulmala, M.; Donahue, N. M. *Nat. Geosci.* **2012**, *5*, 453.

(128) (a) Odum, J. R.; Hoffmann, T.; Bowman, F.; Collins, D.; Flagan, R. C.; Seinfeld, J. H. *Environ. Sci. Technol.* **1996**, *30*, 2580. (b) Presto, A. A.; Donahue, N. M. *Environ. Sci. Technol.* **2006**, *40*, 3536.

(129) (a) Lipsky, E. M.; Robinson, A. L. *Environ. Sci. Technol.* **2006**, *40*, 155. (b) Shrivastava, M. K.; Lipsky, E. M.; Stanier, C. O.; Robinson, A. L. *Environ. Sci. Technol.* **2006**, *40*, 2671. (c) Grieshop, A. P.; Miracolo, M. A.; Donahue, N. M.; Robinson, A. L. *Environ. Sci. Technol.* **2009**, *43*, 4750.

(130) Trump, E. R.; Donahue, N. M. *Atmos. Chem. Phys.* **2014**, *14*, 3691.

(131) Cappa, C. D.; Wilson, K. R. *Atmos. Chem. Phys.* **2011**, *11*, 1895.

(132) (a) Burtscher, H.; Baltensperger, U.; Bukowiecki, N.; Cohn, P.; Huglin, C.; Mohr, M.; Matter, U.; Nyeki, S.; Schmatloch, V.; Streit, N.; Weingartner, E. *J. Aerosol Sci.* **2001**, *32*, 427. (b) Cappa, C. D.; Jimenez, J. L. *Atmos. Chem. Phys.* **2010**, *10*, 5409. (c) Kalberer, M.; Paulsen, D.; Sax, M.; Steinbacher, M.; Dommen, J.; Prevot, A. S. H.; Fisseha, R.; Weingartner, E.; Frankevich, V.; Zenobi, R.; Baltensperger, U. *Science* **2004**, *303*, 1659. (d) An, W. J.; Pathak, R. K.; Lee, B. H.; Pandis, S. N. *J. Aerosol Sci.* **2007**, *38*, 305. (e) Jonsson, A. M.; Hallquist, M.; Saathoff, H. *J. Aerosol Sci.* **2007**, *38*, 843. (f) Salo, K.; Hallquist, M.; Jonsson, A. M.; Saathoff, H.; Naumann, K. H.; Spindler, C.; Tillmann, R.; Fuchs, H.; Bohn, B.; Rubach, F.; Mentel, T. F.; Muller, L.; Reinnig, M.; Hoffmann, T.; Donahue, N. M. *Atmos. Chem. Phys.* **2011**, *11*, 11055. (g) Tritscher, T.; Dommen, J.; DeCarlo, P. F.; Gysel, M.; Barmet, P. B.; Praplan, A. P.; Weingartner, E.; Prevot, A. S. H.; Riipinen, I.; Donahue, N. M.; Baltensperger, U. *Atmos. Chem. Phys.* **2011**, *11*, 11477. (h) Emanuelsson, E. U.; Mentel, T. F.; Watne, Å. K.; Spindler, C.; Bohn, B.; Brauers, T.; Dorn, H.-P.; Hallquist, Å. M.; Häseler, R.; Kiendler-Scharr, A.; Müller, K.-P.; Pleijel, H.; Rohrer, F.; Rubach, F.; Schlosser, E.; Tillmann, R.; Hallquist, M. *Environ. Sci. Technol.* **2014**, *48*, 6168.

(133) (a) Fuentes, E.; McFiggans, G. *Atmos. Meas. Tech.* **2012**, *5*, 735. (b) Karnezi, E.; Riipinen, I.; Pandis, S. N. *Atmos. Meas. Tech. Discuss.* **2014**, *7*, 859.

(134) (a) Crump, J. G.; Seinfeld, J. H. *J. Aerosol Sci.* **1981**, *12*, 405. (b) McMurry, P. H.; Rader, D. J. *Aerosol Sci. Technol.* **1985**, *4*, 249.

(135) Pierce, J. R.; Engelhart, G. J.; Hildebrandt, L.; Weitkamp, E. A.; Pathak, R. K.; Donahue, N. M.; Robinson, A. L.; Adams, P. J.; Pandis, S. N. *Aerosol Sci. Technol.* **2008**, *42*, 1001.

(136) McMurry, P. H.; Grosjean, D. *Environ. Sci. Technol.* **1985**, *19*, 1176.

(137) (a) Matsunaga, A.; Ziemann, P. J. *Aerosol Sci. Technol.* **2010**, *44*, 881. (b) McVay, R. C.; Cappa, C. D.; Seinfeld, J. H. *Environ. Sci. Technol.* **2014**. (c) McVay, R. C.; Cappa, C. D.; Seinfeld, J. H. *Environ. Sci. Technol.* **2014**, *48*, 10251.

(138) Riipinen, I.; Pierce, J. R.; Donahue, N. M.; Pandis, S. N. *Atmos. Environ.* **2010**, *44*, 597.

(139) Saleh, R.; Donahue, N. M.; Robinson, A. L. *Environ. Sci. Technol.* **2013**, *47*, 5588.

(140) (a) Grieshop, A. P.; Donahue, N. M.; Robinson, A. L. *Geophys. Res. Lett.* **2007**, *34*, L14810. (b) Vaden, T. D.; Song, C.; Zaveri, R. A.; Imre, D.; Zelenyuk, A. *Proc. Natl. Acad. Sci. U. S. A.* **2010**, *107*, 6658.

(141) (a) Pankow, J. F.; Chang, E. I. *Environ. Sci. Technol.* **2008**, *42*, 7321. (b) Prisle, N. L.; Engelhart, G. J.; Bilde, M.; Donahue, N. M. *Geophys. Res. Lett.* **2010**, *37*, L01802.

(142) (a) You, Y.; Smith, M. L.; Song, M. J.; Martin, S. T.; Bertram, A. K. *Int. Rev. Phys. Chem.* **2014**, *33*, 43. (b) You, Y.; Renbaum-Wolff, L.; Bertram, A. K. *Atmos. Chem. Phys.* **2013**, *13*, 11723. (c) Song, M.; Marcolli, C.; Krieger, U. K.; Zuend, A.; Peter, T. *Geophys. Res. Lett.* **2012**, *39*, L19801. (d) Zuend, A.; Seinfeld, J. H. *Fluid Phase Equilib.* **2013**, *337*, 201.

(143) Kokkola, H.; Yli-Pirila, P.; Vesterinen, M.; Korhonen, H.; Keskinen, H.; Romakkaniemi, S.; Hao, L.; Kortelainen, A.; Joutsensaari, J.; Worsnop, D. R.; Virtanen, A.; Lehtinen, K. E. J. *Atmos. Chem. Phys.* **2014**, *14*, 1689.

(144) Jang, M. S.; Czoschke, N. M.; Lee, S.; Kamens, R. M. *Science* **2002**, *298*, 814.

(145) Koponen, I. K.; Riipinen, I.; Hienola, A.; Kulmala, M.; Bilde, M. *Environmental Science & Technology* **2007**, *41*, 3926.

(146) Saleh, R.; Shihadeh, A.; Khlystov, A. *J. Aerosol Sci.* **2009**, *40*, 1019.

(147) Roux, M. V.; Temprado, M.; Chickos, J. S. *J. Chem. Thermodyn.* **2005**, *37*, 941.

(148) Huisman, A. J.; Krieger, U. K.; Zuend, A.; Marcolli, C.; Peter, T. *Atmos. Chem. Phys.* **2013**, *13*, 6647.

(149) Ribeiro da Silva, M. A. V.; Monte, M. J. S.; Ribeiro, J. R. *J. Chem. Eng. Data* **2000**, *45*, 756.

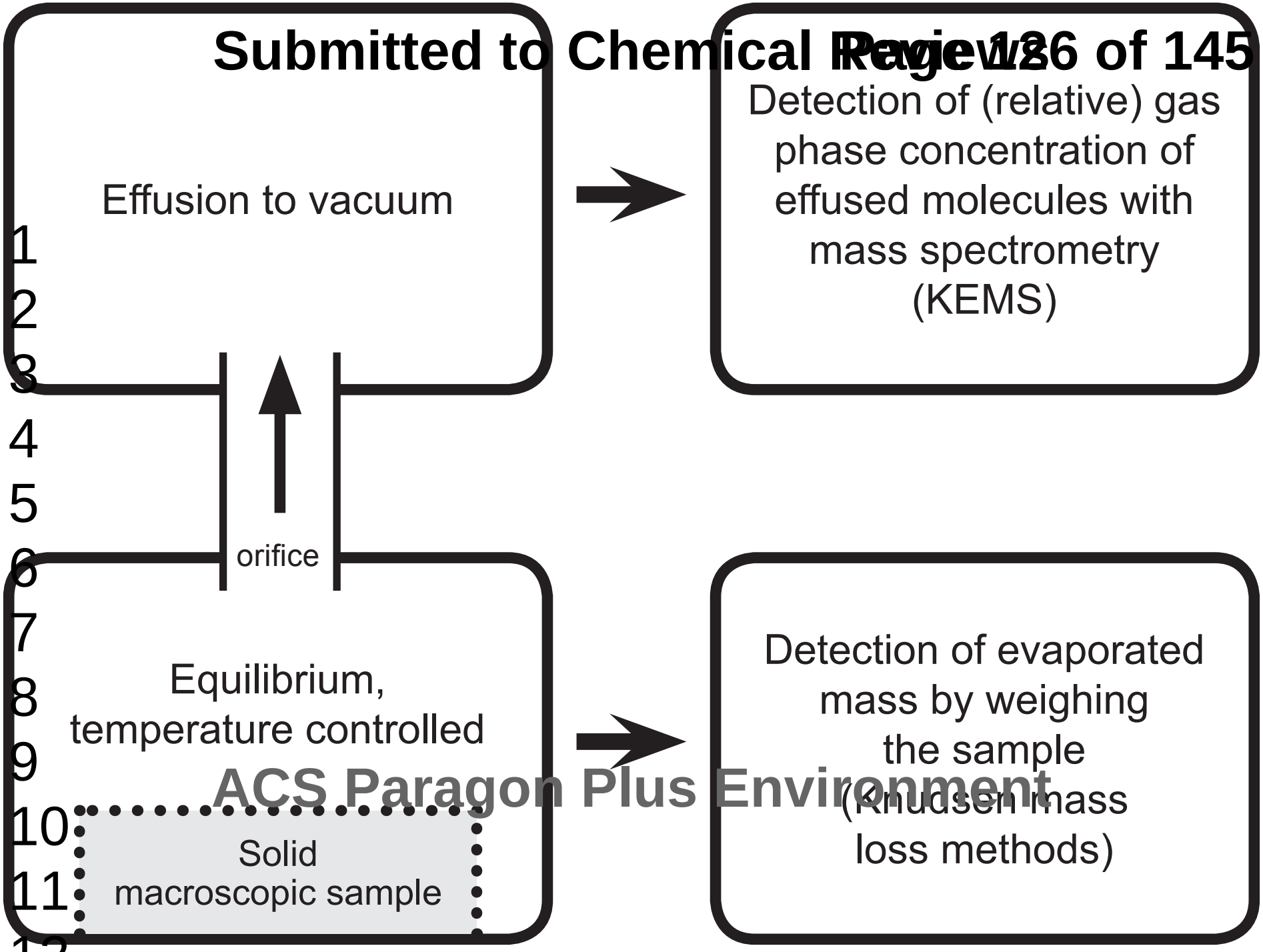

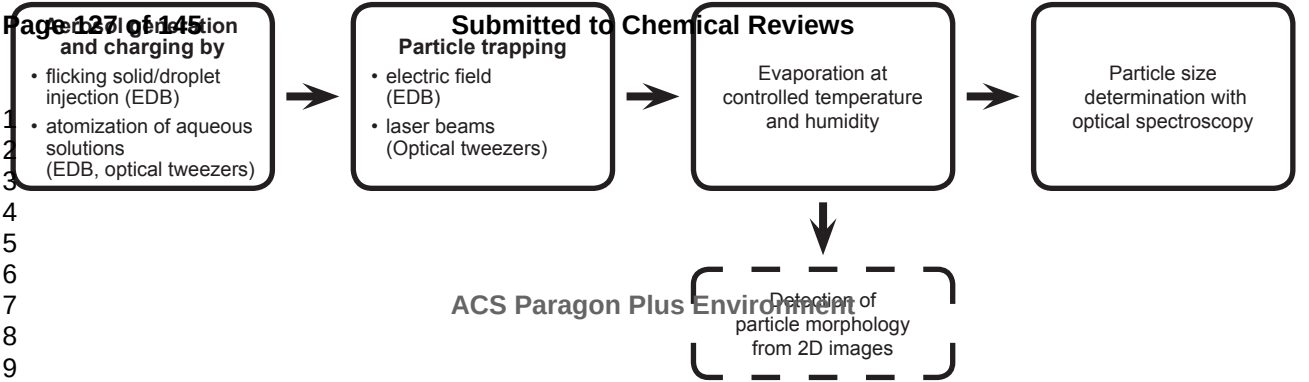

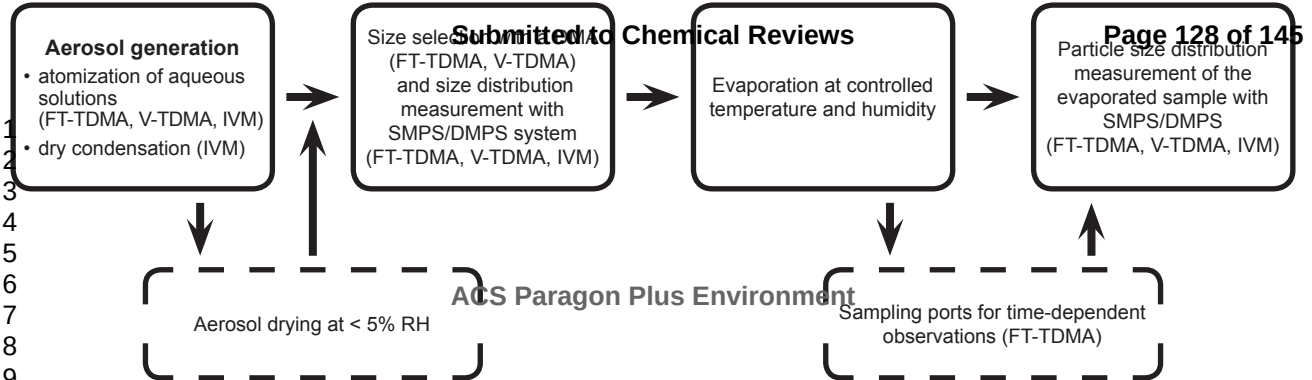
Aerosol generation
• atomization of aqueous solutions (FT-TDMA, V-TDMA, IVM)
• dry condensation (IVM)
Size selection with DMA (FT-TDMA, V-TDMA) and size distribution measurement with SMPS/DMPS system (FT-TDMA, V-TDMA, IVM)
Evaporation at controlled temperature and humidity
Particle size distribution measurement of the evaporated sample with SMPS/DMPS (FT-TDMA, V-TDMA, IVM)
Aerosol drying at < 5% RH
ACS Paragon Plus Environment
Sampling ports for time-dependent observations (FT-TDMA)

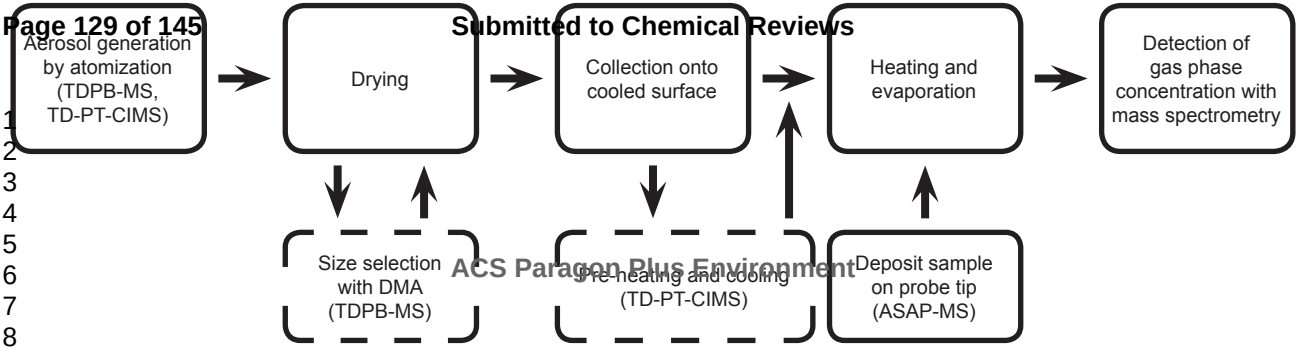

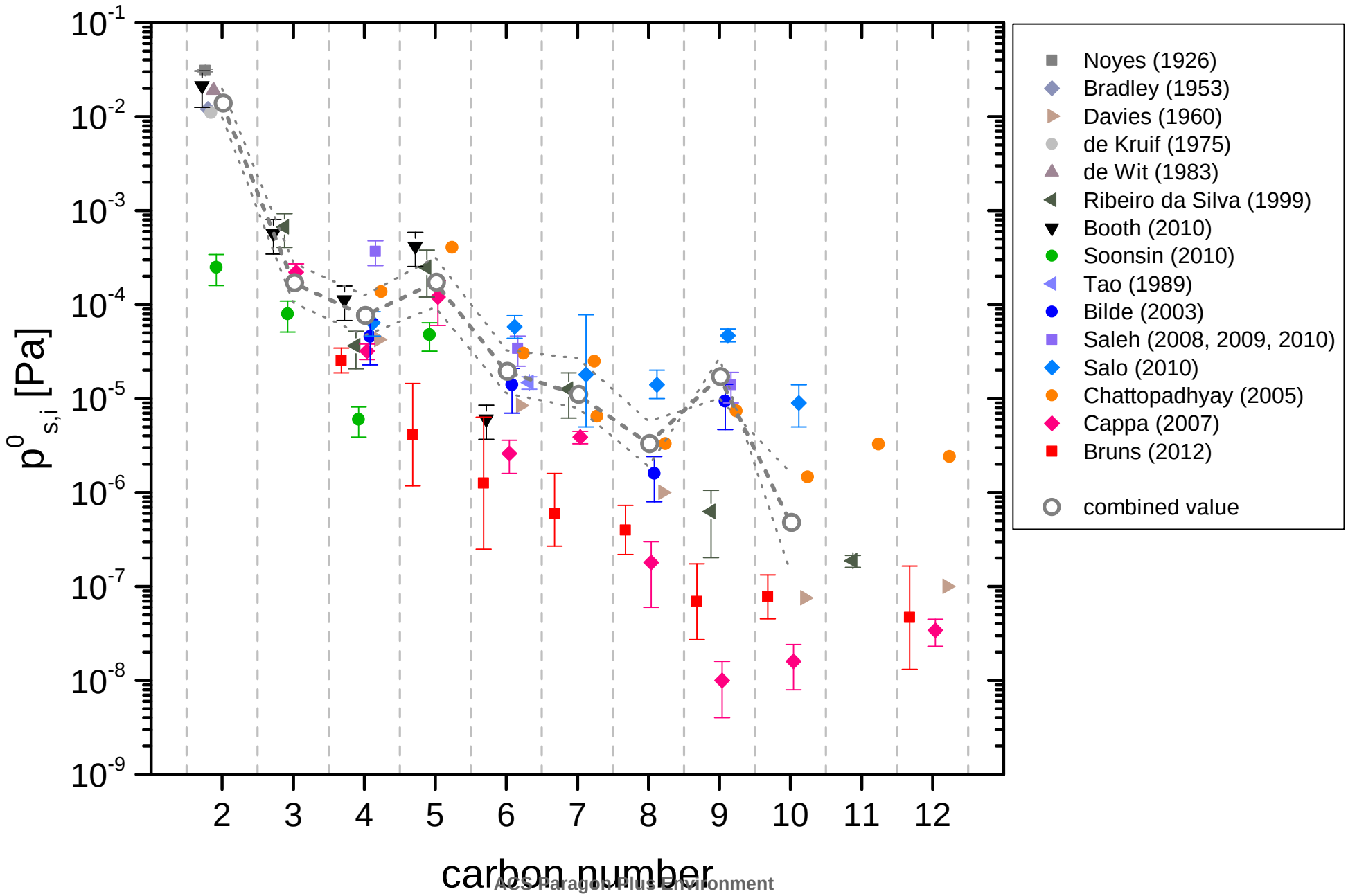
$p^0_{s,i}$ [Pa]
10^{-1}
10^{-2}
10^{-3}
10^{-4}
10^{-5}
10^{-6}
10^{-7}
10^{-8}
10^{-9}
2
3
4
5
6
7
8
9
10
11
12
carbon number
Noyes (1926)
Bradley (1953)
Davies (1960)
de Kruif (1975)
de Wit (1983)
Ribeiro da Silva (1999)
Booth (2010)
Soonsin (2010)
Tao (1989)
Bilde (2003)
Saleh (2008, 2009, 2010)
Salo (2010)
Chattopadhyay (2005)
Cappa (2007)
Bruns (2012)
combined value

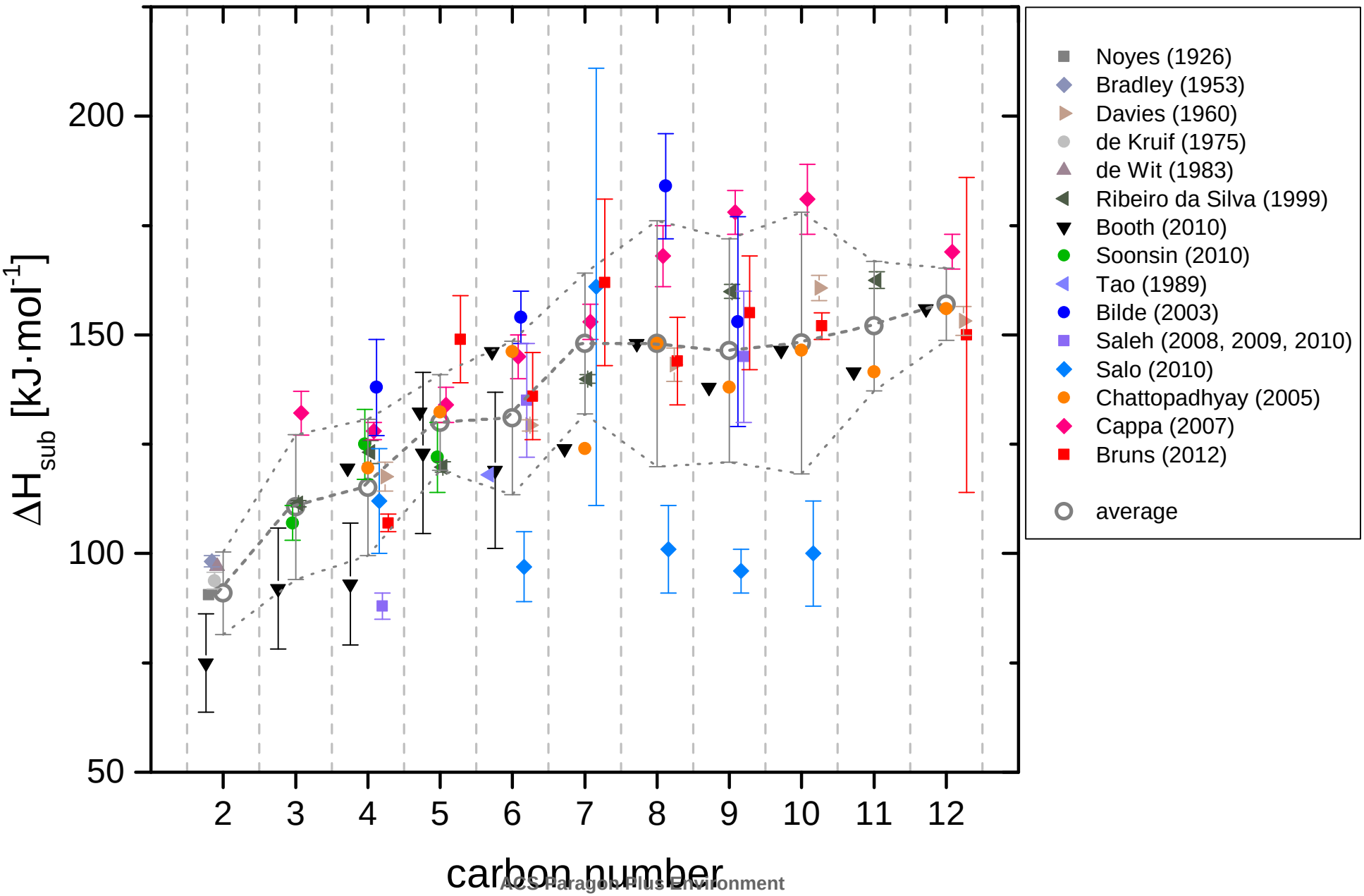
ΔH_sub [kJ·mol^-1]
200
150
100
50
2
3
4
5
6
7
8
9
10
11
12
carbon number
Noyes (1926)
Bradley (1953)
Davies (1960)
de Kruif (1975)
de Wit (1983)
Ribeiro da Silva (1999)
Booth (2010)
Soonsin (2010)
Tao (1989)
Bilde (2003)
Saleh (2008, 2009, 2010)
Salo (2010)
Chattopadhyay (2005)
Cappa (2007)
Bruns (2012)
average

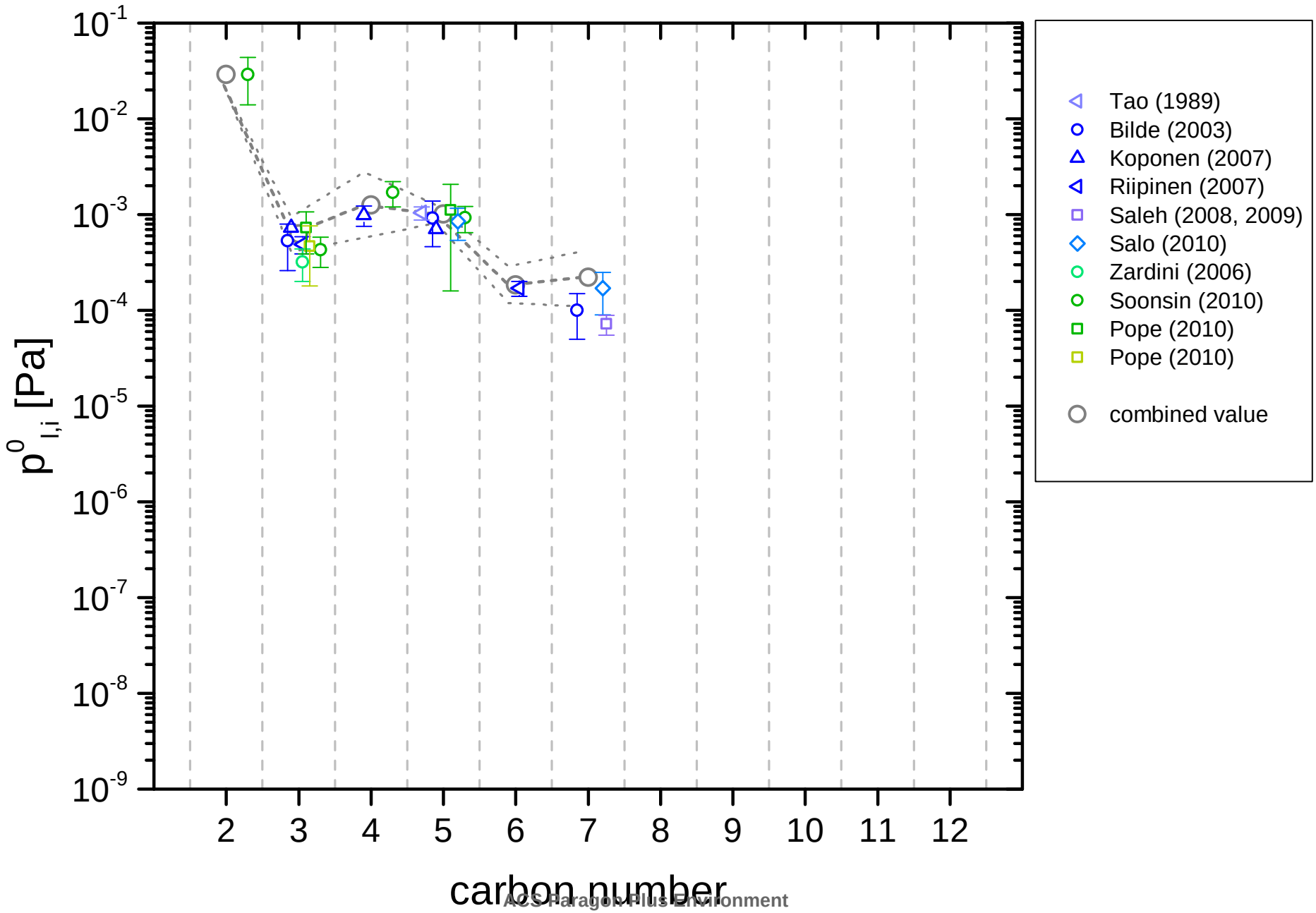
10^{-1}
10^{-2}
10^{-3}
10^{-4}
10^{-5}
10^{-6}
10^{-7}
10^{-8}
10^{-9}
$p^0_{l,i}$ [Pa]
2
3
4
5
6
7
8
9
10
11
12
carbon number
Tao (1989)
Bilde (2003)
Koponen (2007)
Riipinen (2007)
Saleh (2008, 2009)
Salo (2010)
Zardini (2006)
Soonsin (2010)
Pope (2010)
Pope (2010)
combined value

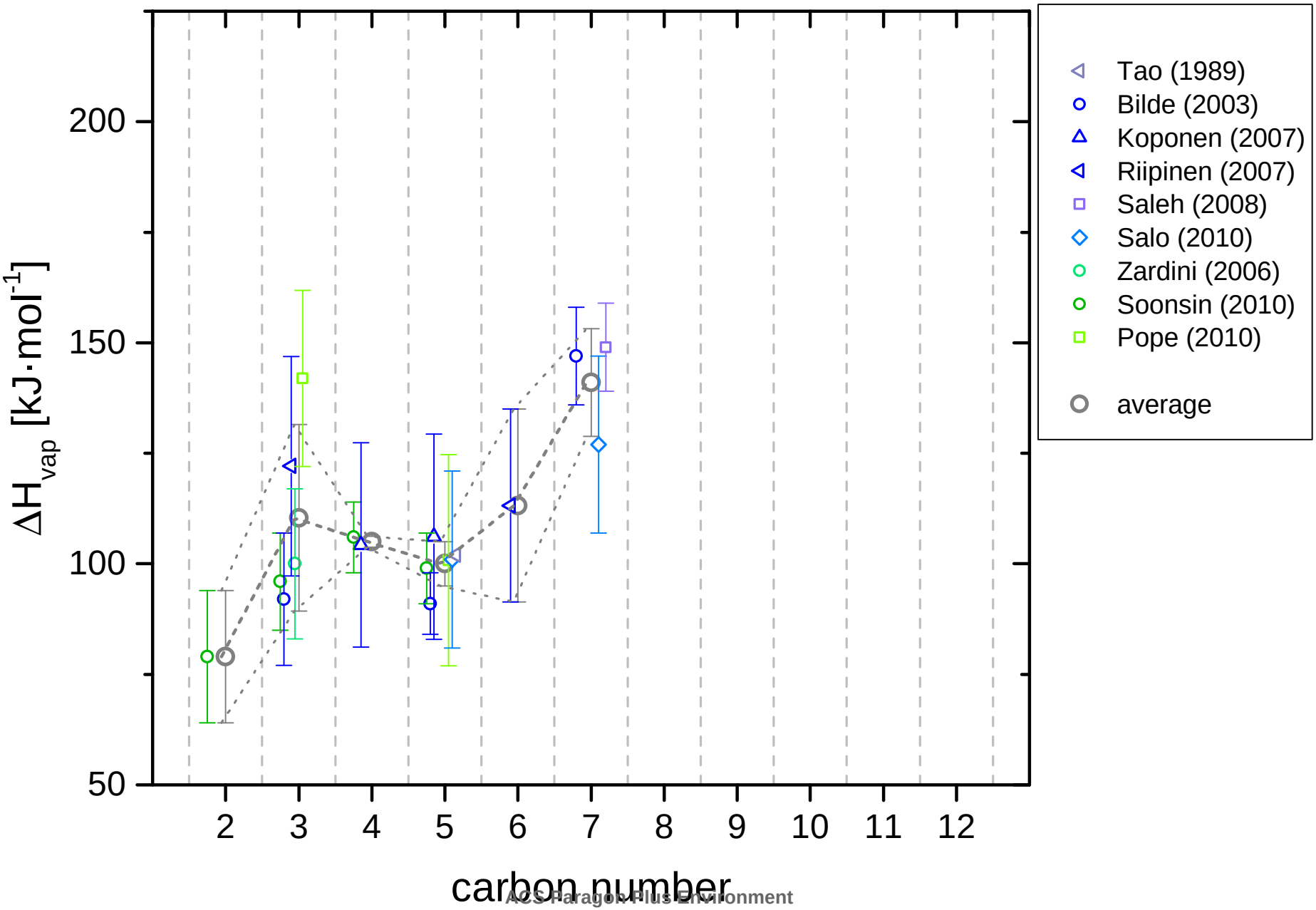
ΔH_vap [kJ·mol^-1]
200
150
100
50
2
3
4
5
6
7
8
9
10
11
12
carbon number
Tao (1989)
Bilde (2003)
Koponen (2007)
Riipinen (2007)
Saleh (2008)
Salo (2010)
Zardini (2006)
Soonsin (2010)
Pope (2010)
average

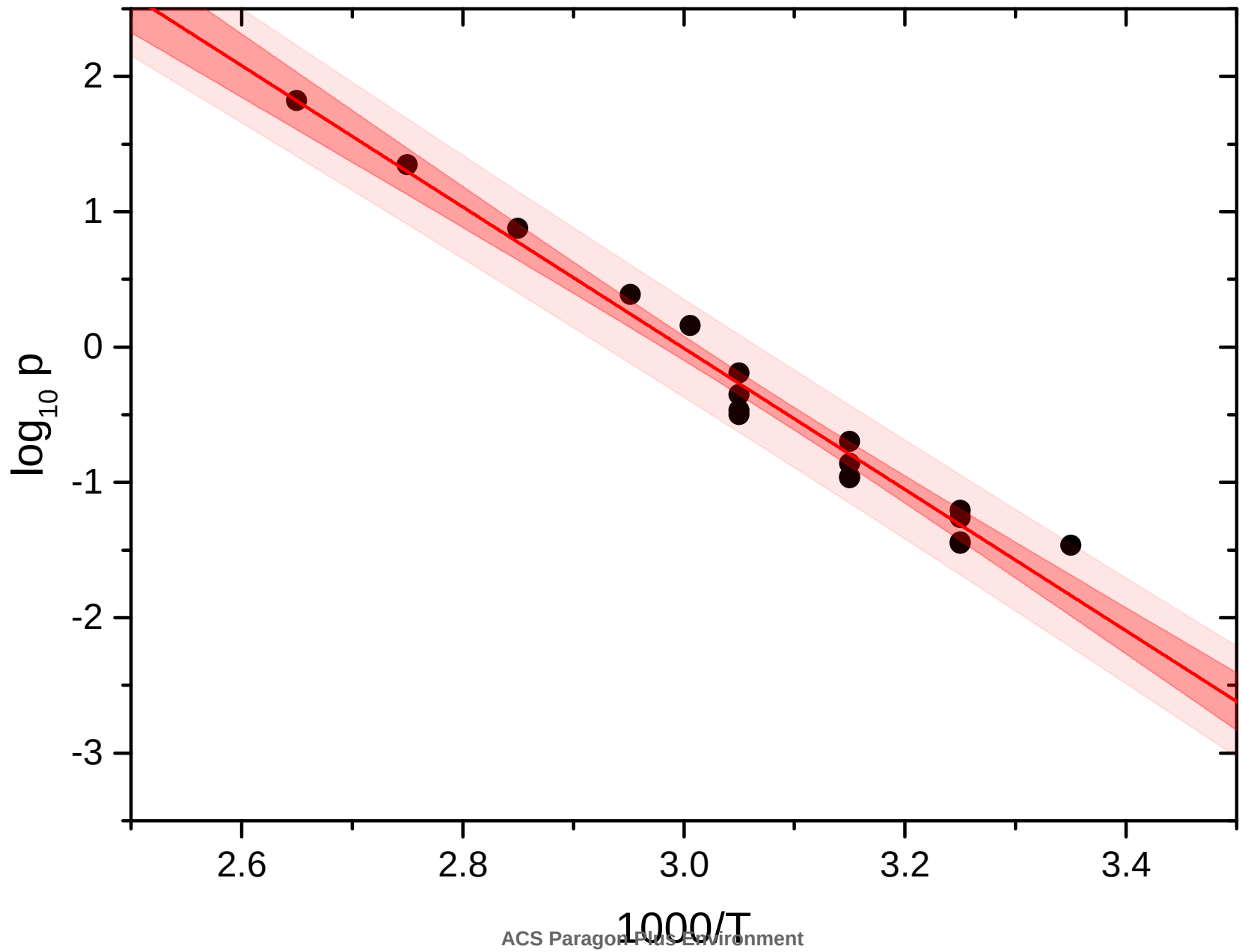
log10 p
2
1
0
-1
-2
-3
2.6
2.8
3.0
3.2
3.4
1000/T

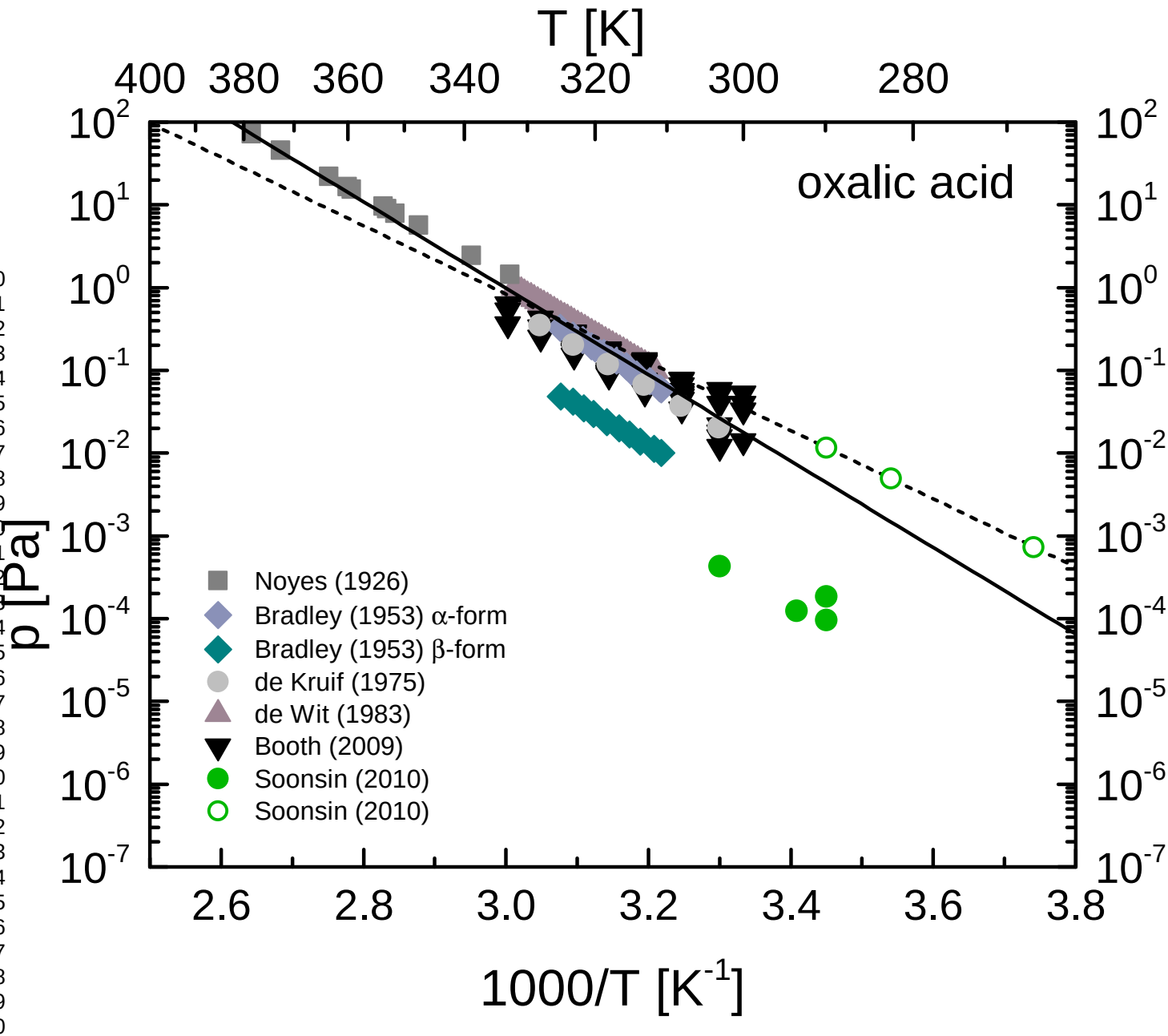
T [K]
400 380 360 340 320 300 280
oxalic acid
p [Pa]
Noyes (1926)
Bradley (1953) α-form
Bradley (1953) β-form
de Kruif (1975)
de Wit (1983)
Booth (2009)
Soonsin (2010)
Soonsin (2010)
2.6 2.8 3.0 3.2 3.4 3.6 3.8
1000/T [K-1]

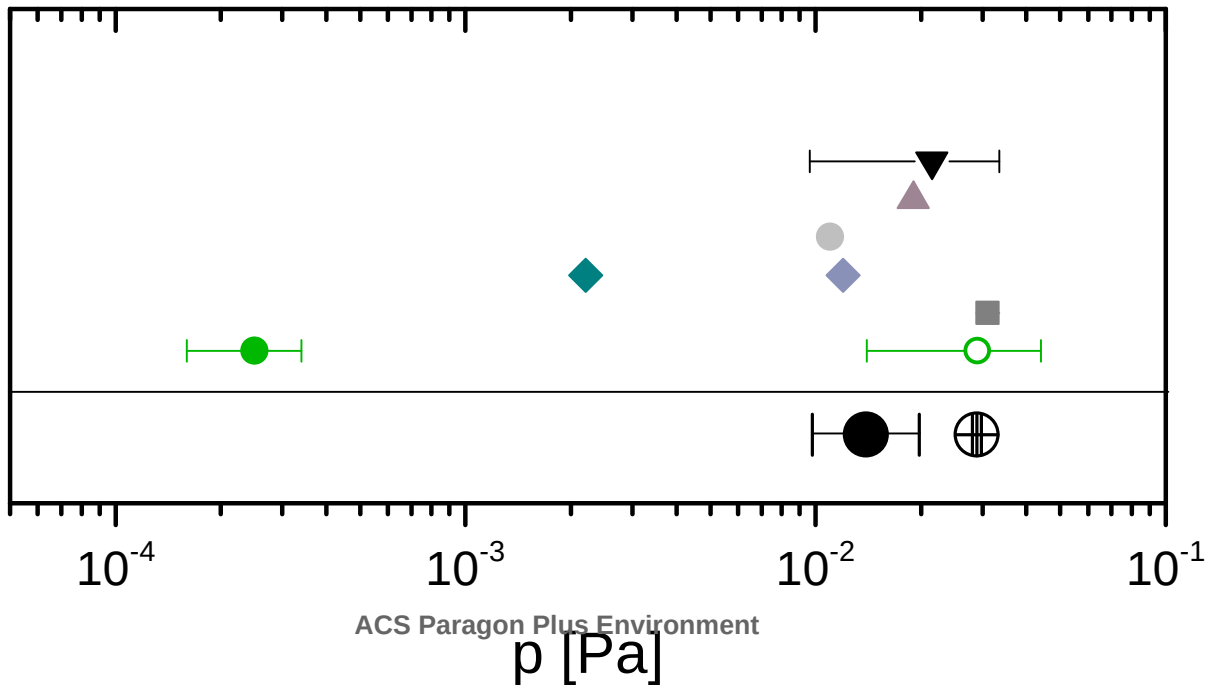
10-4 10-3 10-2 10-1
p [Pa]

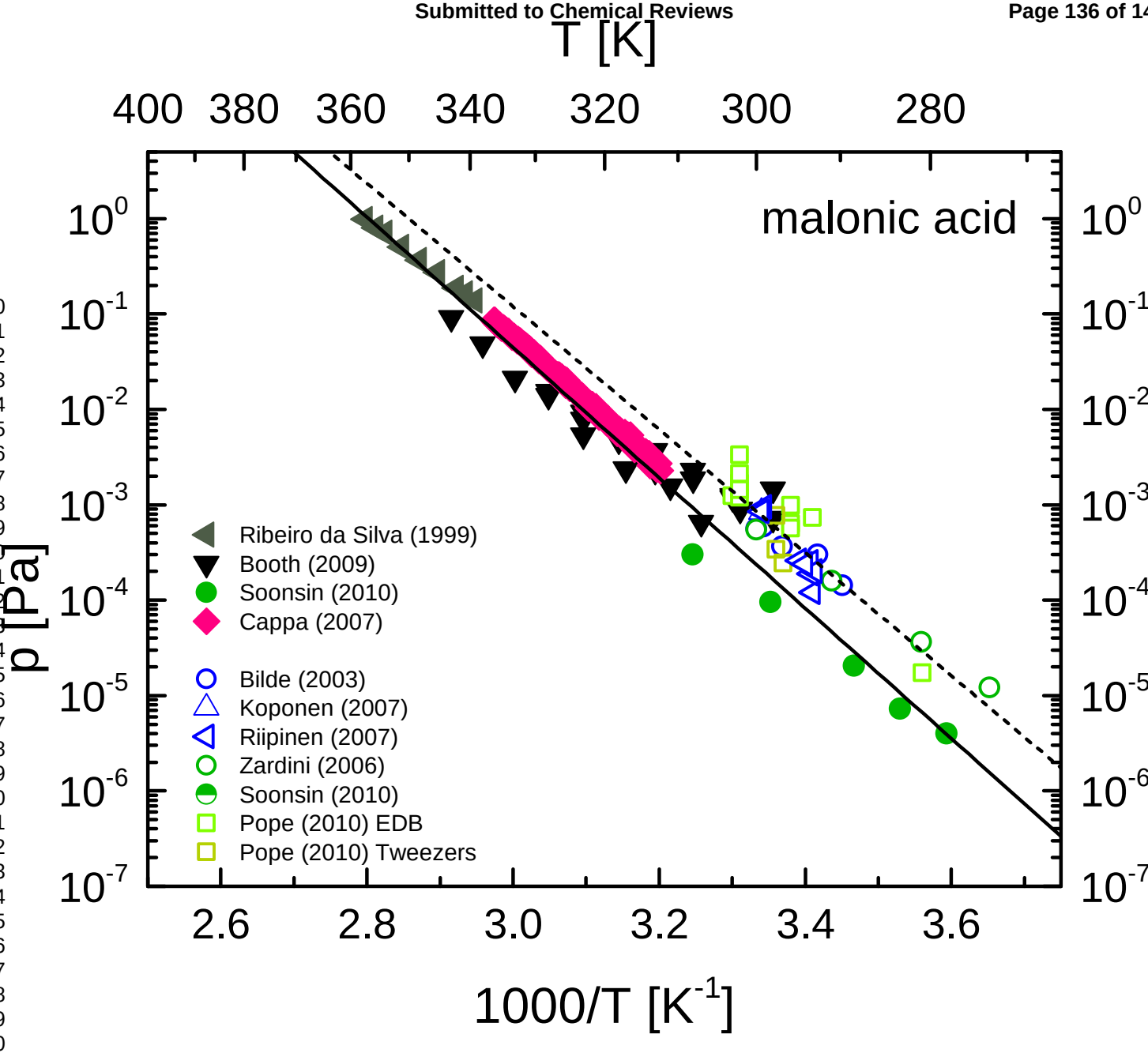
T [K]
400 380 360 340 320 300 280
malonic acid
p [Pa]
Ribeiro da Silva (1999)
Booth (2009)
Soonsin (2010)
Cappa (2007)
Bilde (2003)
Koponen (2007)
Riipinen (2007)
Zardini (2006)
Soonsin (2010)
Pope (2010) EDB
Pope (2010) Tweezers
1000/T [K-1]

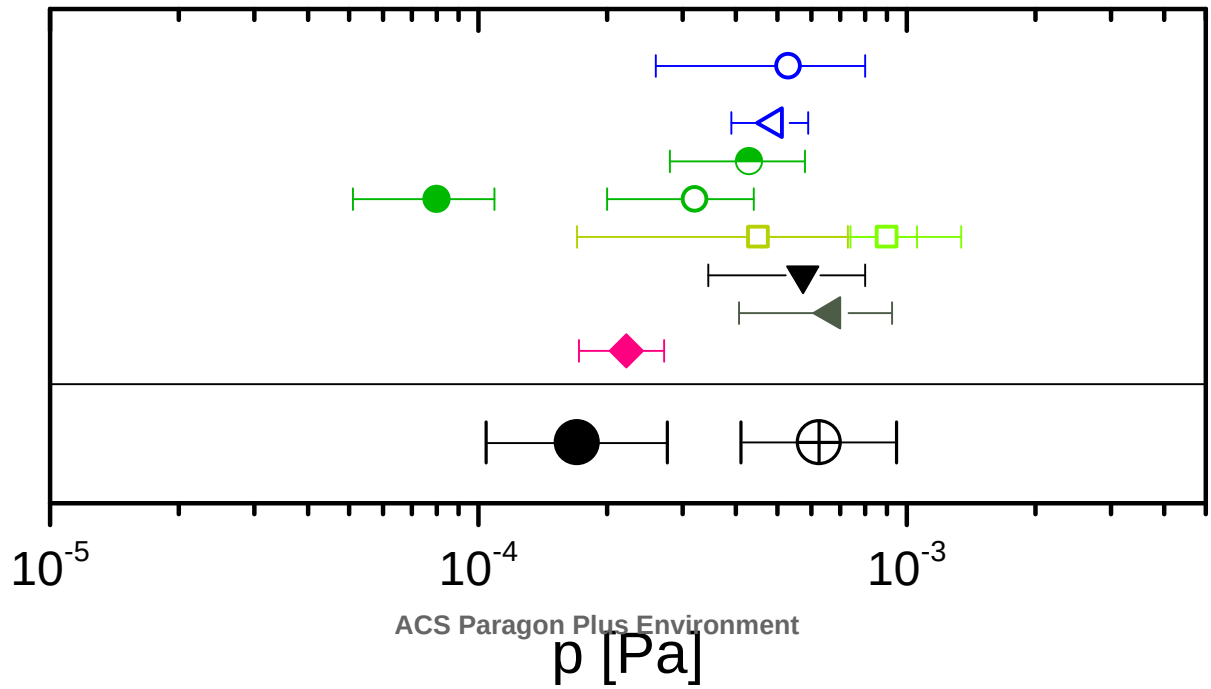
p [Pa]

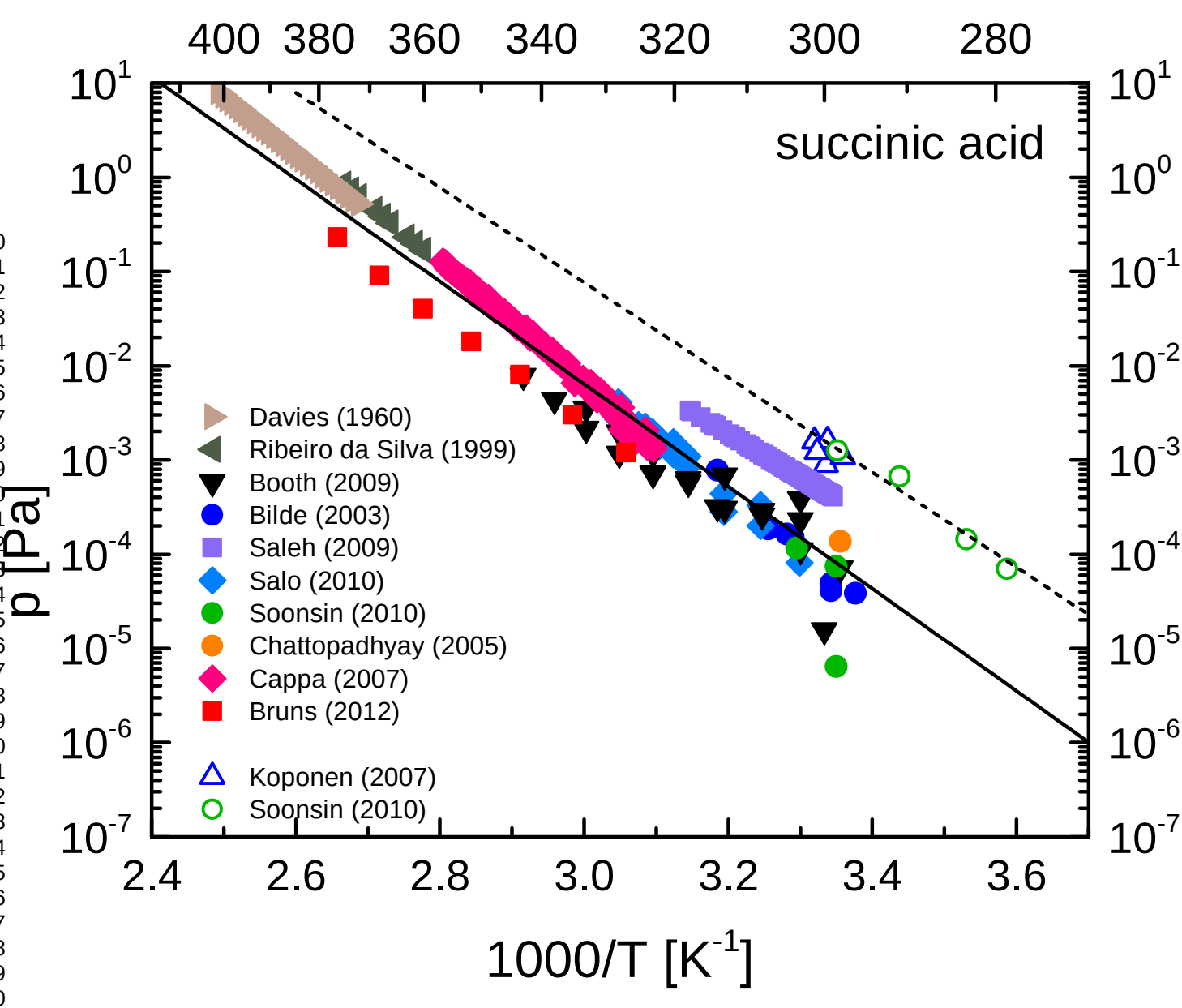
T [K]
400 380 360 340 320 300 280
succinic acid
p [Pa]
Davies (1960)
Ribeiro da Silva (1999)
Booth (2009)
Bilde (2003)
Saleh (2009)
Salo (2010)
Soonsin (2010)
Chattopadhyay (2005)
Cappa (2007)
Bruns (2012)
Koponen (2007)
Soonsin (2010)
1000/T [K-1]

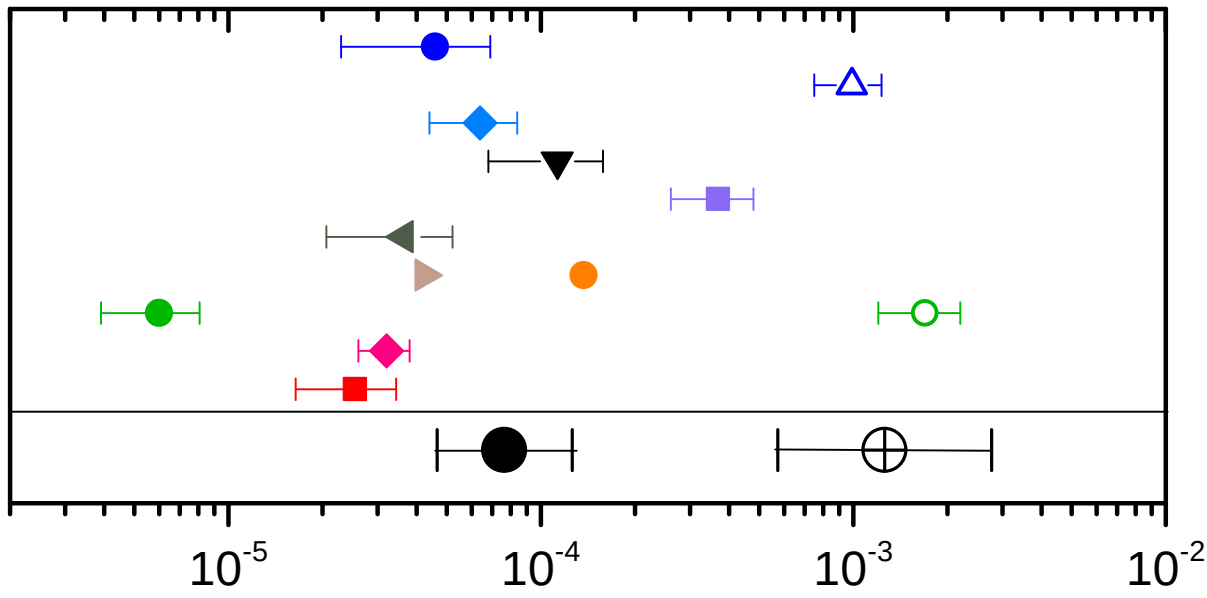
p [Pa]

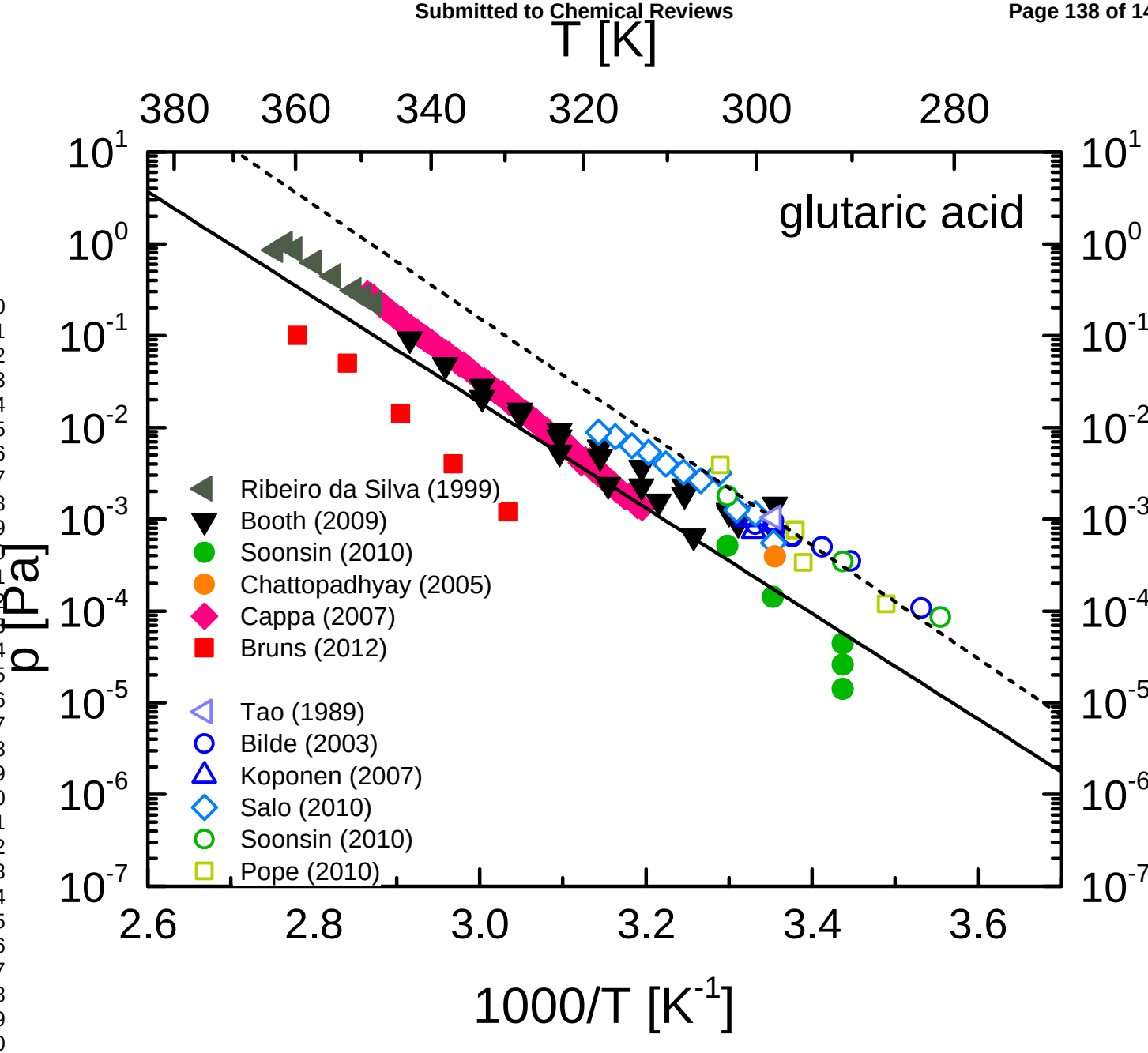
T [K]
380
360
340
320
300
280
glutaric acid
p [Pa]
Ribeiro da Silva (1999)
Booth (2009)
Soonsin (2010)
Chattopadhyay (2005)
Cappa (2007)
Bruns (2012)
Tao (1989)
Bilde (2003)
Koponen (2007)
Salo (2010)
Soonsin (2010)
Pope (2010)
2.6
2.8
3.0
3.2
3.4
3.6
1000/T [K-1]

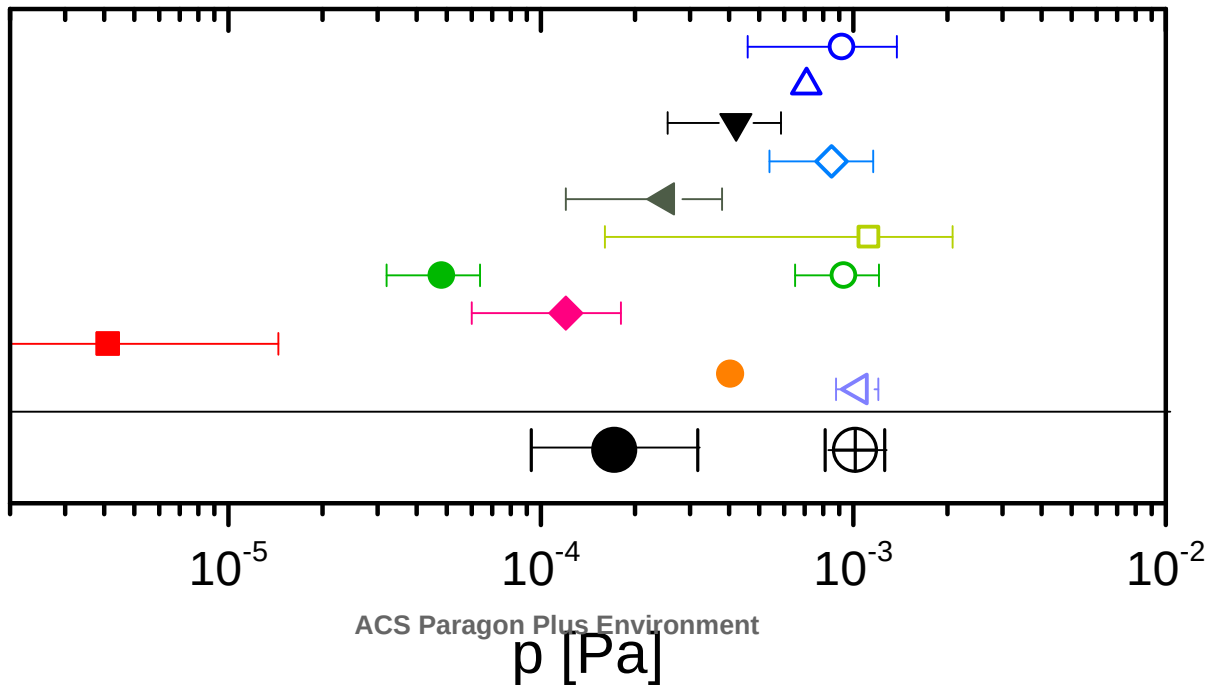
10-5
10-4
10-3
10-2
p [Pa]

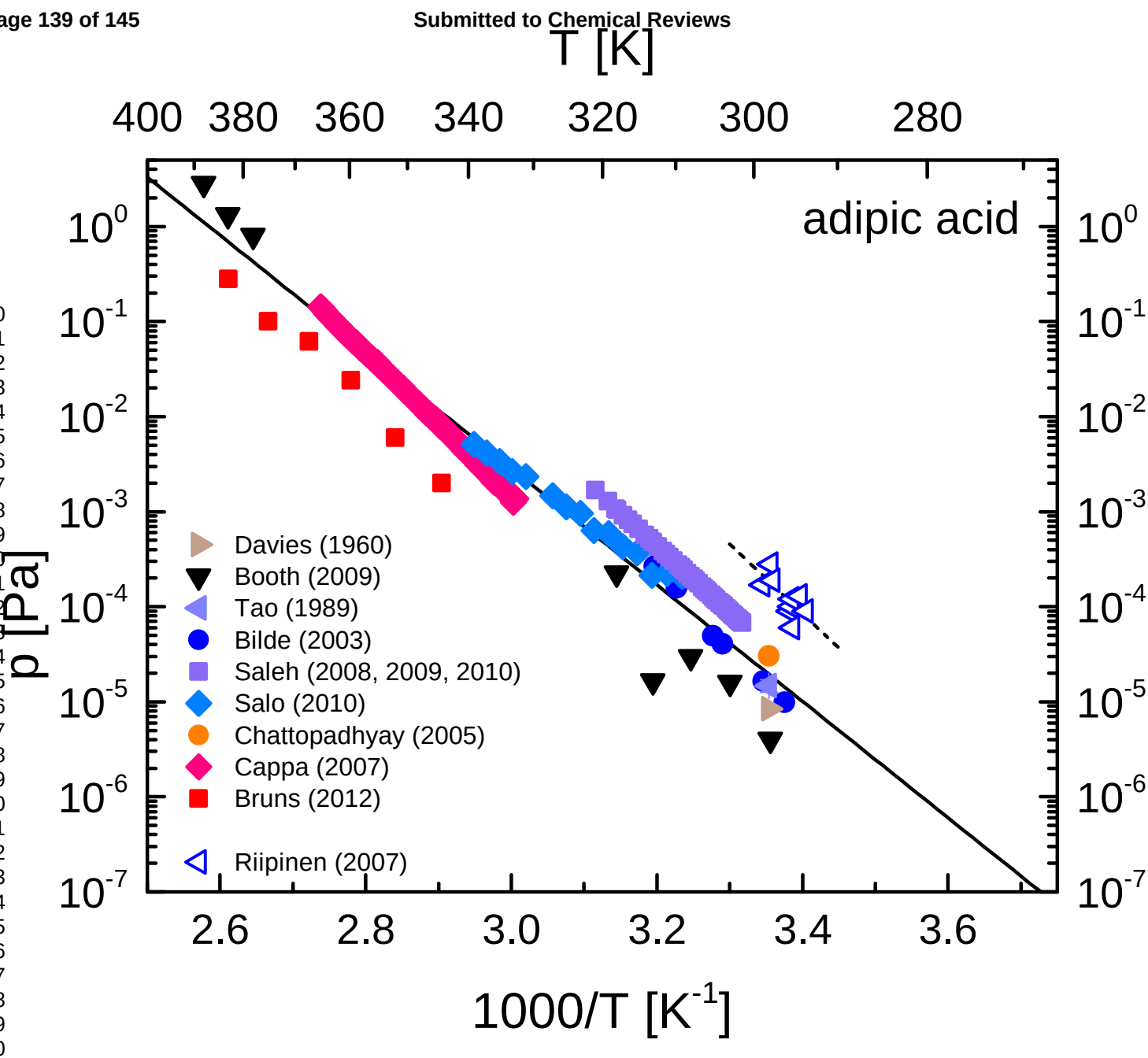
T [K]
400 380 360 340 320 300 280
adipic acid
p [Pa]
10^{0} 10^{-1} 10^{-2} 10^{-3} 10^{-4} 10^{-5} 10^{-6} 10^{-7}
Davies (1960)
Booth (2009)
Tao (1989)
Bilde (2003)
Saleh (2008, 2009, 2010)
Salo (2010)
Chattopadhyay (2005)
Cappa (2007)
Bruns (2012)
Riipinen (2007)
2.6 2.8 3.0 3.2 3.4 3.6
1000/T [K^{-1}]

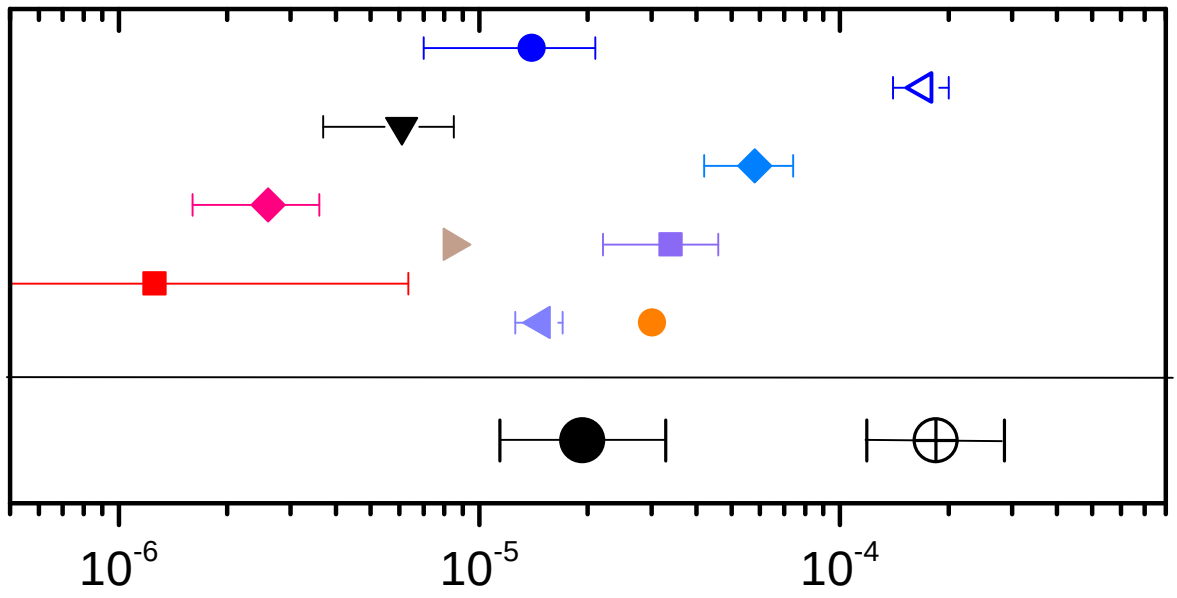
10^{-6} 10^{-5} 10^{-4}
p [Pa]

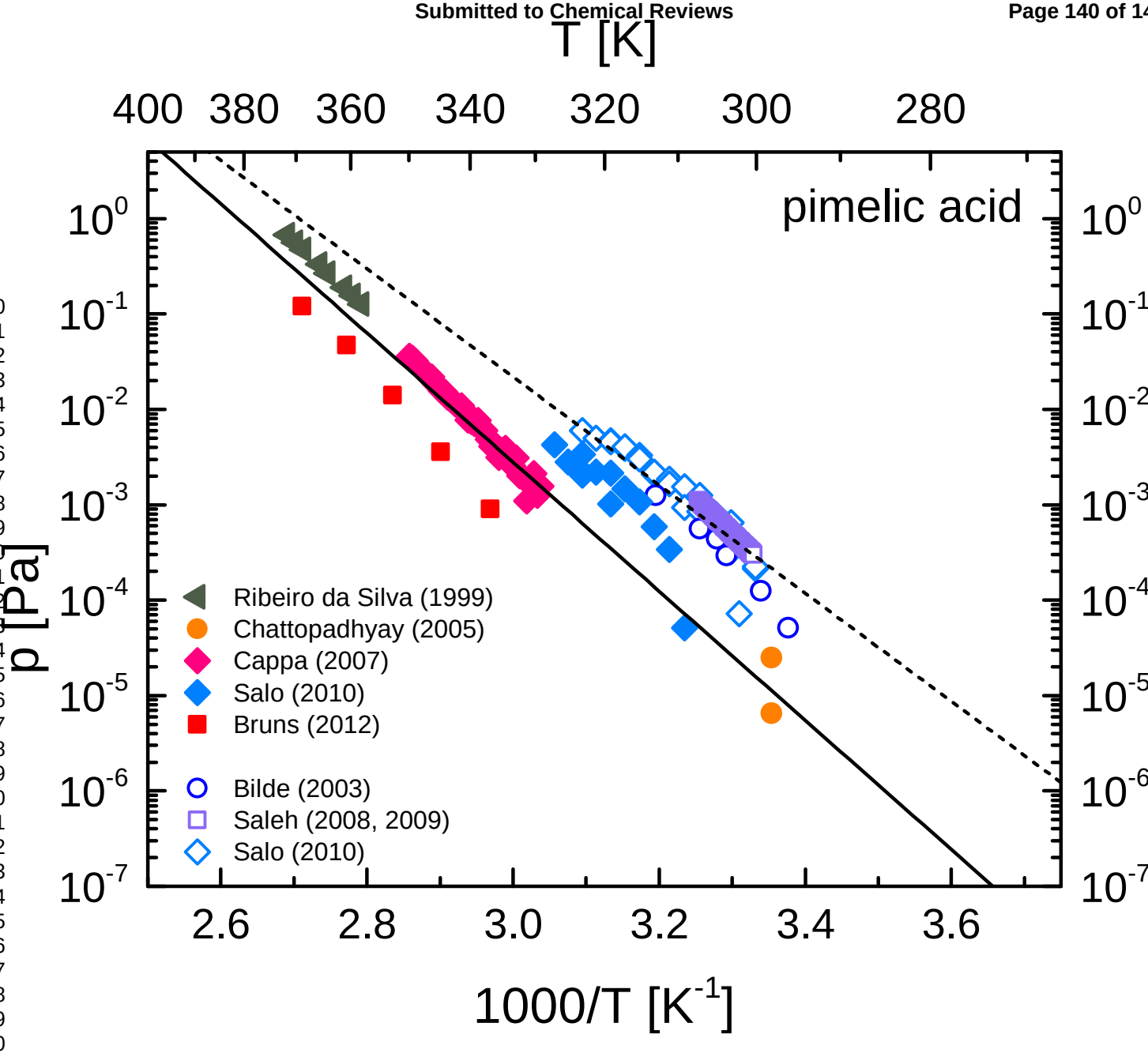
T [K]
400 380 360 340 320 300 280
pimelic acid
p [Pa]
Ribeiro da Silva (1999)
Chattopadhyay (2005)
Cappa (2007)
Salo (2010)
Bruns (2012)
Bilde (2003)
Saleh (2008, 2009)
Salo (2010)
2.6 2.8 3.0 3.2 3.4 3.6
1000/T [K-1]

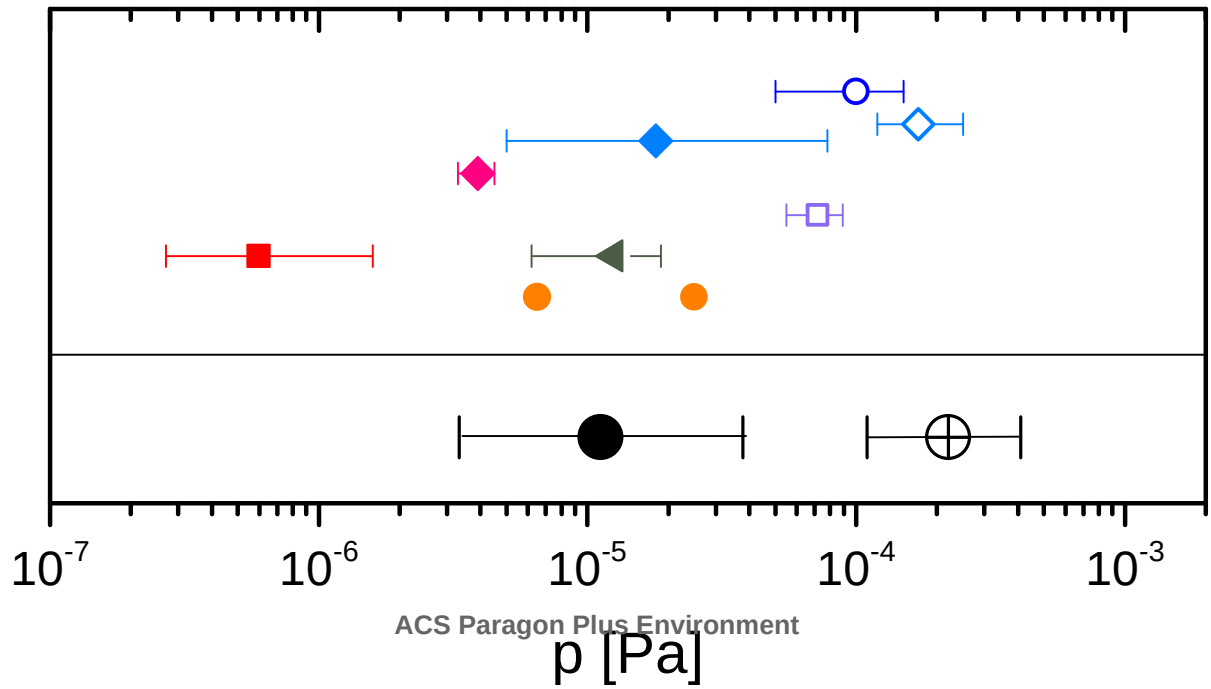
10-7 10-6 10-5 10-4 10-3
p [Pa]

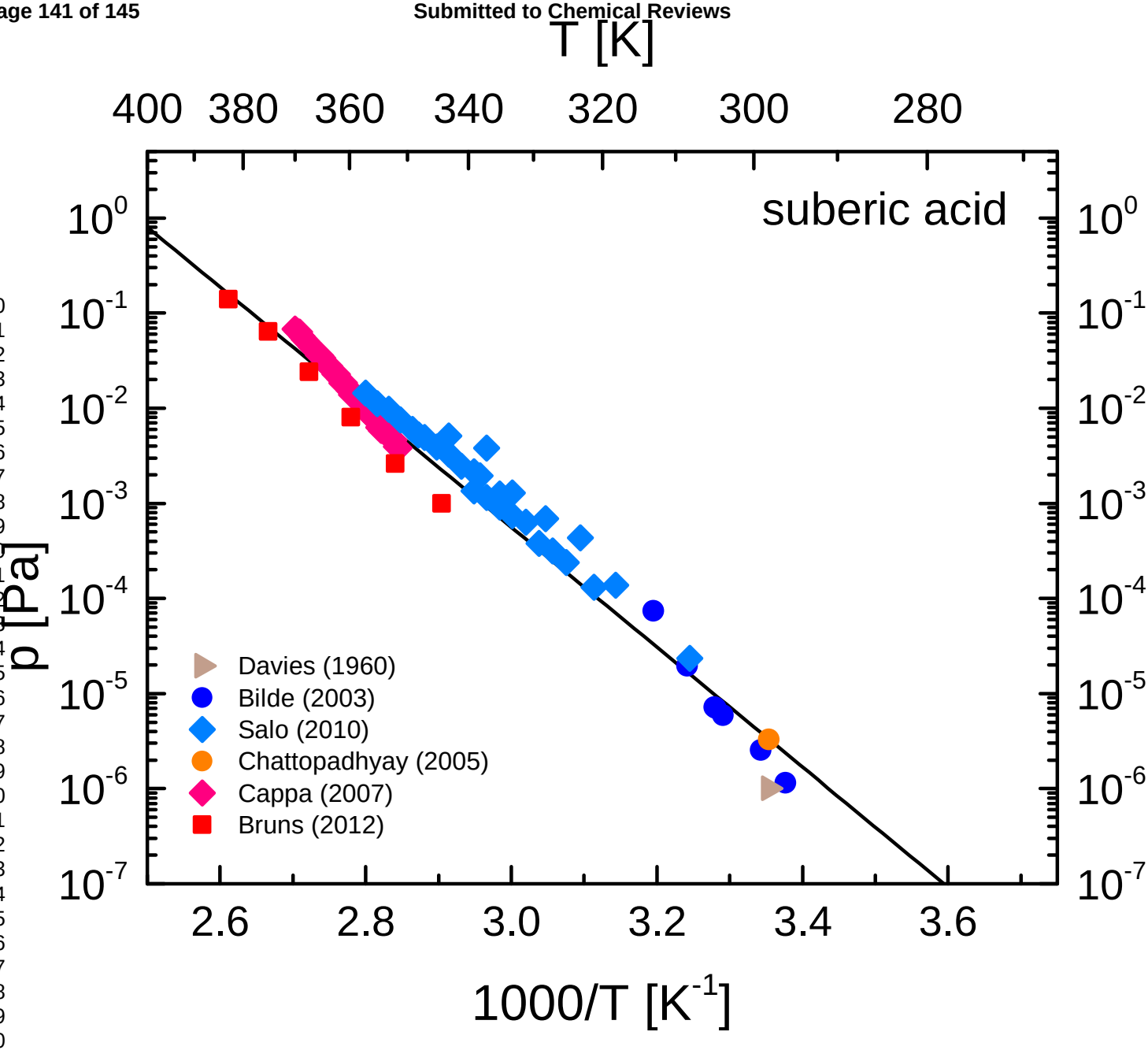
T [K]
400 380 360 340 320 300 280
suberic acid
p [Pa]
1000/T [K-1]
Davies (1960)
Bilde (2003)
Salo (2010)
Chattopadhyay (2005)
Cappa (2007)
Bruns (2012)

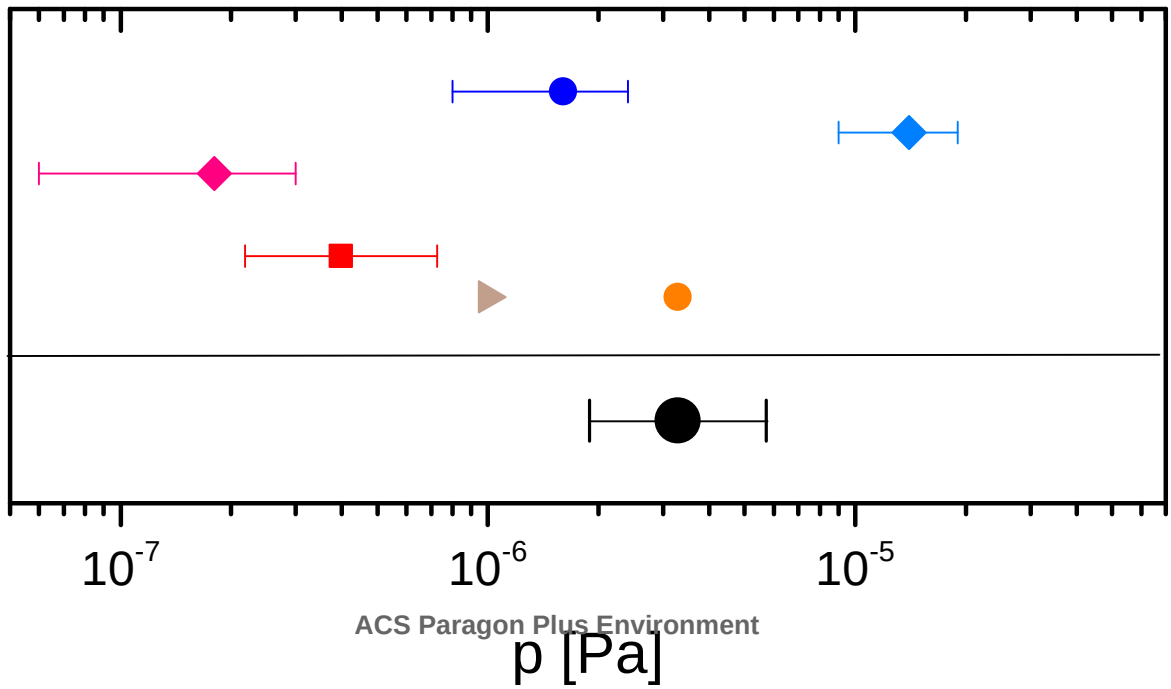
p [Pa]

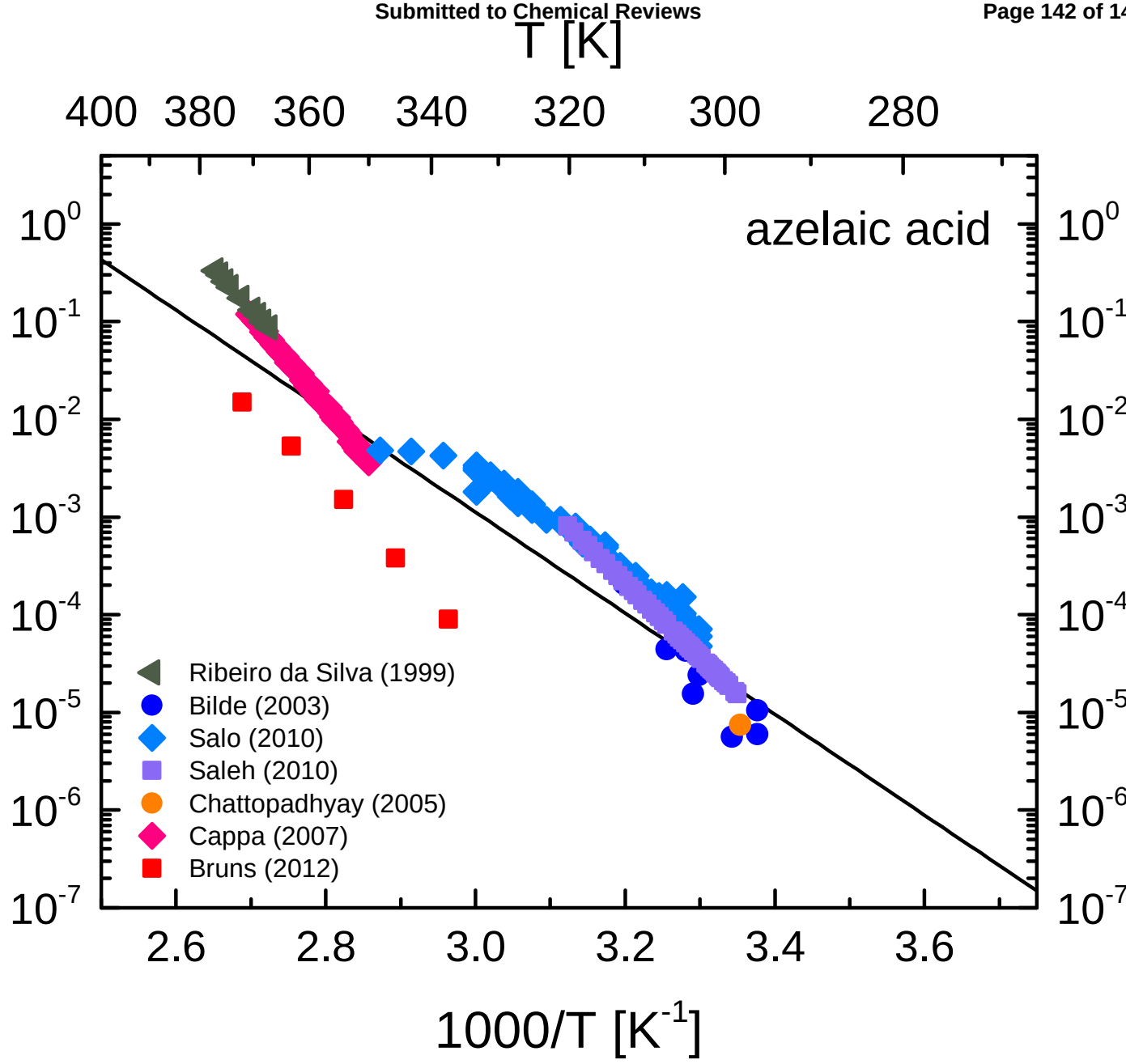
T [K]
400 380 360 340 320 300 280
azelaic acid
Ribeiro da Silva (1999)
Bilde (2003)
Salo (2010)
Saleh (2010)
Chattopadhyay (2005)
Cappa (2007)
Bruns (2012)
2.6 2.8 3.0 3.2 3.4 3.6
1000/T [K-1]

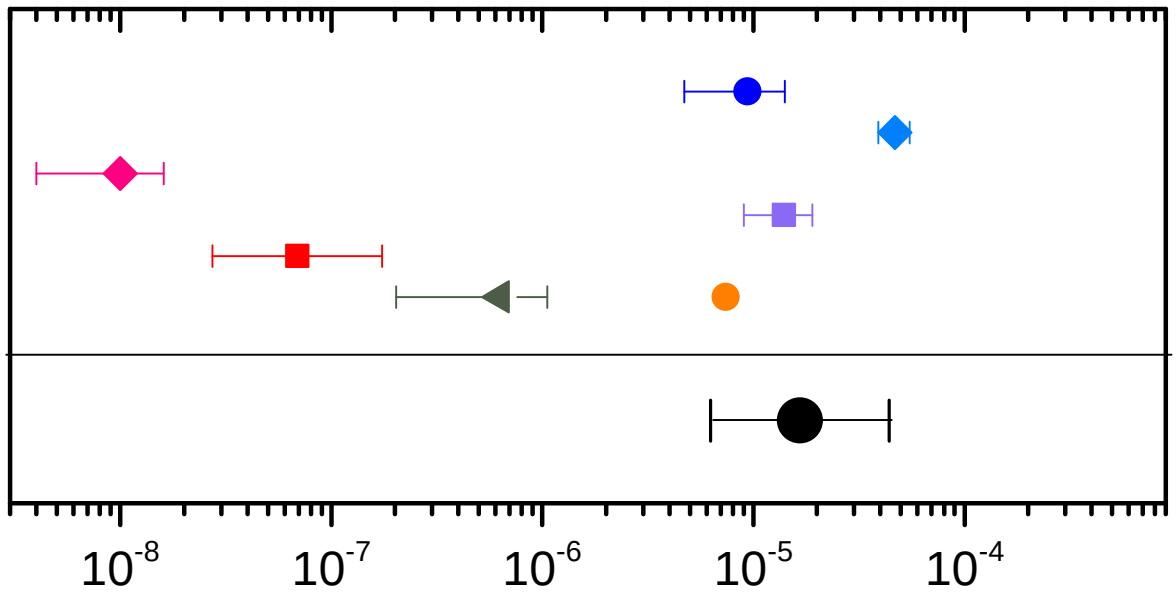
10-8 10-7 10-6 10-5 10-4
p [Pa]

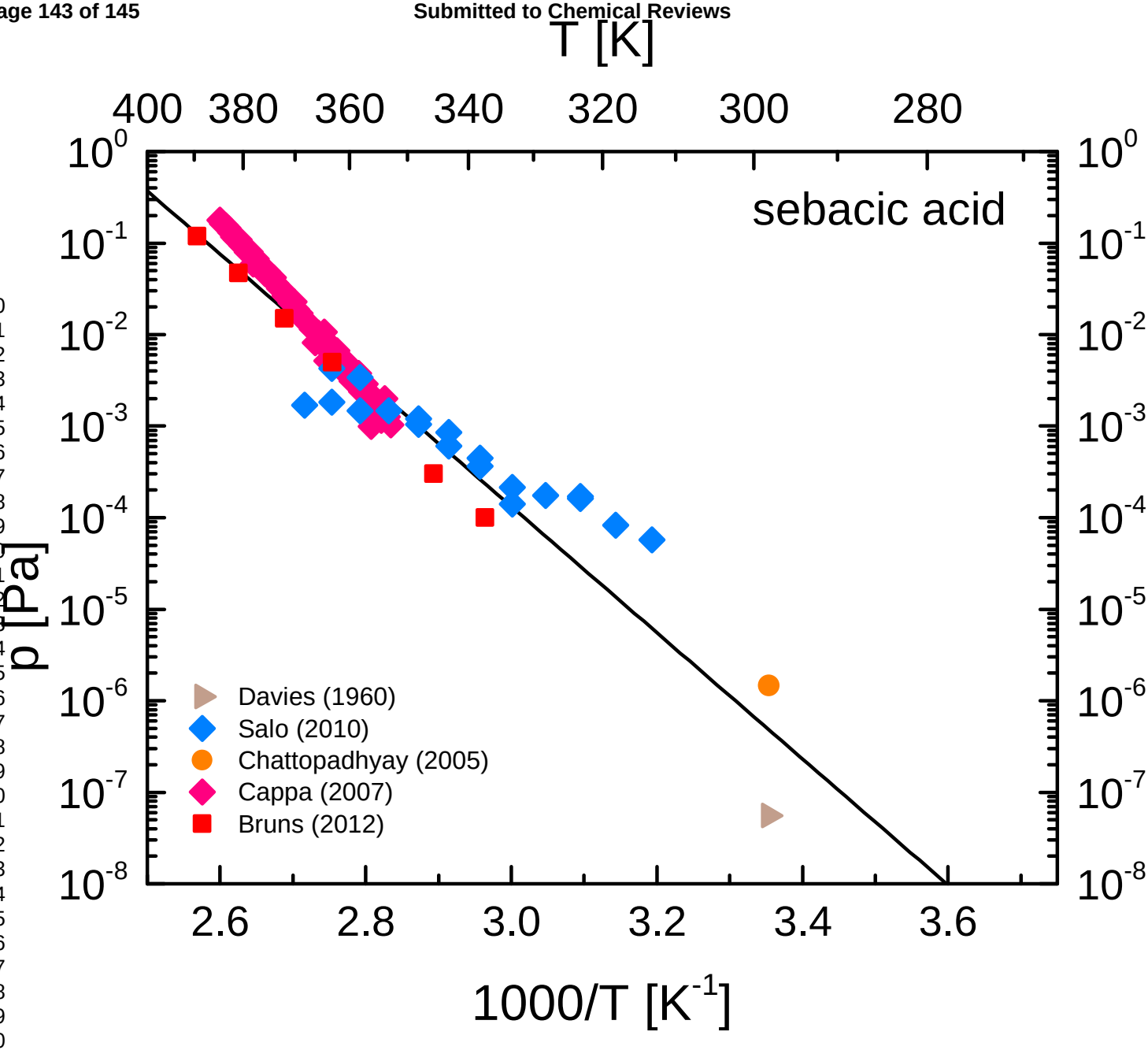
T [K]
400 380 360 340 320 300 280
sebacic acid
p [Pa]
Davies (1960)
Salo (2010)
Chattopadhyay (2005)
Cappa (2007)
Bruns (2012)
2.6 2.8 3.0 3.2 3.4 3.6
1000/T [K-1]

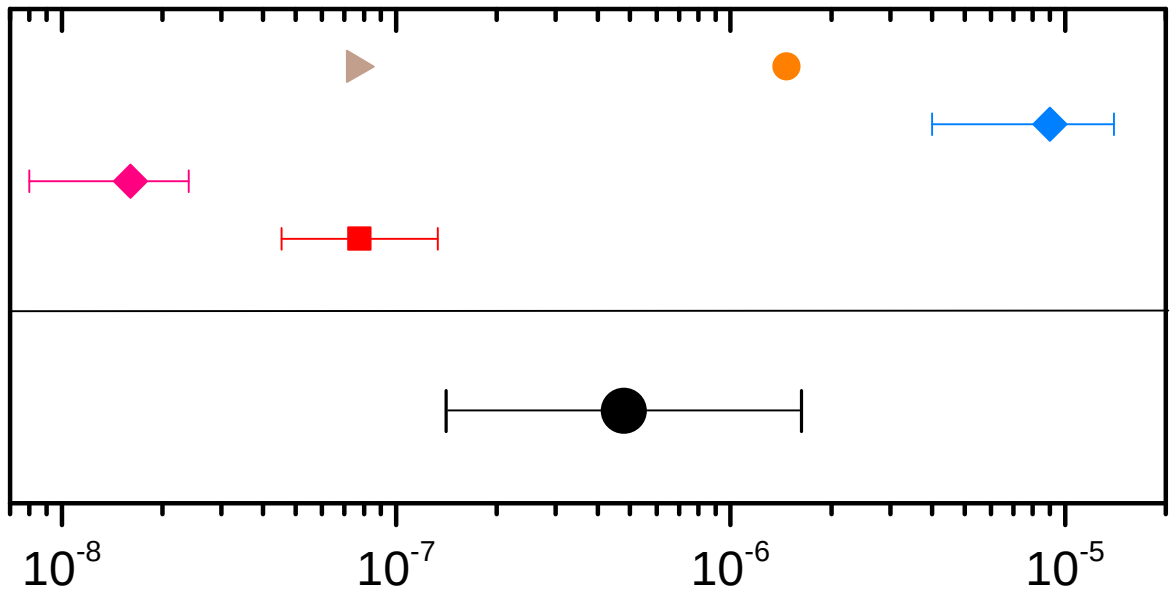
10-8 10-7 10-6 10-5
p [Pa]

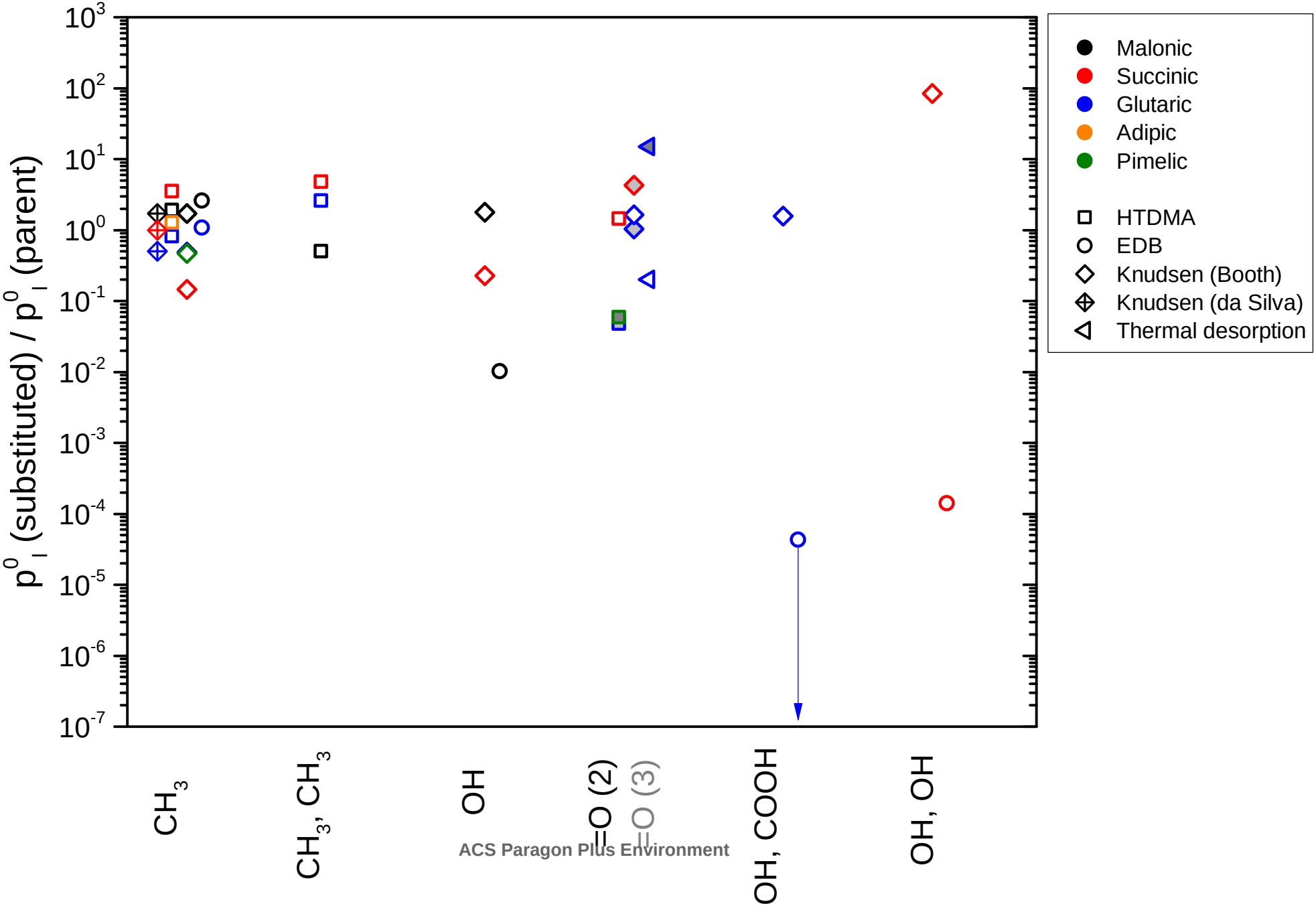
p^0_l (substituted) / p^0_l (parent)
10^3
10^2
10^1
10^0
10^{-1}
10^{-2}
10^{-3}
10^{-4}
10^{-5}
10^{-6}
10^{-7}
CH_3
CH_3, CH_3
OH
=O (2)
=O (3)
OH, COOH
OH, OH
Malonic
Succinic
Glutaric
Adipic
Pimelic
HTDMA
EDB
Knudsen (Booth)
Knudsen (da Silva)
Thermal desorption